Active Lateral Force Feedback in Dynamic Environments

Capabilities of Active Lateral Force Feedback in Point-Following-Tasks

RO57035: RO MSc Thesis

Kenny Brandon

Delft University of Technology

TU Delft

Active Lateral Force Feedback in Dynamic Environments

Capabilities of Active Lateral Force Feedback in Point-Following-Tasks

by

Kenny Brandon

Kenny
Brandon

Instructor:	M. Wiertlewski
Teaching Assistant:	Z. Cai & L. Stracovsky
Project Duration:	October, 2024 - November, 2025
Faculty:	Faculty of Cognitive Robotics, Delft

TU Delft

Preface

This thesis is a research prepared as part of the MSc. Robotics thesis by the designated student. It is aimed at scientists seeking to address challenges in haptic-based applications and developing strategies to enhance usability and task performance in innovative tactile displays, particularly for the latest invention called the Ultraloop. The author sincerely thanks Dr. M. Wiertlewski, L. Stracovsky, and Dr. Z. Cai for their invaluable guidance and support during this research.

Kenny Brandon
Delft, December 2025

Abstract

The absence of haptic feedback on touchscreens creates a big reliance on visual attention, leading to reduced focus and increased cognitive load, especially in dynamic real-world scenarios like driving or using interactive media. While previous research has extensively explored static pointing tasks, a significant gap exists in understanding interactions with moving targets. This thesis investigates the effect of active lateral force feedback, generated specifically by the Ultraloop haptic device, on user performance in dynamic point-following-tasks.

An experiment with 11 participants was carried out to separate the effect of vision and compare different types of haptic feedback across four conditions: Vision Only, Vision with Active Force, No Vision with Friction Modulation, and No Vision with Active Force. In this task, participants moved their finger on the Ultraloop to track a target that moved along a one-dimensional randomized multi-sine path. Then, their performance for each condition was evaluated by measuring the mean tracking error during their experimental trials. Then, their performance was evaluated with a McRuer crossover model analysis to measure human control behavior during the continuous pointing task by estimating parameters such as crossover frequency, lead and lag for each experimental condition.

The results demonstrate that active lateral force feedback significantly minimizes tracking error. It served as an additional cue in visual conditions, reducing the average tracking error by 24.1%, and acted as an effective sensory substitute in non-visual conditions, drastically outperforming friction modulation feedback by reducing the average tracking error by 34.8%. The McRuer analysis showed that it is possible to identify a human control behavior for visual conditions, but becomes quite complicated for non-visual conditions. Also, participants employed predictive control in visual conditions but reverted to reactive, heavily filtered strategies when relying solely on haptic feedback.

In conclusion, this experiment demonstrated that programmable active lateral force feedback is an effective tool for improving touch-enabled interactions in dynamic tasks. These findings expand the usability of active surface haptics, thereby advancing the development of more intuitive and efficient haptic touch interfaces in the future.

Contents

1

Introduction

Touchscreens and touchpads are becoming more essential in daily life, not only on mobile phones and tablets but also as replacements for traditional buttons, dials, and sliders in various everyday interactions. These devices have many advantages for the user due to great stimulus-response compatibility [1], which refers to how efficiently a user can respond to a stimulus, with performance improving when the stimulus and required action are intuitively aligned. Despite the increasing use of traditional touchscreens, they provide little or very primitive haptic feedback, which is essentially vibrotactile feedback. This creates a significant demand on the visual attention of the user[2], which can deteriorate during multitasking or when visuals are masked due to external factors [3], such as when driving. This makes interacting with moving elements particularly risky due to significantly increasing cognitive load. These could involve continuous interaction with moving targets, such as tracking an enemy in a fast-paced action or racing video game, where players must continuously track and target moving enemies or navigate through dynamic courses. Lateral force feedback could guide the player's fingers, improving accuracy and reaction time without relying solely on visual cues. Another example could be following a cursor on a military radar display where an operator using a touchscreen to track a moving drone or vehicle on a digital map requires precision under high-stress conditions. Haptic guidance on the screen would reduce the risk of losing the target, allowing the operator to maintain situational awareness with less focused visual attention.

Recent advancements in surface haptics, particularly in systems like the Ultraloop developed by Cai and Wiertlewski [4], have demonstrated the effectiveness of velocity-dependent lateral force feedback in improving touchscreen interaction. Their study showed that positive damping, where the lateral force increases with finger speed, enables users to complete pointing tasks faster and with greater accuracy. This result suggests that dynamic haptic feedback can support smoother and more efficient target acquisition by minimizing corrective movements, especially during the fine-targeting phase of interaction. Therefore, lateral forces are becoming indispensable for the implementation of haptic feedback in modern tactile touchscreens.

However, current research remains largely limited to static pointing tasks [5], typically modeled using Fitts' Law, which is a predictive model used to measure the speed-accuracy trade-off in human movement, particularly in pointing tasks. It is primarily applied in human-computer interaction to evaluate and optimize the design of interface elements, such as button sizes and distances, by estimating the time required to accurately acquire a target. While these tasks offer a robust framework for evaluating different feedback modalities, they do not fully represent the dynamic interactions where targets are moving or the goals are changing. Dynamic tasks introduce complex elements of prediction and continuous error correction that static Fitts' Law models cannot capture.

Programmable tactile feedback, which directly engages the user's finger, is a promising solution to overcome these limitations. Recent advancements in surface haptics, such as the Ultraloop device, have demonstrated that velocity-dependent lateral force feedback can improve speed and accuracy in static pointing tasks. However, this foundational research fails to address the possibility of dynamic pointing tasks, which can be the next step for modern interfaces. This gap leads to our research question:

Does the lateral force feedback from the Ultraloop reduce a user's tracking error in a dynamic target-following-task?

One of the following composed hypotheses is that the presence of lateral force feedback generated by the Ultraloop will improve user performance in dynamic pointing tasks by reducing tracking errors for target acquisition compared to non-feedback conditions. In addition, it is hypothesized that active lateral force feedback will lead to better performance than other forms of tactile feedback, specifically friction modulation. This thesis aims to investigate how the active lateral force feedback generated by the Ultraloop affects the user with respect to these feedback conditions.

2

Background & Relatable Work

This chapter elaborates on the background of the research to give context to the conducted experiment. It explains the core technology supporting this study, beginning with the working principle of the Ultraloop haptic device and analyzing the key experimental findings from earlier work, which serve as an important stepping stone for the experiment presented in this thesis. Furthermore, it introduces the McRuer crossover model, a framework from manual control theory, which is used in this work to measurably analyze human control dynamics during the haptic tracking task. By covering these key areas—the device and its precedent studies-this chapter provides the necessary foundation for understanding the methodology and analysis of the present investigation.

2.1. Ultraloop Device

To understand the concept of active lateral force feedback provided by the Ultraloop, it is essential to first explain the underlying working principle of the implemented device. The Ultraloop is a unique haptic device introduced and developed by Z. Cai and M. Wiertlewski [6], designed to generate controllable lateral forces on a user's fingertip through high-frequency surface vibrations. The device consists of a ring-shaped aluminum structure with multiple piezoelectric actuators mounted symmetrically around its base; see figure 2.1. These actuators excite the structure at ultrasonic frequencies to produce controlled wave propagation along the surface. By precisely tuning the input signals, the system can synthesize traveling waves that exert tangential forces on the fingertip, creating the sensation of a guided or resistive motion without any displacement of the surface.

The working principle relies on two orthogonal resonant standing waves of the ring structure. When these waves are simultaneously excited with a ±90° phase shift, they combine to form a traveling wave. This traveling wave induces elliptical surface particle motion, resulting in an active net force applied to the skin in the direction of wave propagation. The resulting tangential force arises from the momentum transfer between the oscillating surface and the finger's skin friction, effectively pushing or pulling the fingertip along the tactile surface. This mechanism allows the Ultraloop to deliver continuous and controllable lateral forces of up to approximately 300 mN, even when the finger remains stationary on the surface. The ring geometry of the Ultraloop provides mechanical symmetry, which ensures uniform propagation of the resonant waves and minimizes unwanted disturbance of the traveling waves. This design enables precise and repeatable tactile feedback over the entire contact area. Furthermore, the combination of ultrasonic actuation and high structural stiffness ensures minimal vertical displacement, preserving a stable and rigid interaction surface while allowing rich tangential feedback.

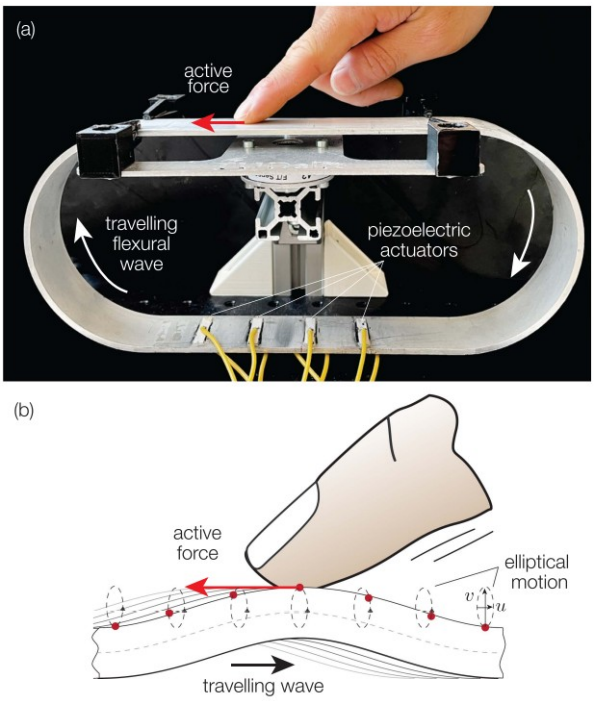

Figure 2.1: (a) The Ultraloop functions as a traveling-wave surface haptic interface, where piezoelectric actuators excite two structural modes that interact to produce a traveling wave. (b) This wave drives an elliptical motion of the surface, which in turn applies controlled lateral forces to the fingertip. [6]

Overall, the Ultraloop enables the active rendering of tactile cues such as friction modulation, directional force guidance, and virtual surface contours [7]. Its working principle bridges the gap between vibration-based haptic feedback and force feedback systems, making it a versatile platform for exploring realistic touch interactions and sensorimotor control in human–machine interfaces. For more info and schematics, see Appendix C.

2.2. Related Work

Before discussing the foundational work, it is essential to clarify how pointing-tasks are modeled during continuous interaction from a control-theoretic perspective. Control theory frames behavior in terms of signals, systems, goals, states, error, feedback, and feedforward, and these relationships are often illustrated using block diagrams that show how signals move through a system with feedback. The signals shown as arrows vary over time, while systems—shown as boxes—transform these signals and may contain internal states. In pointing tasks, the system state is not limited to position but also includes higher-order terms such as velocity, and potentially acceleration, which relates to muscle activation.

An example is given in figure 2.2, which shows a general control theoretic framework for continuous interaction as a second-order lag (2OL) model. The second-order lag (2OL) model is a simple linear model in control theory, characterized by its oscillatory step response before reaching steady state, with its behavior defined by two key parameters: a natural frequency controlling oscillation speed and a damping ratio controlling the damping rate, determining if the system is underdamped, critically damped, or overdamped [8]. The interaction of the framework is modeled as a control loop between the human and the computer. The user forms an intention, compares it with the observed system state, which forms a certain error, and generates a control signal that drives the biomechanics in his arm, producing motion sensed by the input device(mouse). This signal is filtered, transformed by the device's transfer function, and interpreted as position, velocity, or acceleration control, depending on the integration applied. The application then updates its state, which can be simply shown during desktop tasks, and this updated state is displayed back to the user, closing the loop.

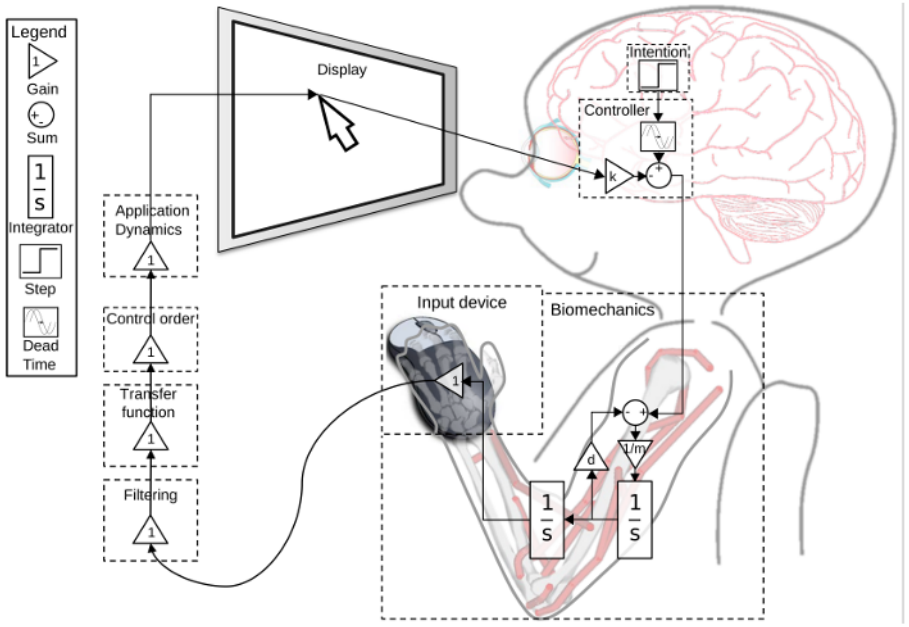

Figure 2.2: A general control-theoretic framework for modeling continuous human–computer interaction is presented. As an illustrative example, the framework is instantiated using the block diagram of the second order lag (2OL) model. [8]

To identify the human element in figure 2.2, the manual control literature offers numerous models, which vary in assumptions, complexity, and parameters, each based on different assumptions about human behavior [8]. One of the most influential frameworks in human–computer interaction is Fitts' Law, which describes pointing as a speed–accuracy trade-off: the time to acquire a target increases with the distance to the target and decreases with the target width [9]. Although originally formulated for discrete movements, Fitts' Law has been widely applied to pointing devices and remains the standard predictive model for movement time in Human Computer Interaction (HCI).

In earlier research conducted by Z. Cai [7], he investigated the possibilities of active lateral force feedback of the Ultraloop by testing whether active force feedback can improve the performance in Fitts's pointing task, which is a standardized motor-control experiment in which a participant must move as quickly and accurately as possible between targets of varying size and distance. Here, a one-dimensional pointing task was designed where participants had to slide against the tactile surface of the Ultraloop to locate a target using different kinds of feedback conditions. The tested targets had 3 different widths (16, 32, and 48 pixels) and 3 different distances (200, 400, and 600 pixels). The tested feedback conditions were active force, friction modulation, vision-only, and vision combined with active force. Figure 2.3 shows the implementation of the force and friction profiles of the different types of feedback conditions. In the first two conditions, the targets were invisible and had to be located purely by touch, while in the last two conditions, the targets were visible, enabling a comparison of performance with and without active lateral force feedback. For the friction modulation, a friction profile was implemented, which gives the feeling of high friction inside the target and low friction outside it. While for the conditions with active force, a force profile was implemented that excites a directing lateral force while outside the target and no force at all while inside the target.

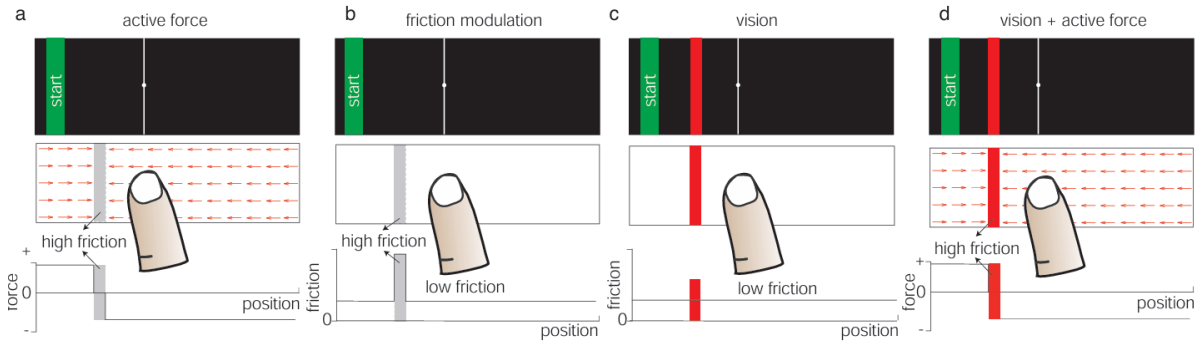

Figure 2.3: (a) Active force and (d) vision + active force conditions share an identical force profile, where forces consistently push the finger toward the target. In the (b) friction modulation condition, friction is high inside and low outside the target area. In (c) vision condition, friction remains consistently low. Targets are visible only in conditions (c) and (d). [7]

For this experiment all the participants used their index finger to slide across the surface to locate and select a target as quickly and accurately as possible. Each trial started with a green start area appearing randomly on the left or right side to avoid orientation bias. In visual conditions, the red target was also visible. Participants moved the white cursor—representing their finger position—into the start area and held it there for 0.6 s until a timer began. Then they slid their finger across the surface to locate the target using either visual or haptic cues, freely moving back and forth to confirm its position. Finally, they lifted their finger at the perceived target location, which triggered the confirmation and saving of the completion time of the trial.

Figure 2.4a shows the mean completion times of the tasks in the nine movement conditions and four feedback conditions. In the haptic-only conditions, active force feedback consistently resulted in shorter completion times than friction modulation across all movements, with a statistically significant difference. These results demonstrate the clear advantage of active force feedback in non-visual conditions. When visual feedback was available, active force feedback further reduced completion time, with the difference between vision and vision + active force also reaching statistical significance across all movement conditions. The Fitts's law analysis in figure 2.4b shows a clear linear relationship between completion time and task difficulty for all feedback conditions. The resulting performance indices indicate that active force feedback leads to more efficient targeting than friction modulation in haptic-only conditions and also improves performance when combined with vision. These findings raise the question of how active lateral force feedback will influence user performance in dynamic environments with a continuously moving target.

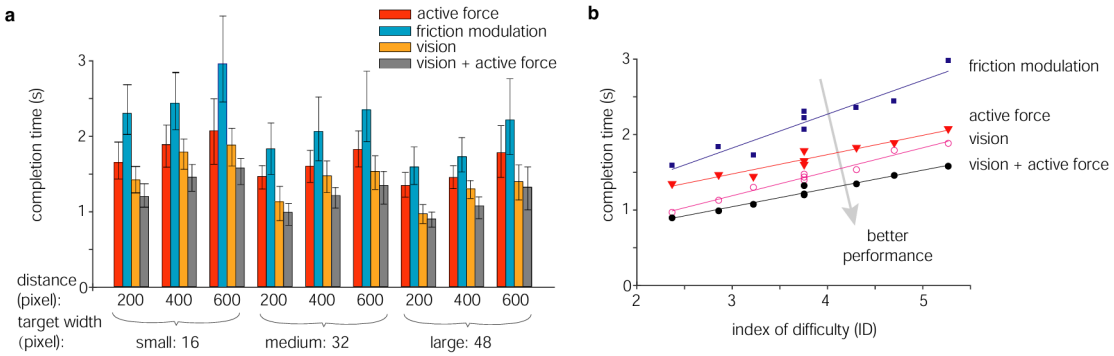

Figure 2.4: (a) Mean completion time in a pointing task across nine movement conditions. (b) Linear regression for mean completion time based on Fitts's indices of difficulty (ID). [7]

2.3. McRuer Crossover Model

Another control model that can identify human behavior during human-computer interaction is the McRuer Crossover Model, which describes how a human behaves as part of a closed-loop control system, where the goal is to maintain stable and accurate control of a dynamic process [10]. Originally developed to model pilot behavior in aerospace systems [11], this model has since been widely applied to study human performance in manual control tasks such as driving, tele-operation and human–machine interfaces. The core idea behind the model is that the human operator continuously observes the difference between the desired state (the target) and the actual state (the system response) and then generates corrective control actions to minimize this error over time. This base principle of the pilot continuously adapting their control actions to match the dynamics of the system being controlled, can be expressed mathematically in the frequency domain as follows:

$$Y_p(s)Y_c(s) = \frac{\omega_c}{s} e^{-\tau_e s} \tag{2.1}$$

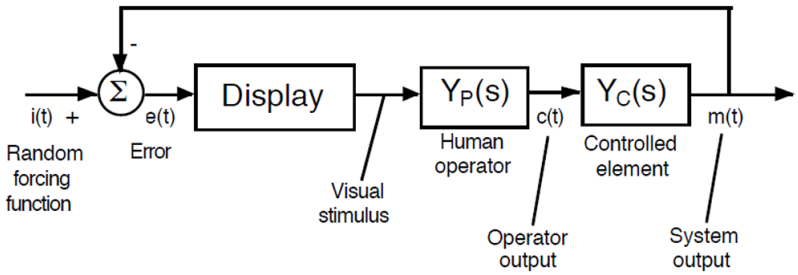

Figure 2.5: Pilot-vehicle block diagram [12]

where Y_p represents the pilot , Y_c the controlled element, and their product Y_pY_c forms the open-loop transfer function, which is visible in the pilot-vehicle block diagram shown in figure 2.5, while ω_c denotes the crossover frequency and τ_e the effective time delay. The crossover model does not capture the entire frequency response of human tracking; it is a local linear approximation that works only near crossover frequency ω_c, where the human closed-loop behavior resembles a first-order, slope-controlled system. By rearranging the formula of equation 2.1 it is possible to obtain the pilot transfer function in the crossover region:

$$Y_p(s) = Y_c^{-1}(s)\frac{\omega_c}{s} e^{-\tau_e s}. \tag{2.2}$$

Determining the exact inverse $Y_c^{-1}(s)$ is complex. McRuer found that the pilot's primary observed goal is not to exactly invert $Y_c(s)$, but to shape the combined open-loop response $Y_p(s)Y_c(s)$ to achieve the critical -20 dB/decade slope in the crossover region, which means that the human pilot adjusts their control strategy so that the total gain of the human-machine system decreases at a precise rate around the critical frequency where stability is determined, producing good tracking performance and sufficient stability margins. This procedure of shaping the pilot's response is referred to as equalization [12]. McRuer noted that, because of inherent cognitive and motor limitations, a human operator cannot have more than one lead term and one lag term. This observation leads to the simplified equalization model:

$$Y_p e \approx K_p \frac{1 + T_L s}{1 + T_I s}, \tag{2.3}$$

where K_p represents the operator's sensitivity or gain, describing how strongly the participant reacts to the perceived error signal. The relationship $\omega_c \approx K_p K_c$ links the pilot gain to the controlled-element gain K_c, showing that both determine the crossover frequency.

The parameter T_I is the human lag time constant, it models that humans do not react instantaneously, but with some lag, whereas T_L is the human lead time constant, it gives the system "lead" to counteract lag and stabilize the loop.

McRuer's analysis [13] indicates that the overall time delay in the loop can be expressed as:

$$\tau_e = \tau_0 - \Delta\tau(\omega_i) \tag{2.4}$$

where τ_e is the effective time delay, representing all latencies in the loop, including visual perception, neural transmission, display latency, and device feedback delay. The variable ω_i represents the bandwidth of the forcing function applied during the task(closed-loop system input). As for the crossover frequency:

$$\omega_c = \omega_{c0} + \Delta\omega(\omega_i). \tag{2.5}$$

For most modeling purposes, the correction term $\Delta\omega(\omega_i)$ can be considered negligible. According to McRuer [13] it is proven that:

$$\omega_{c0}\tau_0 = \frac{\pi}{2}. \tag{2.6}$$

Using this property, the crossover frequency may be approximated as:

$$\omega_c \approx \frac{\pi}{2\tau_0}, \tag{2.7}$$

which allows one to compute the pilot gain K_p, yielding the familiar crossover-form pilot model:

$$Y_p(s) = K_p \frac{(1 + T_L s)}{(1 + T_I s)} e^{-\tau_e s}. \tag{2.8}$$

To account for the dynamics of the human neuromuscular system, an additional first-order lag is typically included:

$$N(s) = \frac{1}{1 + T_n s}. \tag{2.9}$$

Here, T_n represents the neuromuscular time constant, modeling muscle activation dynamics and the mechanical delay between neural commands and applied force.

By combining the equalization term (2.3), the neuromuscular dynamics (2.9), and the effective delay τ_e yields the commonly used Tustin–McRuer pilot model:

$$Y_p(s) = K_p \cdot \frac{1 + T_L s}{1 + T_I s} \cdot \frac{1}{1 + T_n s} \cdot e^{-\tau_e s}. \tag{2.10}$$

One of the key insights of the McRuer crossover model is that humans adapt their internal control strategy to the dynamics of the system they are interacting with. For example, when controlling a sluggish or highly delayed system, people tend to reduce their control gain and increase their reliance on predictive actions to maintain stability. Conversely, when interacting with a fast or responsive system, they increase their gain to achieve more precise tracking. This adaptive nature explains why the model can describe a wide range of behaviors across different domains — from aircraft piloting to precise finger movements on touch interfaces. Ultimately, the McRuer crossover model provides a framework for measuring human-in-the-loop dynamics by treating the human operator as an adaptive, dynamic element within a feedback system, which makes this model a good candidate for evaluating dynamic tracking tasks.

3

Experimental Method

Understanding how humans respond to different forms of haptic feedback is essential for improving surface haptic interfaces and optimizing their integration in dynamic interaction tasks. To explore this, an experimental study was conducted using the Ultraloop device, focusing on how users track a moving target under various sensory and feedback conditions. This chapter outlines the experimental method used to investigate human performance during target-following-tasks with the Ultraloop surface haptic device. The aim of these experiments is to evaluate how different feedback conditions in visual and non-visual situations affect users' tracking accuracy. The following sections describe the experimental setup, including participant preparation, familiarization with the haptic feedback conditions, and implementation of multiple randomized trials across the haptic feedback conditions.

The Ultraloop is capable of implementing friction modulation and active lateral force feedback. To test both forms of haptic feedback on participants fingers while interacting with the Ultraloop, a total of 11 young adult participants (aged 20–30, from the TU Delft campus) participated in the experiments. Each participant washed and dried their hands to ensure that they had a clear tactile sense of the surface. Before the participants started the experiment, they first had to complete an introduction trial, where they could experience friction modulation and active lateral force feedback and get acquainted with them. Shown earlier in chapter 2, during friction modulation, participants experience the feeling of a bump when they move their finger over the moving target, while active lateral force feedback gives participants the feeling of a pulling force on the contact surface of the Ultraloop that will direct their finger towards the moving target. Both these forms of feedback are shown in figure 3.1.

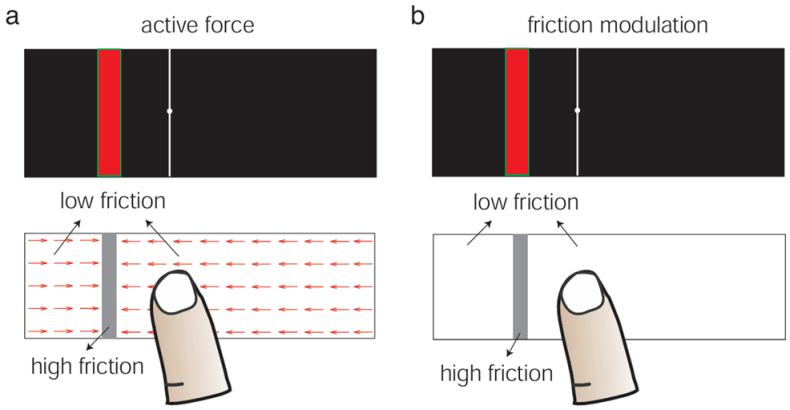

Figure 3.1: The top shows the GUI of the dynamic following-task. The bottom shows the active force or friction field in active force (a) or friction modulation (b) condition, respectively. [7]

For the experimental setup with respect to the hardware, the Ultraloop (see Fig 3.2) device was implemented to interact with the participant's finger as a contactor. Participants used their right index finger on the Ultraloop contact surface to follow the horizontally moving target, which is virtually displayed on a laptop screen as the cursor. The red area indicates where the virtual moving target is at a specific moment, while the Ultraloop uses friction modulation or active lateral force feedback to guide participants to that specific area. This red area matches the movement of the virtual moving object.

Figure 3.2: The Ultraloop contact surface for the participants to follow the moving virtual target, indicated by the red overlaid rectangle. Also, a position sensor is mounted on top to measure the finger position of the participant.

This virtual target-tracking task is programmed with Python using a Pygame library, where the target moves only horizontally with sinusoidal behavior. When the participant's finger is within the moving object, it turns green (see figure 3.3), which is an indication of perfect tracking, but when the finger is outside the moving object, it turns red (see figure 3.4). When the target becomes red, the program starts collecting error measurements, such as the duration of the red state and the positional difference between the target and the participant's finger.

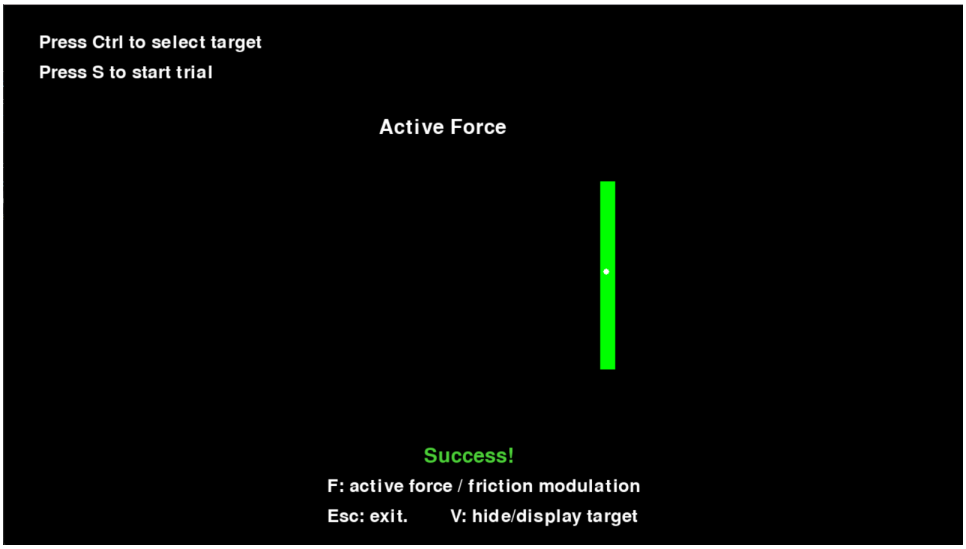

Figure 3.3: The graphical user interface displaying the dynamic following-task. Here the user's cursor is within the region of the target, which is thus displayed in green.

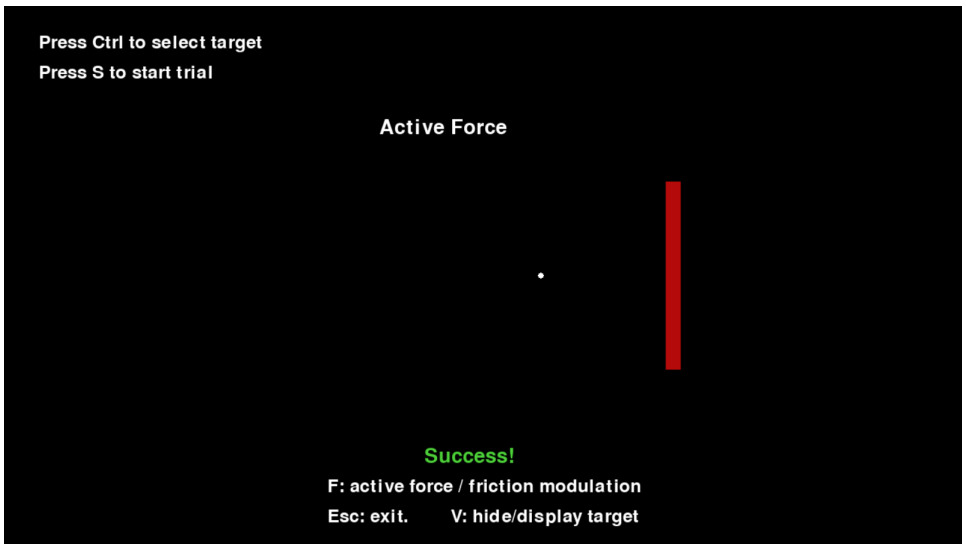

Figure 3.4: The virtual simulation of the dynamic following-task, where the participant is outside the boundary of the dynamic moving object.

Then each participant had to interact with the Ultraloop for five trials of 15 seconds each for 4 different conditions, similar to the earlier research by Cai[7]. The four conditions are described as follows:

1. **Condition 1**: No tactile feedback is implemented and the participant follows the visible moving object.
2. **Condition 2**: Active lateral force feedback is implemented and the participant follows the visible moving object.
3. **Condition 3**: Friction modulation is implemented and the participant follows the invisible moving object.
4. **Condition 4**: Active lateral force feedback is implemented and the participant follows the invisible moving object.

For generating the five 15 seconds trials, a Python script was implemented to generate five different horizontal movement trajectories using the principle of a multiphase multi-sine shown in Figure 3.5. Multiphase multi-sines generate controllable random trajectories ideal for system identification by covering multiple frequencies in a single, reproducible signal [14]. The goal of implementing this principle is to create natural, yet controlled, target motions for experimental trials. Each trial signal is synthesized as a multisine of the form:

$$x(t) = \sum_{i=1}^{N} A_i \, \sin\left(2\pi f_i t + \phi_i\right) \tag{3.1}$$

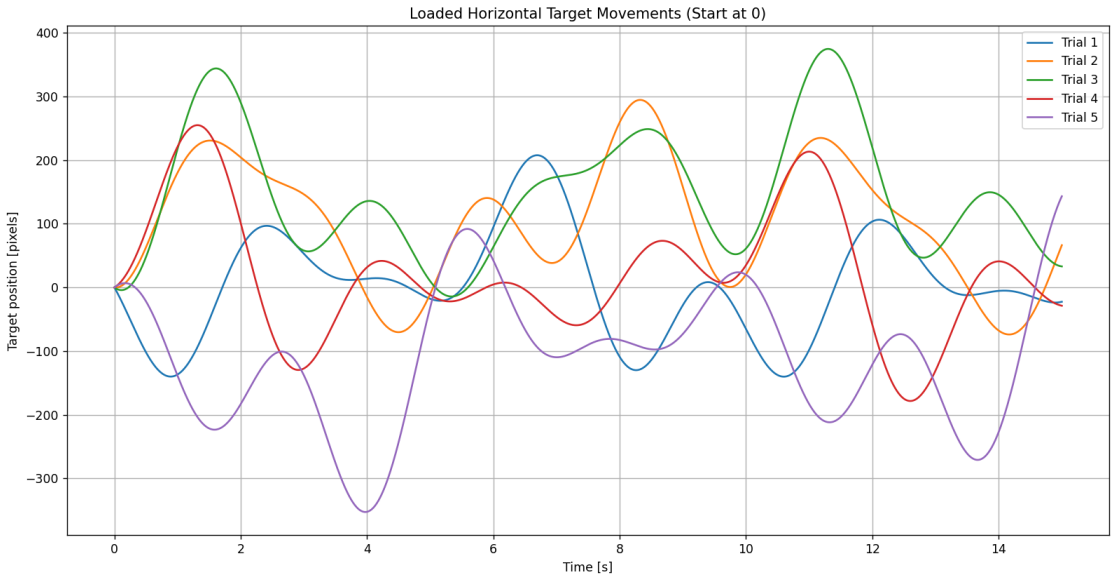

Figure 3.5: The 5 trial movement patterns, which each simulate the movement of the moving target in the following-task.

where f_i are the chosen frequencies, A_i are equal amplitudes, and ϕ_i are the randomized phases. A set of discrete sinusoidal components is defined within a low-frequency range (0.01–0.40 Hz in 0.05 Hz steps). These frequencies represent the building blocks of the target movement. All components are assigned equal amplitudes, ensuring that no single frequency overshoots the motion. For each trial, every frequency component is assigned an independent random phase uniformly distributed between 0 and 2π. This multiphase construction ensures that each trial produces a unique trajectory. Random phases avoid repetition and prevent predictable motion patterns. Finally, the signal is shifted so that it always starts at zero, making the beginning of each trial aligned and comparable across conditions. Also, this way participants cannot recognize movements from the initial point. This process is executed five times with newly randomized phase sets, generating five unique target movements; see table 3.1.

Unfortunately, at the time these randomized multiphase multi-sine paths were generated, the actual random implemented phases were not recorded in the code. At the time of realization, these paths were already implemented for the human experiments and therefore not possible to extract the same exact values back.

Table 3.1: Multisine parameters for generating the trial movements

N	A_i	f_i [rad/s]	ϕ_i [rad]
1	1	0.01	$[0, 2\pi]$
2	1	0.06	$[0, 2\pi]$
3	1	0.11	$[0, 2\pi]$
4	1	0.16	$[0, 2\pi]$
5	1	0.21	$[0, 2\pi]$
6	1	0.26	$[0, 2\pi]$
7	1	0.31	$[0, 2\pi]$
8	1	0.36	$[0, 2\pi]$

With 4 experimental conditions consisting of 5 trials each, it comes down to 20 combinations in total to test. These combinations were given to the participant at random to prevent bias and pattern recognition. For a better visual display, the test matrix is given in table 3.2.

Table 3.2: Testing Matrix for Participants

Condition	Trial Movement Patterns				
1) Vision Only	Trial 1	Trial 2	Trial 3	Trial 4	Trial 5
2) Vision + Active Force Feedback	Trial 1	Trial 2	Trial 3	Trial 4	Trial 5
3) No Vision + Friction Modulation	Trial 1	Trial 2	Trial 3	Trial 4	Trial 5
4) No Vision + Active Force Feedback	Trial 1	Trial 2	Trial 3	Trial 4	Trial 5

During the experiment, there are measured values that are important to give an indication about the participants performance. For example, the principal metric to evaluate the performance of the participants in the tracking task was calculated by analyzing the mean error distance between the moving target and the position of the participant's finger over time. This error represents the deviation between the target trajectory and the participant's cursor trajectory, indicating whether tactile feedback helps participants maintain accurate alignment with the moving target by comparing this for each individual participant in each condition.

To characterize the human-in-the-loop control behavior during the tracking task, the participant's interaction with the Ultraloop system can be represented as a closed-loop control system. Figure 3.6 shows a block diagram of the point-following-task of the participant with the Ultraloop, based of figure 2.5. The movement of the target here is defined as $f(t)$, which is a position function in pixels, where $e(t)$ is the error distance between the moving target and the finger of the participant, $c(t)$ is the operator output and the control input, which is a velocity and finally $y(t)$ is the control output as a position in pixels, which is a feedback that affects the error distance. Also, a small addition to this block diagram is $d(t)$, which represents control noise, intended as the noise introduced by the operator while exerting the control action.

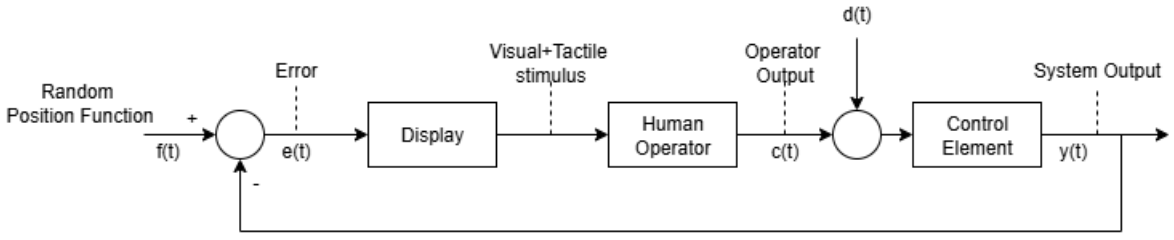

Figure 3.6: Participant-controller block diagram.

In figure 3.7 there is a real-world visualization of the block diagram from figure 3.6, which shows what all the inputs and outputs of the system look like while the participant is interacting in the point-following experiment. In figure 3.7B, a zoomed-in image of the screen the participant looks at during the experiment to see his cursor and the moving target, where sometimes the target is visible or invisible. Figure 3.7C shows the top view of the interacting tactile display (Ultraloop) the participant uses during the experiment, where the tactile stimulus (red arrow) in this case is the active lateral force feedback guiding the finger towards the target.

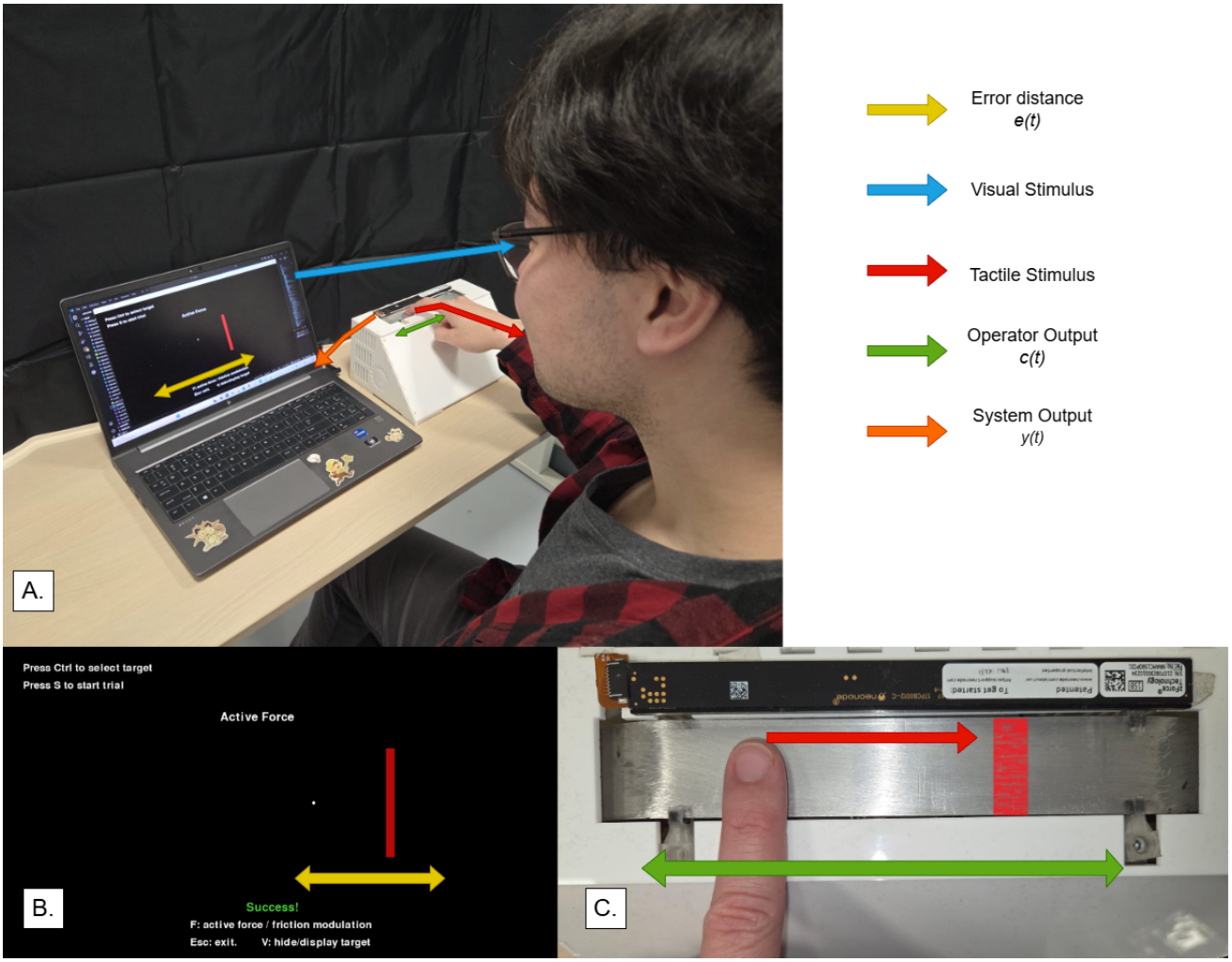

Figure 3.7: A: Participant conducting the point-following experiment visualized with the inputs and outputs of the participant-controller block diagram. B: GUI showing the position of the moving target and cursor of the participant. C: Top view of the interacting display of the Ultraloop.

4

Results

This chapter presents the results of the experiment to evaluate how different haptic feedback conditions influence tracking performance during the dynamic target-following-task with the Ultraloop device. These results show whether active lateral force feedback helps users maintain control, particularly for conditions of varying velocity, unpredictable movement, and occluded vision. The results are structured to address two primary performance indicators. First, an analysis of the mean error distance between the moving target and all the participants' finger positions over time, providing a direct measure of tracking accuracy followed by a more detailed perspective by examining example tracking paths from a representative participant across all feedback conditions, illustrating how resulting paths differed between them. The second part of this chapter presents a dynamic modeling attempt using the McRuer Crossover Model to describe how participants regulate their movements under different haptic feedback conditions.

4.1. Participant Performance

Both RMSE and average error distance are suitable standard accuracy metrics for evaluating target-tracking performance, but because RMSE disproportionately penalizes large deviations, average error distance was chosen as the more appropriate metric in this context [15]. The average error distance between the participant's finger and the moving target is analyzed, providing the mean Euclidean distance between the participant's trajectory and the target trajectory for each condition. These conditions are compared with each other to see the impact of active lateral force feedback in situations with and without visual feedback. For the average error distance, a set of box plots were made for each condition with their five different movement trials to indicate whether all trials are evenly difficult or if one was significantly more complicated than the others. This was not the case according to the results shown in A.1 in the Appendix, where the mean error-distance was determined for each trial-track for all conditions. It shows that there is no specific track with a significantly higher mean error-distance over all four tested conditions, concluding that these movement trials were equally difficult for the participants.

More importantly, the results of the box plot made over all the participants' mean error distances for all conditions. Figure 4.1 shows the performance of all participants for each condition, calculating the mean error-distance for each participant for all five movement trials of that specific condition, and then showing it as a data-point in the box plot. Each data-point has its own specific color indicating to which participant it belongs. Overall, this figure shows a significant difference between the first two conditions (vision) and the last two conditions (no vision). Conditions 1 (Vision Only) and 2 (Vision + Active Force Feedback) show significantly lower mean error-distance compared to conditions 3 (No Vision + Friction Modulation) and 4 (No Vision + Active Force Feedback), clearly demonstrating that visual information plays a dominant role in tracking accuracy, as expected. Also within expectations, Condition 3 (No Vision + Friction Modulation) showed the highest error values, reflecting the difficulty of relying solely on cues from friction modulation, while Condition 4 (No Vision + Active Force Feedback) performed slightly better but still lagged behind the visual conditions, while conditions 1 (Vision Only) and 2 (Vision + Active Force Feedback) consistently showed the lowest overall error distances.

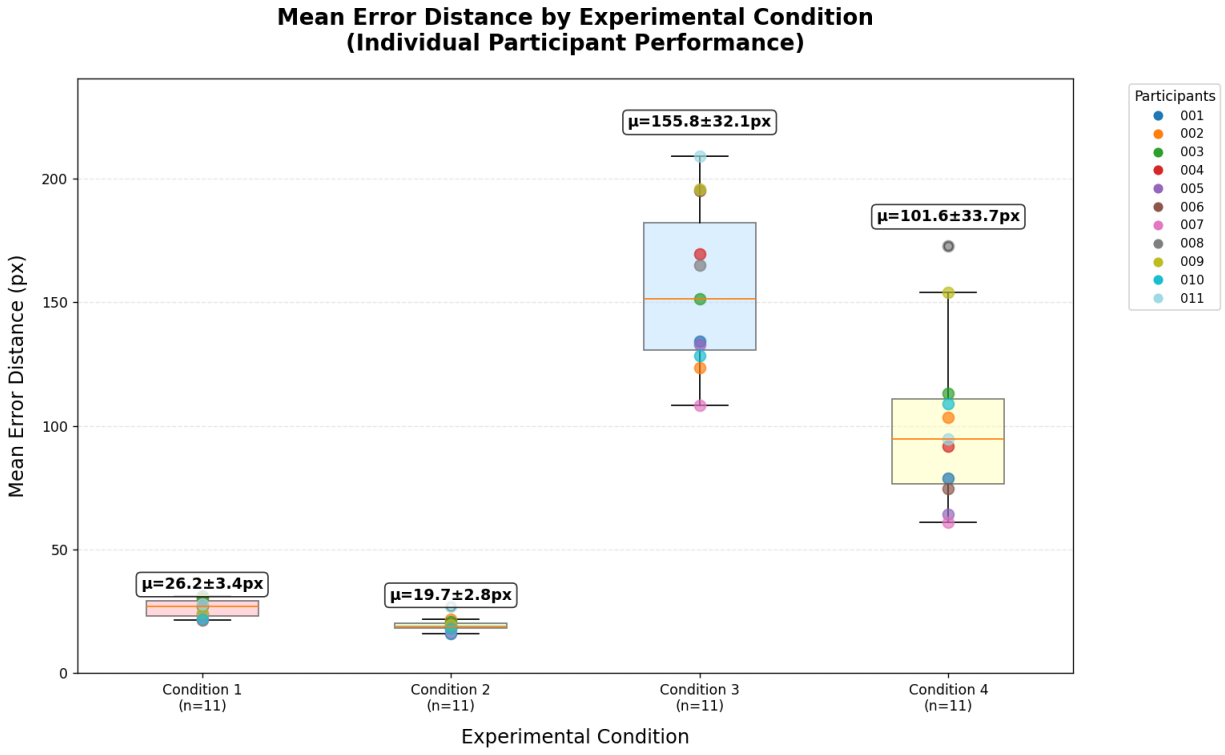

Figure 4.1: Boxplots of all the 11 participants' mean error-distance for each of the 4 testing conditions. Each condition shows a plot of the mean error distance ± standard deviation indicated on top.

4.1.1. Visual Conditions

To enable a clearer comparison of the impact of active lateral force feedback for visible conditions, the focus is placed on conditions 1 (Vision Only) and 2 (Vision + Active Force Feedback). Figure 4.2 shows a zoomed-in part of figure 4.1 with lines connecting the corresponding participants with their mean error-distance for the two conditions. The slope of the connecting lines reflects the extent to which active lateral force feedback influences participant tracking performance. A steeper downward slope indicates a greater positive impact of active lateral force feedback on performance. This figure shows that all participant have a downward slope, meaning that condition 2 (Vision + Active Force Feedback) where the active lateral force is implemented, reduces their mean error-distance. One small detail that causes this is that most participants tend to overshoot in the following-task experiment for condition 1 (Vision Only) when they try to predict the trajectory of the target by going ahead with their finger position, not expecting the small occurring changes in speed and direction. The lateral forces likely help minimize overshoot and fine-tuning corrections, especially during the turning points of the sinusoidal target motion, leading to smoother and more accurate tracking.

By comparing the average error distance between all participants under visual conditions, the results show that implementing active lateral force feedback leads to a reduction of 6.5 pixels, corresponding to a 24.1% improvement in tracking accuracy. It is also shown in the figure that the difference in the mean error-distance is significant because the boxplots do not overlap. Furthermore, a t-test that gives a p-value less than 0.05 ($p = 0.000003$) proves that condition 1 (Vision Only) has a significantly higher error than condition 2 (Vision + Active Force Feedback), indicating that active lateral force feedback has a positive impact on participant performance for visible target-following-tasks.

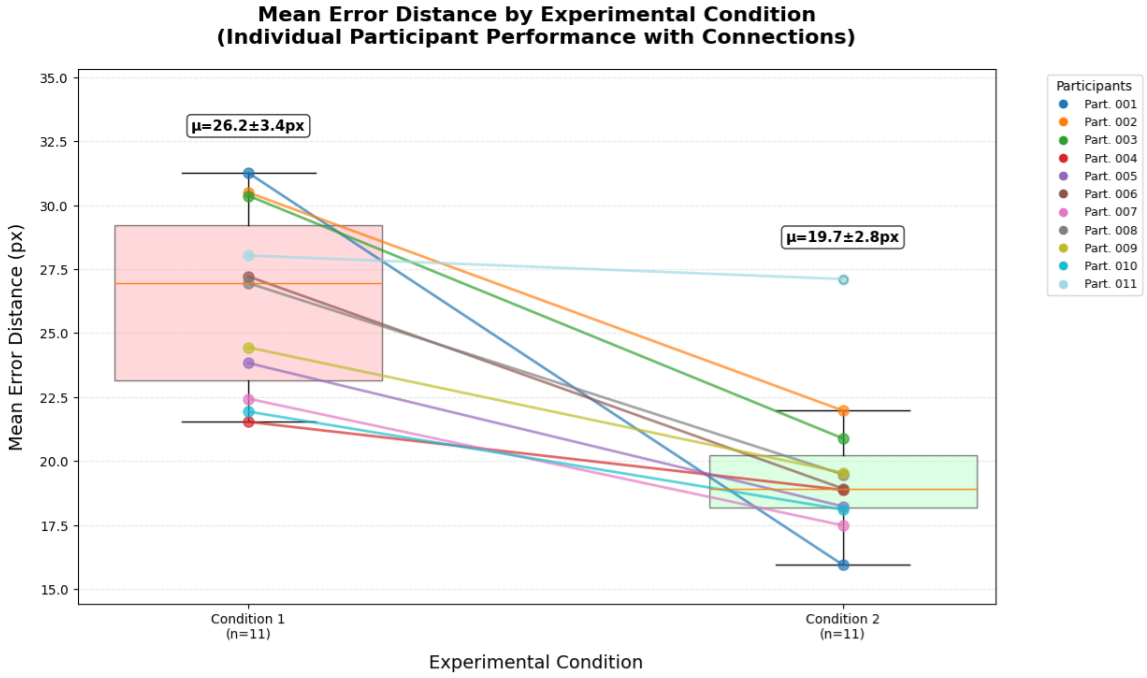

Figure 4.2: Zoomed-in image of the boxplots of all the 11 participants' mean error-distance for each of the 4 testing conditions, focusing on comparing Vision Only (condition 1) to Vision + Active Force Feedback (condition 2).

4.1.2. Non-Visual Conditions

For a specific comparison of the impact of active lateral force feedback for non-visual conditions, the focus is placed on conditions 3 (No Vision + Friction Modulation) and 4 (No Vision + Active Force Feedback). Figure 4.3 also shows a zoomed-in part of figure 4.1 with a line connecting the corresponding participants with their mean error-distance for these two non-visual conditions. The trials with condition 3 (No Vision + Friction Modulation) were, for all participants, the most difficult because this bump they feel when they move over the target is the only feedback that gives an approximate location of the moving target for a certain time instance. Therefore, every participant quickly tends to use their finger for active exploration in order to find the bump of the target. But for condition 4 (No Vision + Active Force Feedback) the trials seemed less difficult due to the guiding feedback of the active lateral force feedback. Here, it is also noticeable that almost all connections show a steep downward slope, which means that the active force did indeed have an impact on the participants' performance. However, individual differences occurred, with some participants (e.g., participant 008, 009) in the non-visual force condition still exhibiting exploratory behaviors similar to those observed in condition 3 (No Vision + Friction Modulation). This might be due to the participant quickly losing the target and then enacting the same behavior as the trials for condition 3 (No Vision + Friction Modulation). This suggests that for certain participants, the active force magnitude may have been insufficient to fully suppress the need for active exploration, or that personal differences in tactile sensitivity and interpretation affected the ability to rely solely on force guidance.

By comparing the average all the mean error distances between all participants under non-visual conditions, the results show that implementing active lateral force feedback compared to only friction modulation leads to a reduction of 54.2 pixels, corresponding to a 34.8% improvement in tracking accuracy. Also, a t-test that gives a p-value less than 0.05 ($p \approx 0.00$) shows that condition 3 (No Vision + Friction Modulation) has a significantly higher error than condition 4 (No Vision + Active Force Feedback), indicating that active lateral force feedback has a positive impact on participant performance for invisible target-following-tasks.

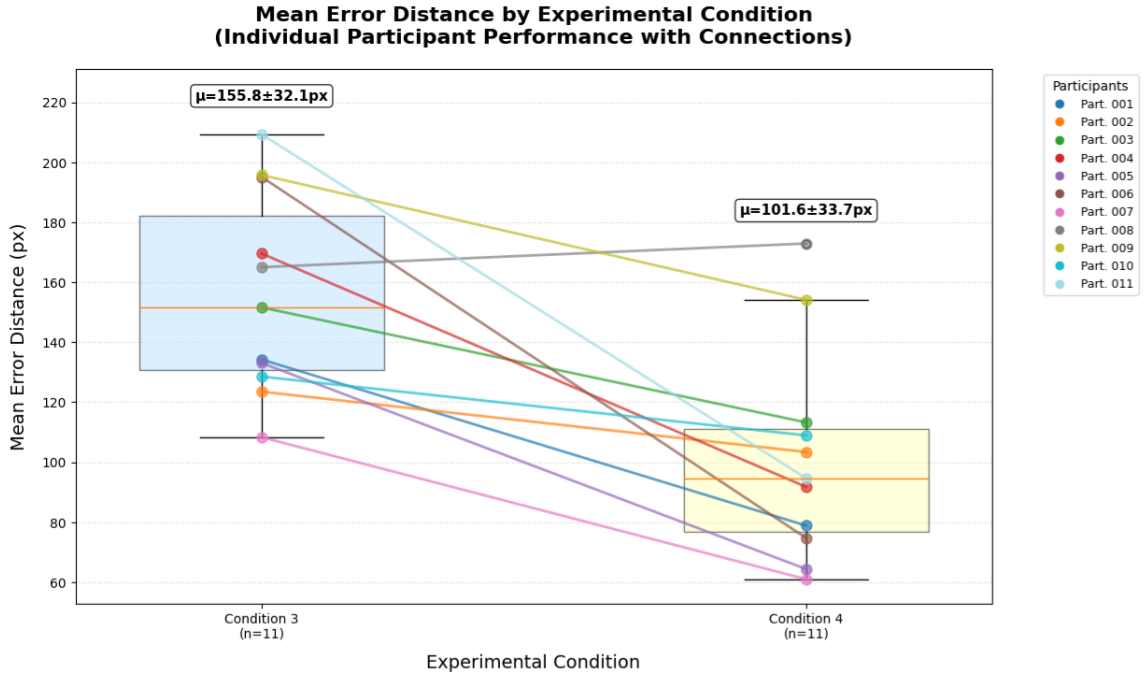

Figure 4.3: Zoomed-in image of the boxplots of all the 11 participants' mean error-distance for each of the 4 testing conditions, focusing on comparing No Vision + Friction Modulation (condition 3) to No Vision + Active Force Feedback (condition 4).

4.2. Tracking Behavior

The overall results revealed clear differences in mean error-distance across the four experimental conditions (Figure 4.1), particularly between visual and non-visual settings. To review the resulting tracking paths for deeper insight participant 007 was selected because his performance consistently demonstrated one of the lowest error levels across all conditions.

4.2.1. Visual Conditions

To provide a clearer view of how these errors manifest, trial path 1 in figure 3.5 from this participant is shown for each experimental condition. As expected for condition 1 (Vision Only) in figure 4.4, the participant tracks the target very accurately, while the mean error-distance remains consistently low throughout the trial, with smooth transitions during direction changes. At the peaks of the movement pattern of the moving target, which indicate a change of moving direction, it is slightly noticeable that the participant's resulting path shows some overshoots, which might be due to unexpected changes in the moving direction the participant cannot predict.

For condition 2 (Vision + Active Force Feedback) in figure 4.5, there are barely any differences compared to the paths in condition 1 (Vision Only). However, it is slightly noticeable the participant initiates movement more quickly and exhibits less overshoot at peaks of the trajectory ($t = 1, 7, 14$) compared to the Vision Only condition. The tactile cues appear to enhance the participant's ability to make finer, more immediate corrections and minimize positional error during rapid direction changes. So, the addition of active force feedback to visual information results in slightly improved tracking precision.

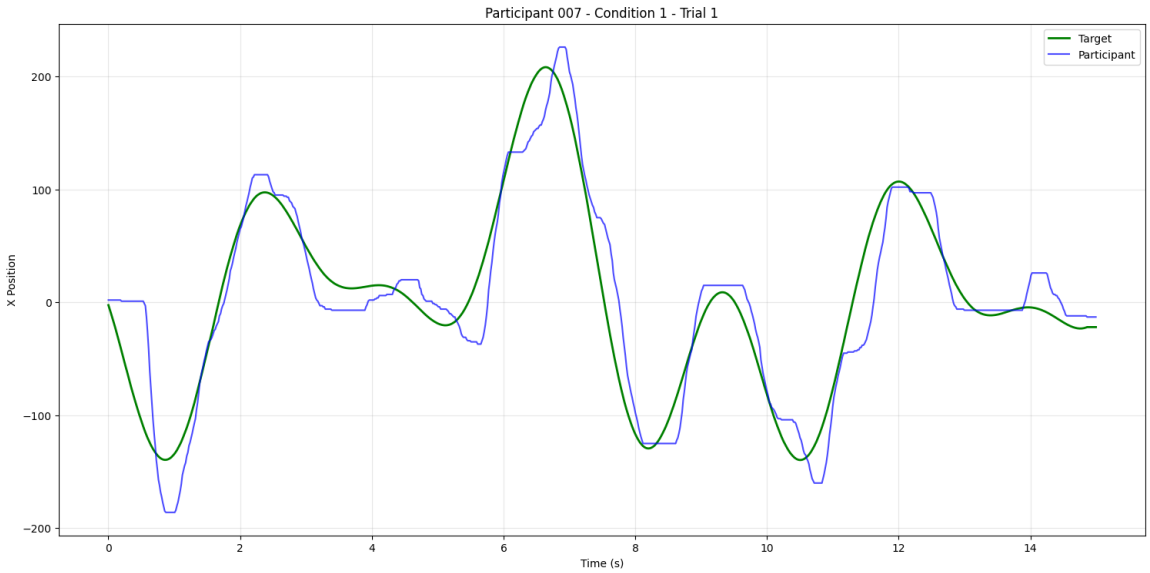

Figure 4.4: Resulting paths generated by the moving target(green) and the participant(blue). These results come from participant 007, condition 1 (Vision Only), movement trial 1.

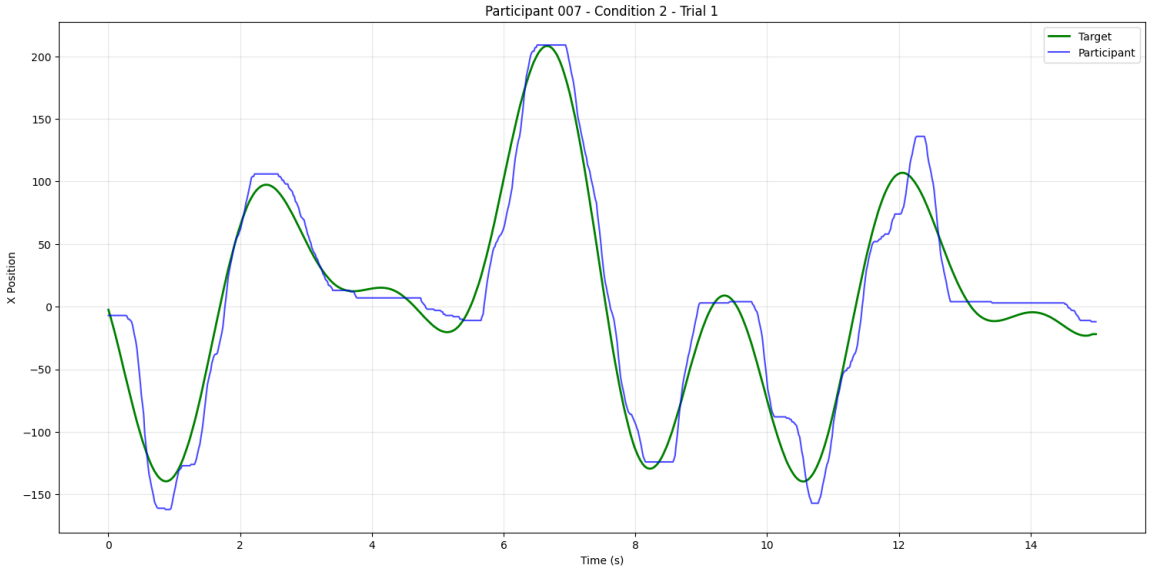

Figure 4.5: Resulting paths generated by the moving target(green) and the participant(blue). These results come from participant 007, condition 2 (Vision + Active Force Feedback), movement trial 1.

4.2.2. Non-Visual Conditions

The result of participant 007 for condition 3 (No Vision + Friction Modulation) in figure 4.6 shows that the participant experiences difficulties in trying to match the movement of the target. This is expected due to significant challenges in tracking performance when visual feedback is removed and only haptic information from friction modulation is available. The path of the participant contains many irregular oscillations, with peak locations and movement directions frequently misaligned with the target path. These mismatches suggest that the participant is actively exploring the surface to locate the moving target rather than accurately tracking it. Even though the participant's path occasionally intersects with the target path, which results in a tactile input from the friction modulation, he still struggles to determine the direction of the target's movement.

In Condition 4 (No Vision + Active Force), where directional lateral force feedback replaces visual information, participant 007 shows improved performance compared to Condition 3 (No Vision + Friction Modulation); see figure 4.7. Although the tracking error remains degraded relative to the visual conditions, the movement path shows more systematic corrections and a clearer overall trajectory than in condition 3 (No Vision + Friction Modulation). This shows that the active force feedback provides useful directional guidance in contrast to friction modulation but cannot yet fully compensate for the absence of visual position information. However, the tracking still shows small occasional directional uncertainties, particularly at a small distance after a change of direction indicated by peaks($t = 7, 9, 14$).

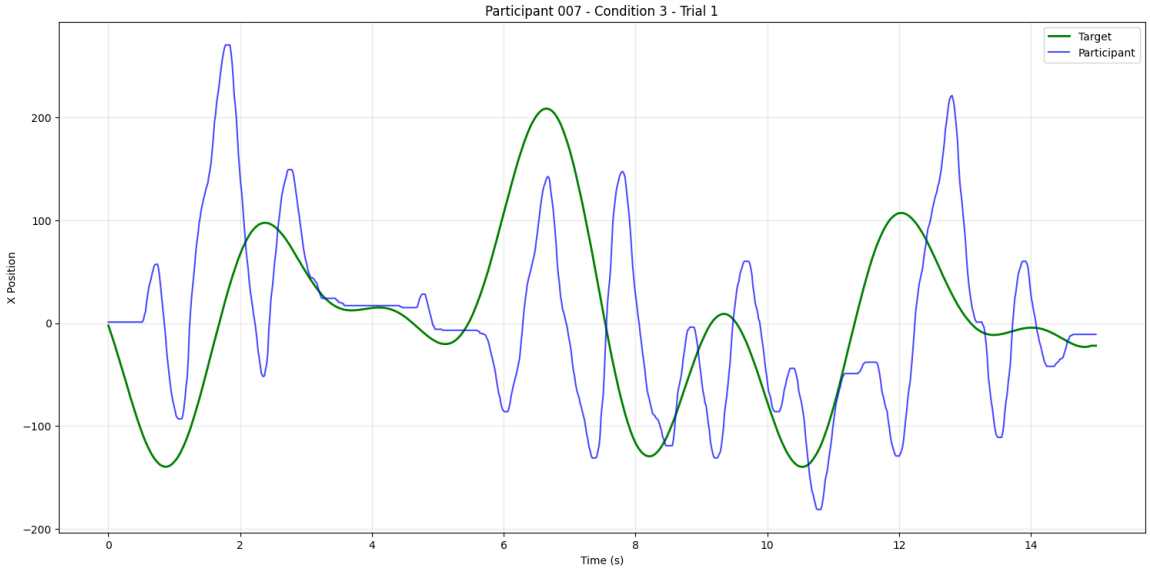

Figure 4.6: Resulting paths generated by the moving target(green) and the participant(blue). These results come from participant 007, condition 3 (No Vision + Friction Modulation), movement trial 1.

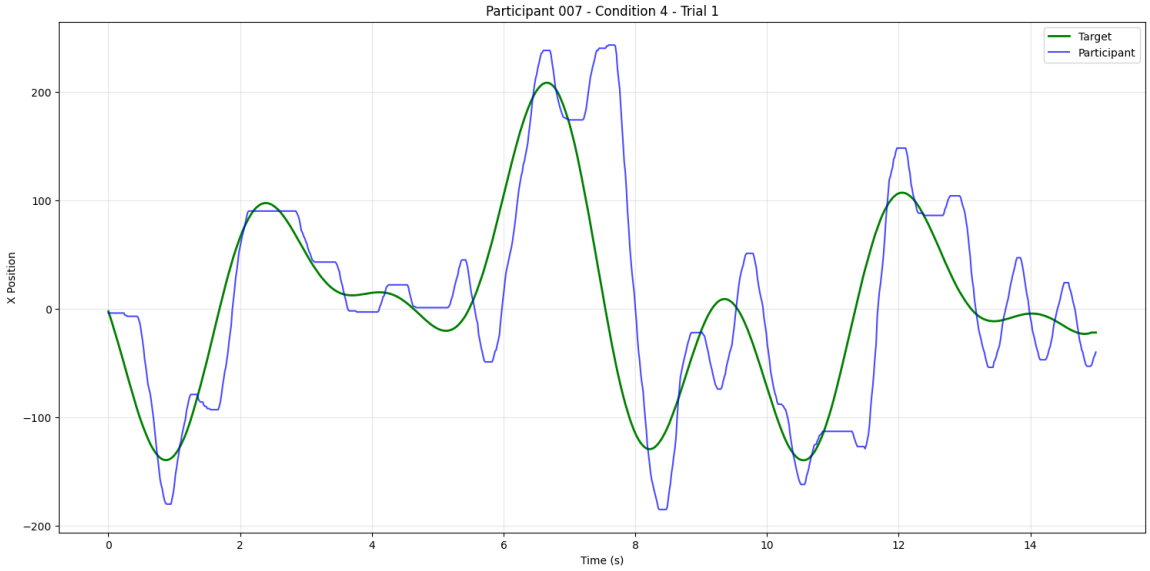

Figure 4.7: Resulting paths generated by the moving target(green) and the participant(blue). These results come from participant 007, condition 4 (No Vision + Active Force Feedback), movement trial 1.

4.3. McRuer Analysis

For the human tracking experiment using the McRuer Crossover Model, a Python script was implemented to perform individual participant analyses for each condition. The collected tracking data include a time array in which, at each timestep, the cursor position, target position, and their corresponding tracking-error were recorded. After pre-processing the participants' tracking data where it resamples to 60 Hz uniform time steps and normalizes positions to center around the screen midpoint, it implements the tracking-error which is the fundamental closed-loop feedback signal. The model converts this error into a velocity command, which is then integrated to yield a predicted cursor position. This cursor position was predicted for each resulting path of the participant across the four experimental conditions: (1) visible target without tactile feedback, (2) visible target with active lateral force feedback, (3) invisible target with friction modulation feedback, and (4) invisible target with active lateral force feedback.

Fitting of the McRuer crossover model parameters was performed jointly across all the five trials per condition by using the Differential Evolution (DE) algorithm implemented in SciPy. Differential evolution is a population-based stochastic optimization method that is particularly effective for nonlinear, multi-parameter problems—such as fitting models, where parameter landscapes often contain multiple local minima [16]. The goal of the optimization is to find the set of parameters [K_p, T_L, T_I, T_n, τ_e] that minimizes the sum of the root mean squared error (RMSE) between the simulated model output (model-predicted cursor position) and the participant's actual cursor trajectory across all trials in a given condition. The optimization function evaluates how well the simulated model reproduces the participant's tracking behavior. This approach offers several advantages for McRuer model fitting, like it avoids becoming trapped in local minima, which is common with gradient-based methods. Also, it can handle noisy or discontinuous objective functions, which may arise from measurement noise in behavioral data. Eventually, this optimization procedure provided a distinct set of parameters for every participant and condition, resulting in 44 identified models. The following bounds for these parameters are shown in table 4.1 below, which are based on plausible estimates from literature [11]. Two boundary sets were used to take into account that people control movement differently depending on whether they can see the target or not. Therefore, the model uses different parameter ranges for visual and non-visual conditions to match these natural differences in human control. Typical human parameters reported in the literature suggest fixed values of approximately $T_n \approx 0.1$ s for neuromuscular lag and $\tau_e \approx 0.2$ s for effective delay [12].

Table 4.1: Boundary interval for the McRuer Crossover Parameters for identifying the participant.

Parameter	**Visual conditions**	**Non-visual conditions**
K_p (Human Gain)	[0.001, 30.0]	[0.001, 10.0]
T_L (Lead time constant)	[0.05, 0.3]	[0.05, 0.15]
T_I (Lag time constant)	[0.01, 0.5]	[0.01, 1.0]
T_n (Neuromuscular time constant)	0.1	0.1
τ_e (Effective time delay constant)	0.2	0.2

After optimizing the model for each individual participant-condition combination, the script visualizes a box-plot of the parameters, which shows distribution of fitted parameters across conditions with individual participant data points colored by participant. This analysis helps understand how control parameters change across different experimental conditions and which parameters are most varying between participants. With these optimized parameters the McRuer model attempts to reproduce the general tracking behavior of participants across all conditions, each with its own fitting errors (RMSE), measuring the difficulty of identifying their control behavior. The parameters fitted to each participant [K_p, T_L, T_I] revealed clear trends that reflect the influence of visual and tactile feedback on control performance. Although it is important to note that the model's fit was not optimal across all experimental conditions—particularly those without vision—its application offers a valuable, measurable perspective on the adaptability in human control.

4.3.1. Model Fitting Error

Before the optimized fitted McRuer Models are evaluated for their specific parameters it is important to have an indication how well these crossover models performed in identifying the participants' control behavior. The McRuer crossover model demonstrated varying levels of fitting performance across the four experimental conditions in figure 4.8, which shows that participant 007 is a good example, due to having the lowest fitting error in conditions 1 (Vision Only) and 3 (No Vision + Friction Modulation). To give a more insightful explanation about the varying fitting error among the four experimental conditions, a trial path is shown for each of these experimental condition from participant 007. The model achieved its lowest sum of fitting error in conditions 1 (Vision Only) and 2 (Vision + Active Force Feedback), with only minimal difference between these visual conditions. In condition 1 (Vision Only) the sum all the fitting error has a mean value of 490 pixels, while for condition 2 (Vision + Active Force Feedback) the mean of the total fitting error is at 517 pixels. This performance indicates that the McRuer model manages to effectively capture the human control strategy when visual feedback is available, regardless of the addition of tactile cues in Condition 2 (Vision + Active Force Feedback). This is visible in figure 4.9 and 4.10 where the generated model (red) path does not perfectly match with the participant path (blue), however it can capture the behavior of the participant by closely oscillating at the same time. In the legend of the top-left corner the parameters are displayed for the optimized McRuer model for that specific condition including the sum RMSE of all the fitted model paths.

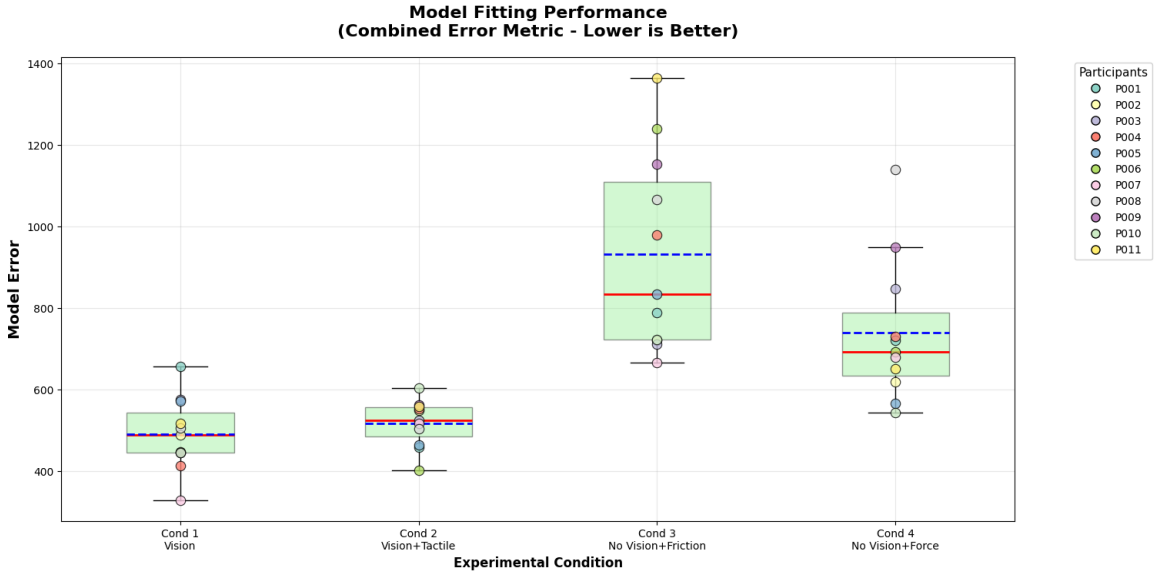

Figure 4.8: Boxplots of all the model fitting error values of each participant-condition combination for the 4 testing conditions. Each condition shows a boxplot of the fitting error values of the optimized McRuer crossover model, which measures how precise control behavior is captured. Red line: Median. Blue line: Mean.

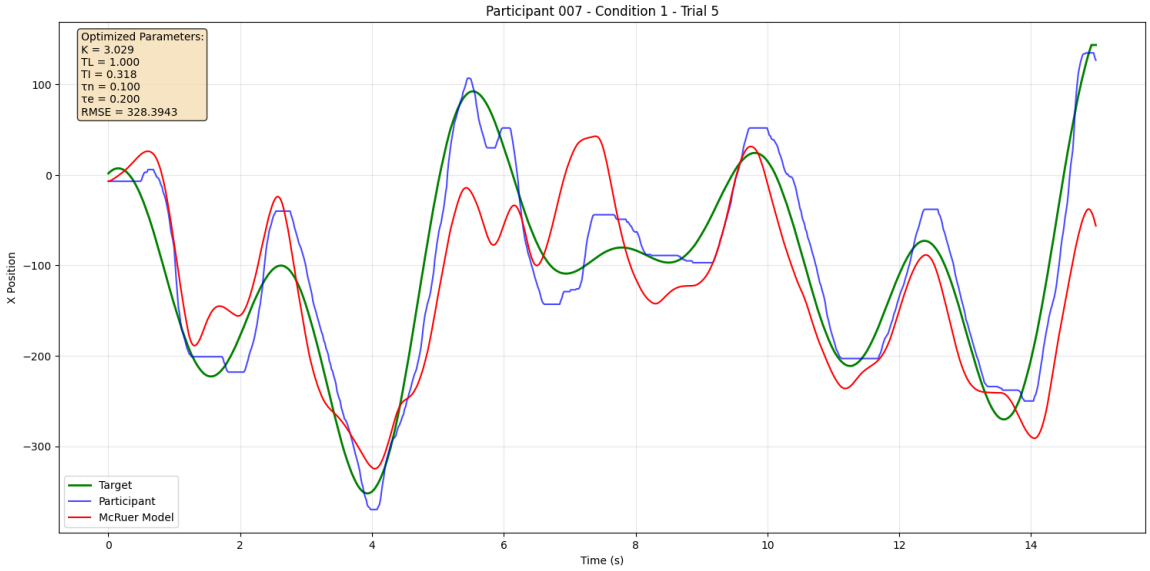

Figure 4.9: Resulting paths generated by the moving target(green), the participant(blue) and the McRuer crossover model(red). Top-right legend displays the optimized parameters for the fitted McRuer model. These results come from participant 007, condition 1 (Vision Only) and movement trial 5.

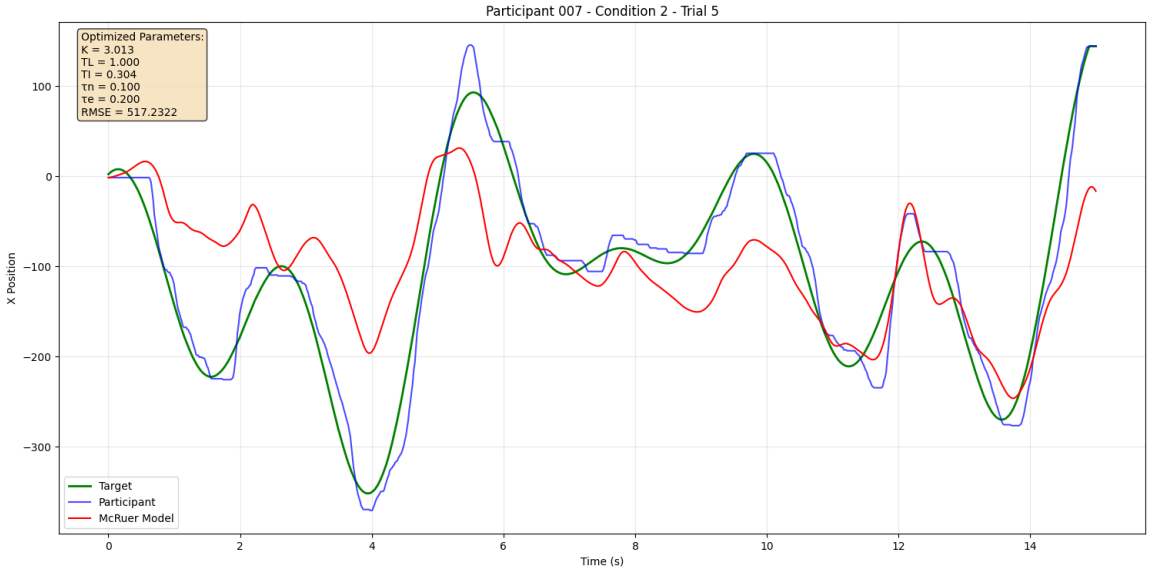

Figure 4.10: Resulting paths generated by the moving target(green), the participant(blue) and the McRuer crossover model(red). Top-right legend displays the optimized parameters for the fitted McRuer model. These results come from participant 007 during condition 2 (Vision + Active Force Feedback) and movement trial 5.

Unfortunately, a significant increase in fitting errors was observed in Condition 3 (No Vision + Friction Modulation), with an average sum of 931 pixels, representing the poorest model performance across all conditions. This deteriorating fit (increasing RMSE) in Condition 3 (No Vision + Friction Modulation) is due to participants using irregular corrections because they only feel bumps and McRuer's continuous feedback model captures average behavior but misses discrete corrections. Figure 4.11 shows the result of participant 007 for condition 3 (No Vision + Friction Modulation) and clearly shows that the participant experiences difficulties in trying to match the movement of the target. The large amount of irregular oscillations that mismatch the moving target make it difficult for the model to identify a certain behavior, especially when the participant does not know where to look, therefore with no visual feedback, the human behavior becomes more unpredictable, making it almost impossible for the model to identify an average behavior.

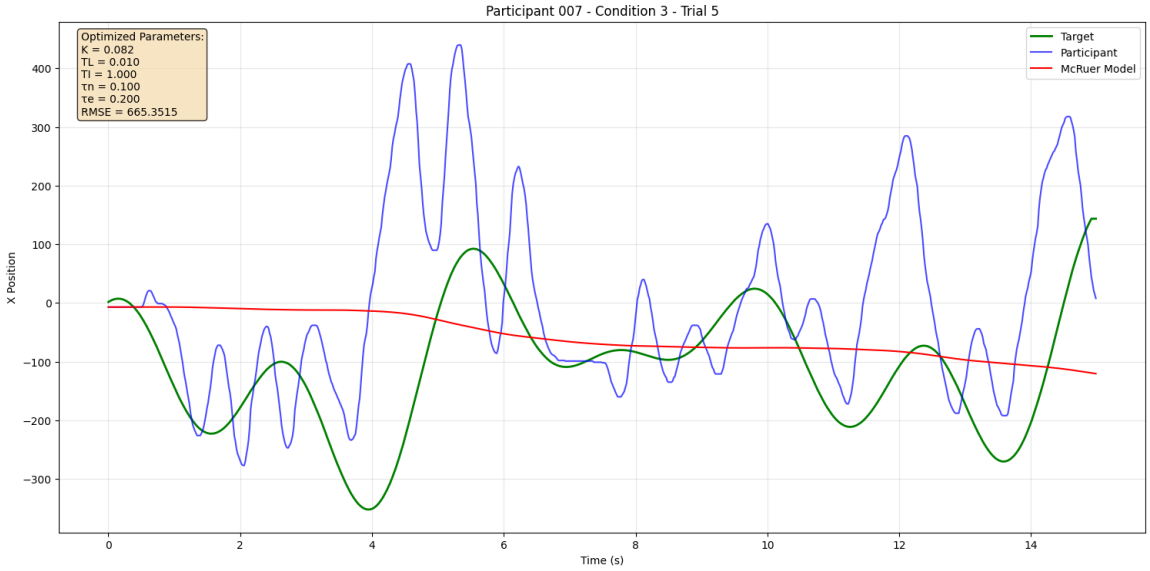

Figure 4.11: Resulting paths generated by the moving target(green), the participant(blue) and the McRuer crossover model(red). Top-right legend displays the optimized parameters for the fitted McRuer model. These results come from participant 007 during condition 3 (No Vision + Friction Modulation) and movement trial 5.

Condition 4 (No Vision + Active Force Feedback) showed moderate fitting performance, with lower fitting errors compared to Condition 3 (No Vision + Friction Modulation) but still relatively high compared to the two visual conditions, with an average sum of 740 pixels as fitting error. This improvement suggests that active lateral force feedback provides more intuitive directional information than friction modulation, enabling participants to develop control strategies that help more to approximate the McRuer crossover model, see figure 4.12. However, the higher fitting errors compared to the visual conditions indicate that even active force in non-visual conditions have different tracking strategies than the visible tracking conditions.

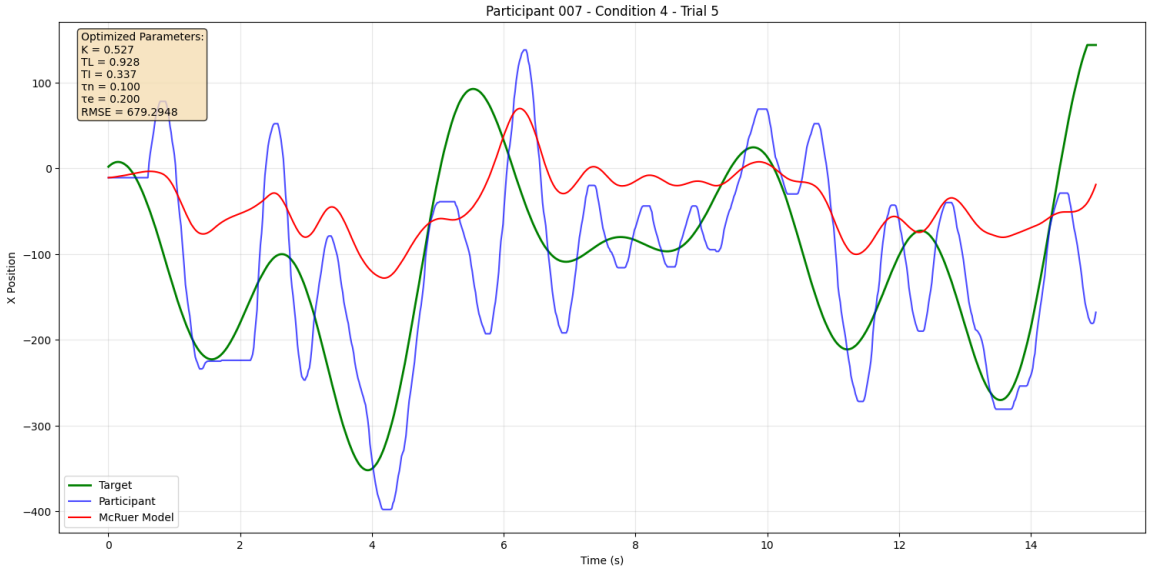

Figure 4.12: Resulting paths generated by the moving target(green), the participant(blue) and the McRuer crossover model(red). Top-right legend displays the optimized parameters for the fitted McRuer model. These results come from participant 007 during condition 4 (No Vision + Active Force Feedback) and movement trial 5.

Overall, in conditions 1 (Vision Only) and 2 (Vision + Active Force Feedback) the participants can see the target, but in conditions 3 (No Vision + Friction Modulation) and 4 (No Vision + Active Force Feedback) they cannot, while the model assumes they can, which means the model is using information the participants do not have access to. Consequently, the resulting model parameters are not a reliable reflection of the human's actual control strategy in those non-visual conditions. The results show that the McRuer crossover model can describe tracking behavior in visual conditions, however, it may need adjustments or even implement other alternative identification models to better capture human control strategies when visual feedback is absent.

4.3.2. Parameter Optimization

Crossover Gain

Figure 4.13 plots the average control gain (K_p) for each condition in the expected descending order of task difficulty: highest for Condition 2 (Vision + Active Force Feedback), followed by Condition 1 (Vision Only), Condition 4 (No Vision + Active Force Feedback), and lowest for Condition 3 (No Vision + Friction Modulation). However, it is crucial to note that the McRuer model fundamentally failed to correctly identify control behavior in Conditions 3 and 4, as its optimization assumes that without visual feedback the participants have sufficient information with haptic feedback only; consequently, the resulting parameters for these non-visual conditions are not reliable indicators of the actual control strategy.

In the visual conditions (see figure 4.14), the model captured the control gains of each individual participant, connected by colored lines, showed mixed responses to the addition of force feedback in Condition 2 (Vision + Active Force Feedback): some increased, some decreased, and others remained similar to Condition 1 (Vision Only). According to the McRuer model, this individual variation resulted in only a negligible mean increase in K_p (0.1), indicating that active lateral force feedback provided barely any improvement to responsiveness when the target was visible.

Unfortunately, for the non-visual conditions (see figure 4.15), the identified parameters reflect an unreliable fit. While fitted gains were typically lowest for Condition 3 (No Vision + Friction Modulation) and showed a slight mean increase (0.07) for Condition 4 (No Vision + Active Force Feedback) with active force feedback, this minimal improvement is an artifact of the failed model identification. The core finding is that the McRuer model is ill-suited to describe behavior when participants cannot see the target, making a clear interpretation of K_p trends in these conditions complicated.

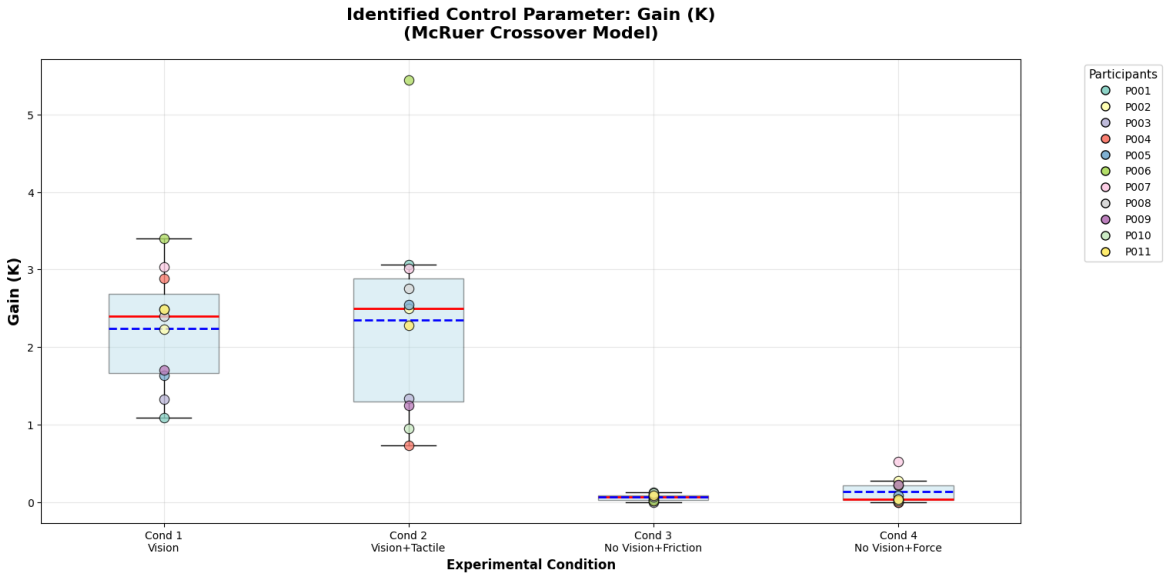

Figure 4.13: Boxplots of all the K_p parameter values of each participant for the 4 testing conditions. Each condition shows a boxplot of the K_p values of the optimized McRuer crossover model, which identifies their control behavior. Red line: Median. Blue line: Mean.

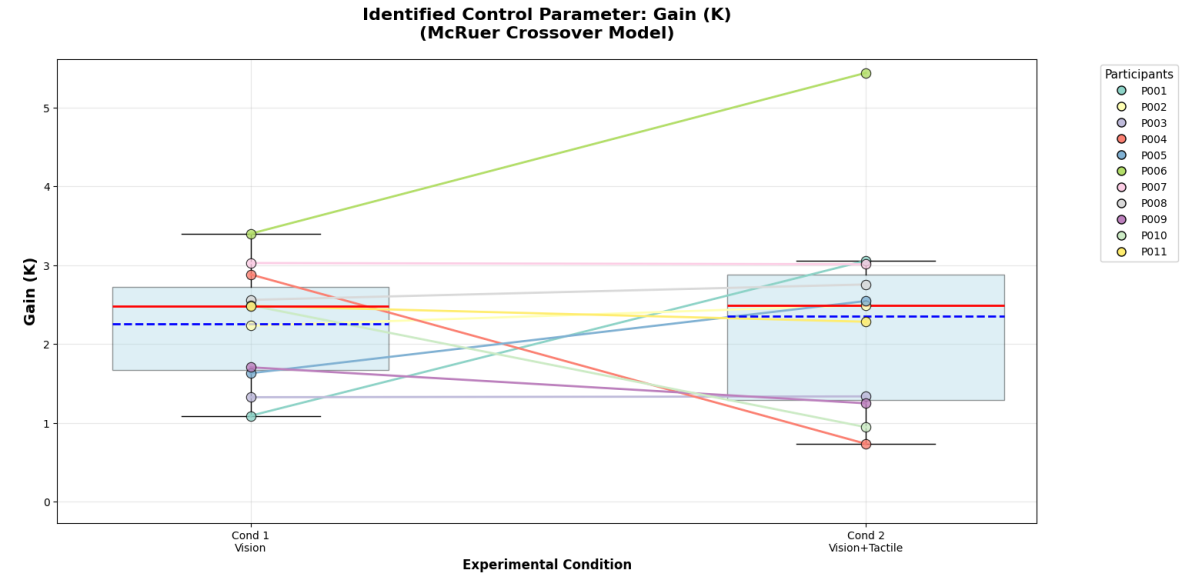

Figure 4.14: Zoomed-in view of the boxplots of parameter values K_p of all optimized McRuer models for each participant-condition combination, focusing on comparing Vision Only (condition 1) to Vision + Active Force Feedback (condition 2). Red line: Median. Blue line: Mean.

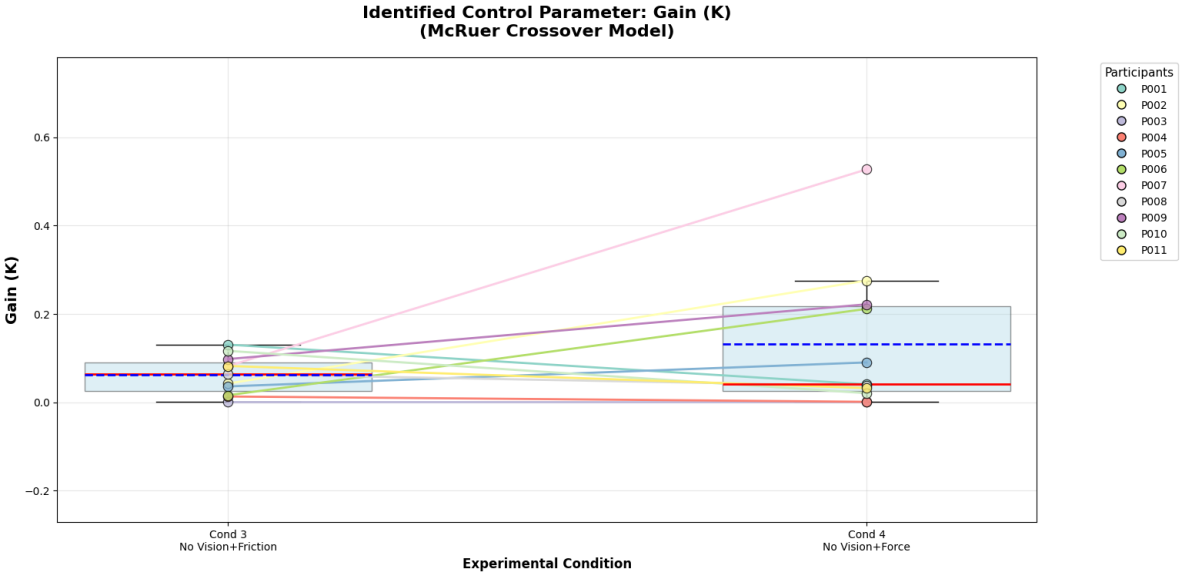

Figure 4.15: Zoomed-in view of the boxplots of parameter values K_p of all optimized McRuer models for each participant-condition combination, focusing on comparing No Vision + Friction Modulation (condition 3) to No Vision + Active Force Feedback (condition 4).

Lead Time Constant

The optimized lead time constants (T_L) presented in Figure 4.16 demonstrate plausible values that reflect varying degrees of anticipatory control across the experimental conditions. The T_L values fall within the expected range, representing realistic human prediction horizons for dynamic tracking tasks. The expected systematic ordering of mean (blue line) T_L values, which is highest in Condition 2, followed by Condition 1, then Conditions 3 and 4, reveals how different forms of tactile feedback conditions influence participants' predictive capabilities.

The slight increase of the mean of the optimized T_L values in Condition 2 (Vision + Active Force) compared to Condition 1 (Vision Only) indicates that the addition of active lateral force feedback slightly enhances participants' ability to anticipate target motion. This effect suggests that combining visual with tactile information enables more confident prediction of trajectory patterns. The remarkable lower T_L values in non-visual Conditions 3 and 4 confirm again the critical factor of visual feedback in enabling predictive control, with participants reverting to primarily exploratory strategies when vision is unavailable. Notably, the minimal difference in T_L between Conditions 3 and 4 indicates that neither friction modulation nor active force feedback can fully give the same predictive capabilities enabled by vision. But then it must be taken into account that the model was not able to fully grasp the continuous behavior for the non-visual conditions.

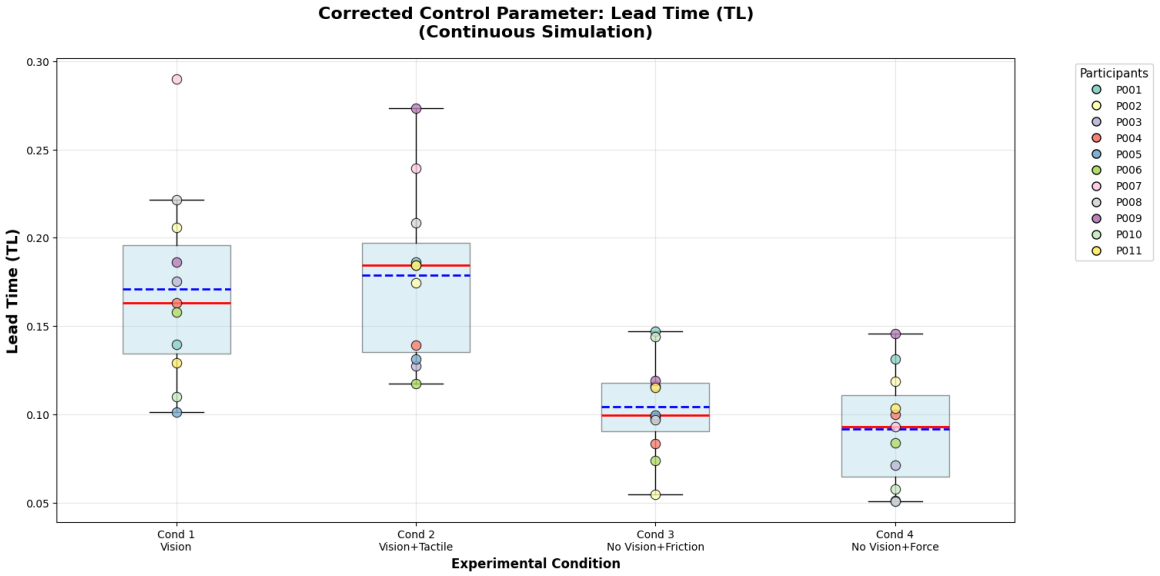

Figure 4.16: Boxplots of all the T_L parameter values of each participant for the 4 testing conditions. Each condition shows a boxplot of the T_L values of the optimized McRuer crossover model, which identifies their control behavior. Red line: Median. Blue line: Mean.

Lag Time Constant

The optimized lag time constants (T_I) presented in Figure 4.17 demonstrate how different sensory feedback modalities influence participants' motor response smoothing strategies. The descending order of the mean optimized T_I values (blue line), which is highest in Condition 4 (No Vision + Active Force), followed by Condition 3 (No Vision + Friction), then Conditions 2 and 1, reveals that their movements became slower and smoother when they were unable to see the target to prevent irregular corrections and maintain stability. The minimal difference in T_I between Conditions 1 and 2 (Vision conditions) suggests that while active force feedback enhances tracking precision, it does not substantially alter the basic smoothing strategy when visual information is available.

This pattern demonstrates that participants adapt their control strategies systematically based on available sensory information, with visual conditions enabling more responsive control compared to non-visual conditions. But then again, capturing the perfect control behavior for these non-visual conditions is quite complicated.

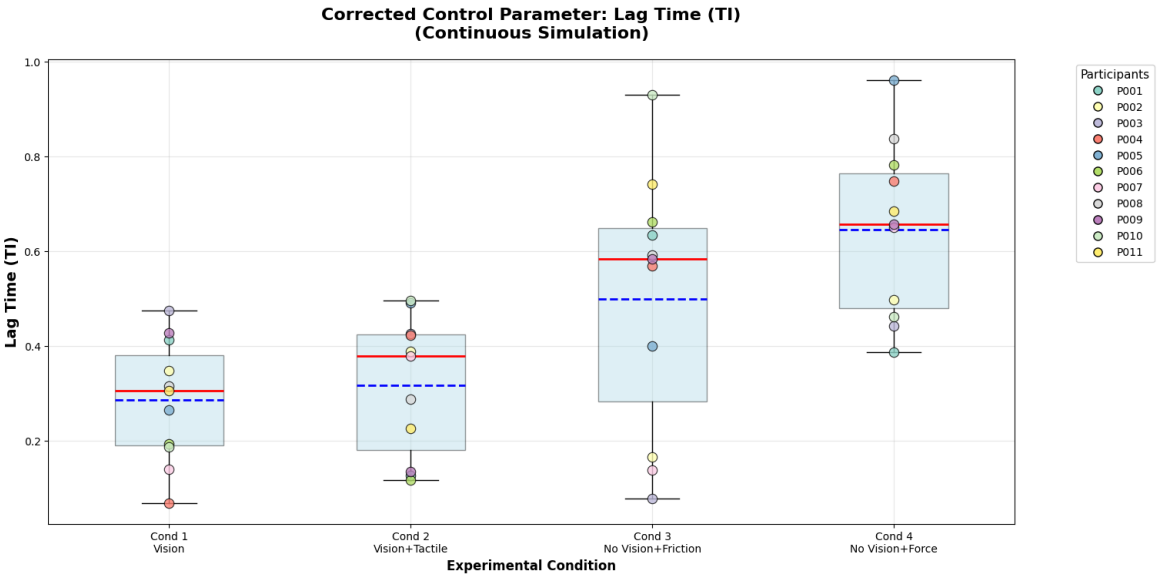

Figure 4.17: Boxplots of all the T_I parameter values of each participant for the 4 testing conditions. Each condition shows a boxplot of the T_I values of the optimized McRuer crossover model, which identifies their control behavior. Red line: Median. Blue line: Mean.

5

Discussion & Conclusion

5.1. Discussion

This section discusses the experimental findings and practical limitations encountered during the user study of surface haptic feedback using the Ultraloop. It focuses on interpreting the results of the target-following experiments conducted with the Ultraloop, highlighting the behavioral differences between friction modulation and active lateral force feedback. Then, it also discusses key limitations and their implications for future research.

5.1.1. Interpretation of Results

The analysis of the mean error-distance between the participant's finger and the moving target demonstrates the increasing performance of active lateral force feedback. In both visual and non-visual scenarios, this form of feedback led to the lowest tracking errors. Condition 2 (Vision + Active Force) resulted in a significant reduction in mean error-distance compared to Condition 1 (Vision Only). This indicates that the active force feedback provided by the Ultraloop is not redundant when vision is available; instead it acts as an extra support that enhances precision.

For the non-visual conditions, Condition 4 (No Vision + Active Force Feedback) showed much improvement compared to Condition 3 (No Vision + Friction Modulation). Friction modulation, which provides only discrete bump cues, proved to be an ineffective tactile guide for a continuous tracking task, resulting in high oscillatory errors. This aligns with observed participant behavior, where users frequently choose to actively explore the surface to detect these cues to locate the target, which comes with increasing delays and errors, especially in the absence of vision.

In contrast, the continuous, directional push/pull of the active lateral force feedback provided participants with a remarkably stable connection with the invisible target. This form of feedback proves to be more effective by replacing the missing visual information with a continuous tactile signal that expresses direction of the targeted position. This finding also addresses the limitation of traditional touchscreens stated in the introduction, stating their heavy reliance on visual attention, by demonstrating that programmable lateral forces can perhaps replace vision for dynamic tasks.

For the McRuer analysis during the model fitting process, significant challenges emerged in parameter optimization, particularly for the non-visual conditions 3 (No Vision + Friction Modulation) and 4 (No Vision + Active Force Feedback). For these conditions, the model showed significant high fitting errors, meaning that it was unable to identify a consistent control behavior from the participants. While active force feedback improves overall tracking performance, it does not significantly enhance predictive control beyond what visual information alone provides. This suggests that trajectory anticipation primarily relies on visual processing pathways, with haptic feedback serving as support for reactive error correction rather than enabling true predictive control capabilities.

5.1.2. Limitations and Future Work

Although the findings demonstrate the potential of active lateral force feedback for improving haptic interaction, several practical and methodological limitations should be noted. For example, each trial was relatively short due to the heat building up on the Ultraloop surface, which may have affected tactile intensity over time. Longer trials could provide more insight into how users adapt and develop behavior models of the device dynamics.

Also, some irregularities in the recorded position data, likely caused by the Neonode sensor's sampling limitations or electrical interference, occasionally required restarting the system. These hardware constraints may have introduced minor inconsistencies in the data. Additionally, the experiments were conducted on the original Ultraloop device, but a newer version was available, the Flatloop; see Appendix D. This device was created during the duration of this thesis but not yet stable enough for the experiments of this study. Future research using this improved hardware could perhaps offer more consistent force outputs and allow for a broader range of feedback conditions.

The predicted cursor paths from the optimized McRuer model parameters visually confirm its core limitations. While it generates plausible trajectories for visual tracking, its predictions fail for non-visual conditions. The poor fit is therefore a direct result of an invalid model structure, not merely an optimization shortcoming for non-visual conditions. This highlights a limitation that the model's structure cannot capture the full complexity of human adaptive control for non-visual condition with multiple paths.

Instead of forcing a single model structure, like McRuer onto all resulting data, a more robust approach would be to develop a framework for multi-model identification. Future studies could involve machine learning or statistical criteria to select the most appropriate model structure for each trial or condition based on the available sensory information and observed participant behavior.

5.2. Conclusion

The goal of this research was to investigate the effect of the Ultraloop's lateral force feedback on user performance in a dynamic point-following-task, specifically focusing on tracking error and the adaptation of human control dynamics. The hypothesis stated that active lateral force feedback would improve performance by reducing tracking errors and enhancing control dynamics compared to non-feedback or alternative feedback conditions. This research shows that the results support the hypothesis while also giving insights into how human participants adapt their control strategy according to each experimental condition, with a clear distinction between the effects of friction modulation and active lateral force feedback on user performance. Active lateral force feedback functioned as a supportive cue in visual conditions, lowering the average tracking error by 24.1%, and served as a highly effective sensory substitute in non-visual conditions, where it outperformed friction modulation by reducing the average tracking error by 34.8%.

Friction modulation feedback does not express the direction of the target; instead, it merely signals when the fingertip crosses a particular target point by creating a localized change in surface resistance. Consequently, this form of feedback supports only detection but not continuous guidance, which limits its application for non-visual dynamics.

In contrast, active lateral force feedback provides a continuous directional cue that directly guides the user's finger towards the moving target. The consistent reduction in mean error distance under active lateral force feedback conditions indicates that participants were able to rely on these cues for real-time correction. The improvement noticeable in non-visual conditions suggests that active lateral forces can serve as effective compensatory feedback in non-visual conditions.

In conclusion, these findings confirm that the Ultraloop's lateral force feedback provides an effective tactile mechanism for minimizing tracking error in dynamic environments. It significantly improves performance as a supporting cue when vision is available and serves as a potential sensory substitute when vision is absent, significantly outperforming friction-based feedback(friction modulation). All in all, the demonstrated effectiveness of active lateral force feedback shows promising possibilities for its application in various scenarios, including assistive technologies and sensory substitution situations.

References

[1] Annie Rydström et al. "Multifunctional systems in vehicles: a usability evaluation". In: *International Cyberspace Conference on Ergonomics: 15/09/2005-15/10/2005*. International Ergonomics Association. 2005, pp. 768–775.

[2] Gary E Burnett and J Mark Porter. "Ubiquitous computing within cars: designing controls for non-visual use". In: *International Journal of Human-Computer Studies* 55.4 (2001), pp. 521–531.

[3] T.J. Brans. "Pseudo Potential Fields on Surface-Haptic Touchscreens using Friction Modulation". MA thesis. Technical University Delft, 2022.

[4] Zhaochong Cai and Michaël Wiertlewski. "Viscous Damping Displayed by Surface Haptics Improves Touchscreen Interactions". In: *International Conference on Human Haptic Sensing and Touch Enabled Computer Applications*. Springer. 2024, pp. 352–364.

[5] Stanislav Aranovskiy et al. "A switched dynamic model for pointing tasks with a computer mouse". In: *Asian Journal of Control* 22.4 (2020), pp. 1387–1400.

[6] Zhaochong Cai and Michaël Wiertlewski. "Ultraloop: Active lateral force feedback using resonant traveling waves". In: *IEEE Transactions on Haptics* 16.4 (2023), pp. 652–657.

[7] Zhaochong Cai, David Abbink, and Michaël Wiertlewski. "Attracting Fingers with Waves: Potential Fields Using Active Lateral Forces Enhance Touch Interactions". In: *Proceedings of the 2025 CHI Conference on Human Factors in Computing Systems*. 2025, pp. 1–13.

[8] Jörg Müller, Antti Oulasvirta, and Roderick Murray-Smith. "Control theoretic models of pointing". In: *ACM Transactions on Computer-Human Interaction (TOCHI)* 24.4 (2017), pp. 1–36.

[9] Paul M Fitts. "The information capacity of the human motor system in controlling the amplitude of movement." In: *Journal of experimental psychology* 47.6 (1954), p. 381.

[10] PETER THOMPSON and DUANE MCRUER. "Comparison of the human optimal control and crossover models". In: *Guidance, Navigation and Control Conference*. 1988, p. 4183.

[11] Duane T McRuer and Henry R Jex. "A review of quasi-linear pilot models". In: *IEEE transactions on human factors in electronics* 3 (2006), pp. 231–249.

[12] Francesca Roncolini, Giuseppe Quaranta, et al. "Virtual pilot: a review of the human pilot's mathematical modeling techniques". In: *Aerospace Europe Conference 2023-Joint 10th EUCASS-9th CEAS Conference*. 2023, pp. 1–14.

[13] Duane T McRuer and Ezra S Krendel. *Mathematical models of human pilot behavior*. Tech. rep. 1974.

[14] Tibor Kimpian and Fulop Augusztinovicz. "Multiphase multisine signals–Theory and practice". In: *Proceedings of ISMA2016 including USD2016, International Conference on Noise and Vibration Engineering*. 2016, pp. 19–21.

[15] Yan Song et al. "Performance evaluation metrics and approaches for target tracking: A survey". In: *Sensors* 22.3 (2022), p. 793.

[16] Wu Deng et al. "An improved differential evolution algorithm and its application in optimization problem." In: *Soft Computing-A Fusion of Foundations, Methodologies & Applications* 25.7 (2021).

[17] Laura Winfield et al. "T-pad: Tactile pattern display through variable friction reduction". In: *Second Joint EuroHaptics Conference and Symposium on Haptic Interfaces for Virtual Environment and Teleoperator Systems (WHC'07)*. IEEE. 2007, pp. 421–426.

[18] Heng Xu, Michael A Peshkin, and J Edward Colgate. "UltraShiver: Lateral force feedback on a bare fingertip via ultrasonic oscillation and electroadhesion". In: *IEEE transactions on haptics* 12.4 (2019), pp. 497–507.

[19] Joseph Mullenbach, Michael Peshkin, and J Edward Colgate. “eShiver: Lateral force feedback on fingertips through oscillatory motion of an electroadhesive surface”. In: *IEEE transactions on haptics* 10.3 (2016), pp. 358–370.

[20] Heng Xu, Michael A Peshkin, and J Edward Colgate. “SwitchPaD: Active lateral force feedback over a large area based on switching resonant modes”. In: *Haptics: Science, Technology, Applications: 12th International Conference, EuroHaptics 2020, Leiden, The Netherlands, September 6–9, 2020, Proceedings 12*. Springer. 2020, pp. 217–225.

[21] Xiaowei Dai, J Edward Colgate, and Michael A Peshkin. “LateralPaD: A surface-haptic device that produces lateral forces on a bare finger”. In: *2012 IEEE Haptics Symposium (HAPTICS)*. IEEE. 2012, pp. 7–14.

A

Appendix

Table A.1: Examples of Active Tactile Surface Devices

Device Name	Type of Haptic Feedback	Purpose / Application
T-PaD [17]	Ultrasonic vibration to modulate shear forces	Creating virtual textures and guiding finger motion
Ultraloop [6]	Ultrasonic vibration for traveling wave-based lateral force actuation	Active lateral force feedback to enhance touch interaction by dynamically guiding finger motion
UltraShiver [18]	Resonant ultrasonic vibration and electroadhesion	Delivers subtle, continuous lateral forces for tactile illusions
eShiver [19]	Electroadhesion-based asymmetric friction	Rendering directional friction and force feedback on surfaces
SwitchPad [20]	In-plane ultrasonic oscillation and out-of-plane electroadhesion	Provides wide-area tactile feedback for immersive interactive surfaces
LateralPad [21]	Ultrasonic vibration in both normal and lateral direction	Generating lateral force feedback on a finger touching a glass

A.1. Results Participants

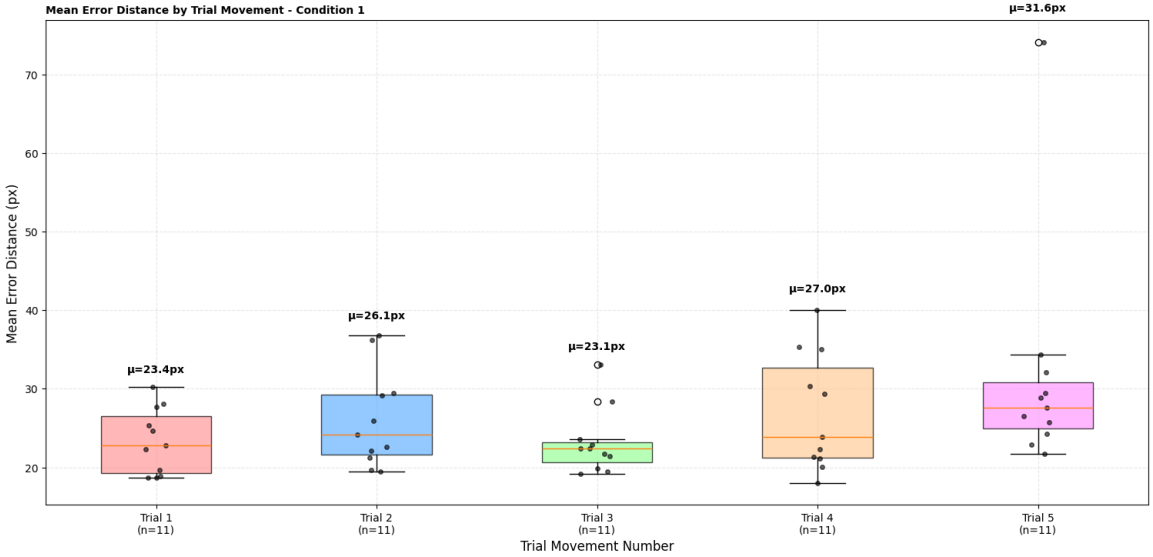

Figure A.1: The boxplot of all the 11 participants their mean error-distance for each of the 5 movement trials for condition 1: Vision Only.

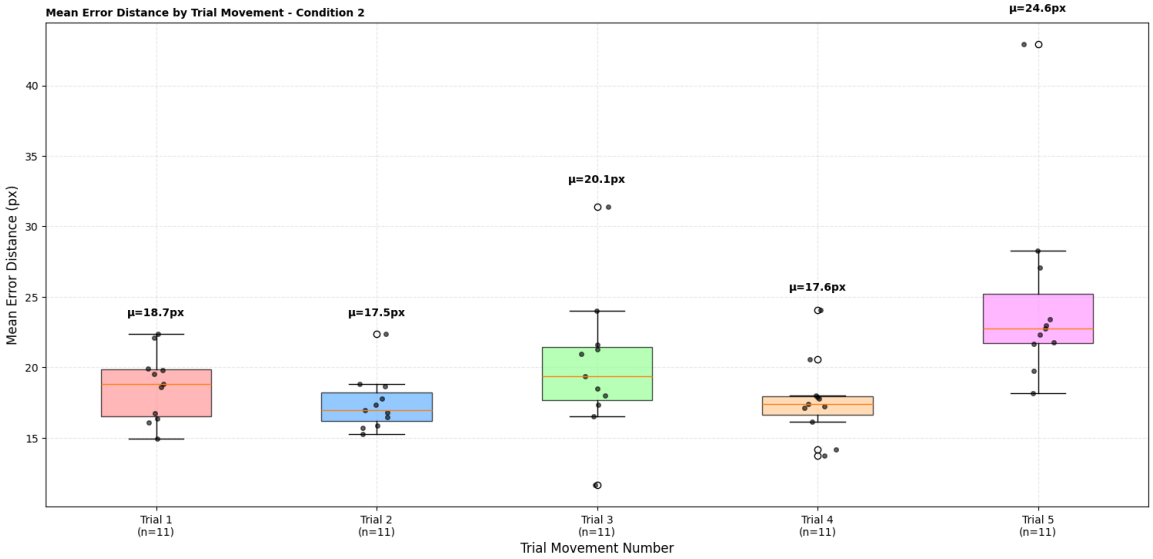

Figure A.2: The boxplot of all the 11 participants their mean error-distance for each of the 5 movement trials for condition 2: Vision + Active Lateral Force.

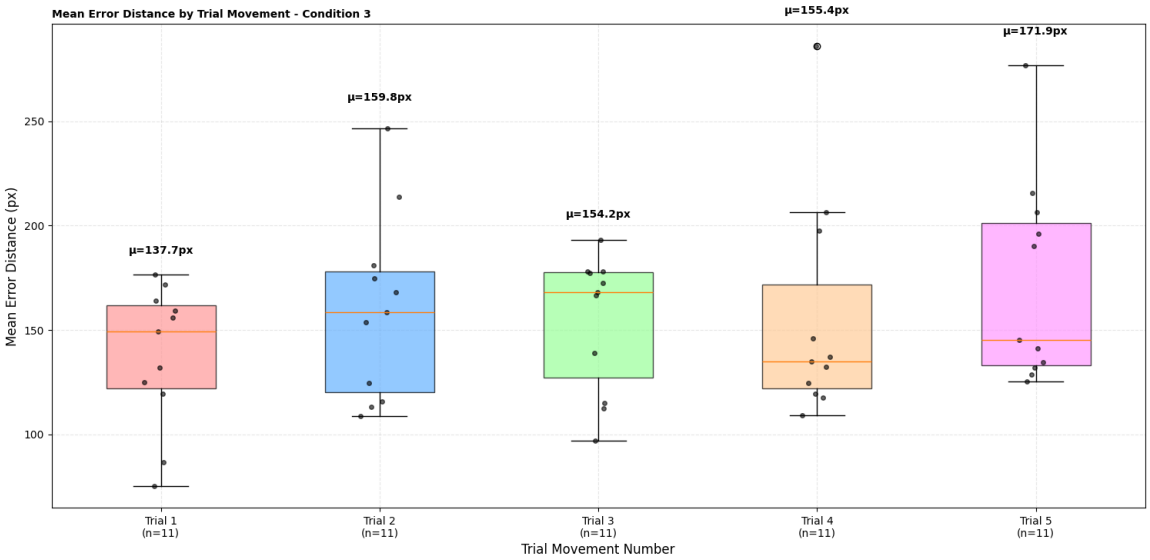

Figure A.3: The boxplot of all the 11 participants their mean error-distance for each of the 5 movement trials for condition 3: No Vision + Friction Modulation.

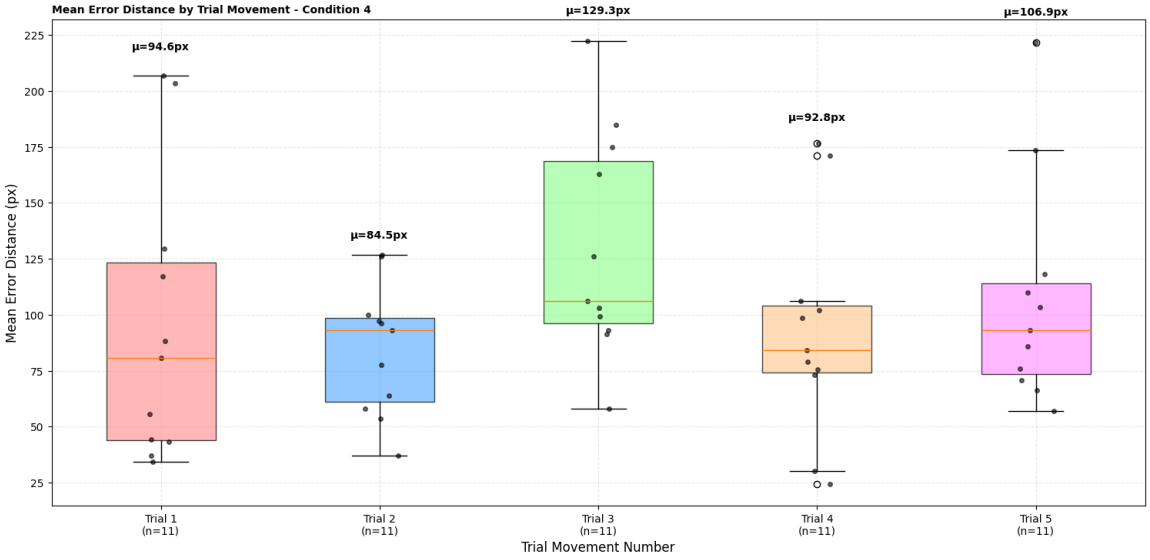

Figure A.4: The boxplot of all the 11 participants their mean error-distance for each of the 5 movement trials for condition 4: No Vision + Active Lateral Force.

B

Appendix - McRuer Analysis

B.1. McRuer Analysis Results

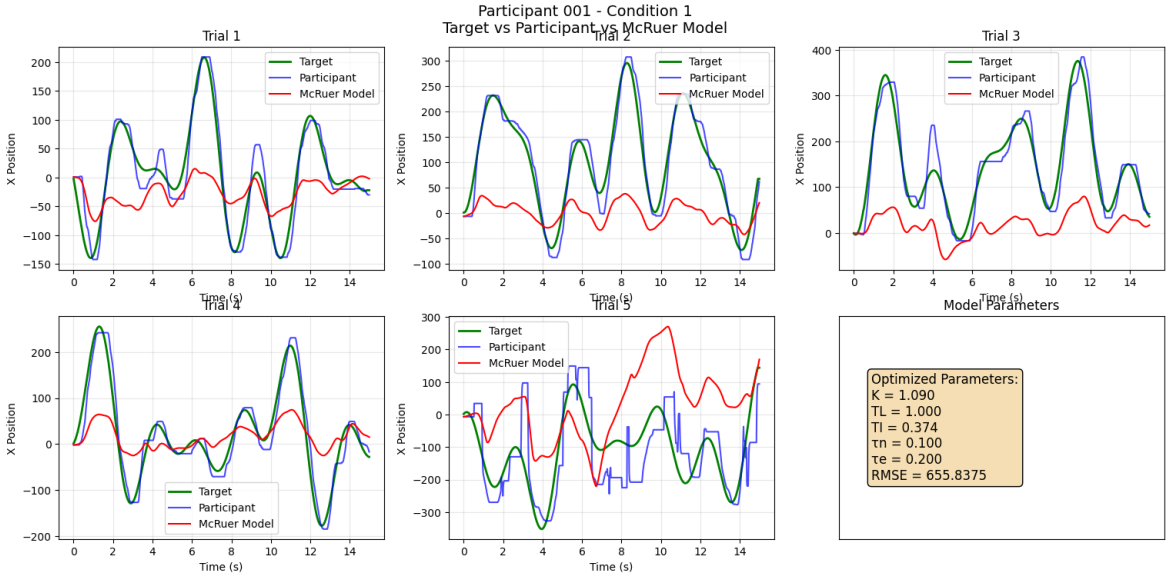

Figure B.1: Experimental results of participant 001, condition 1. Legend bottom-right displaying the optimized McRuer model parameters for generating the model path trying to identify the control behavior for this participant and condition. Green line: Target path. Blue line: Participant path. Red line: Model path.

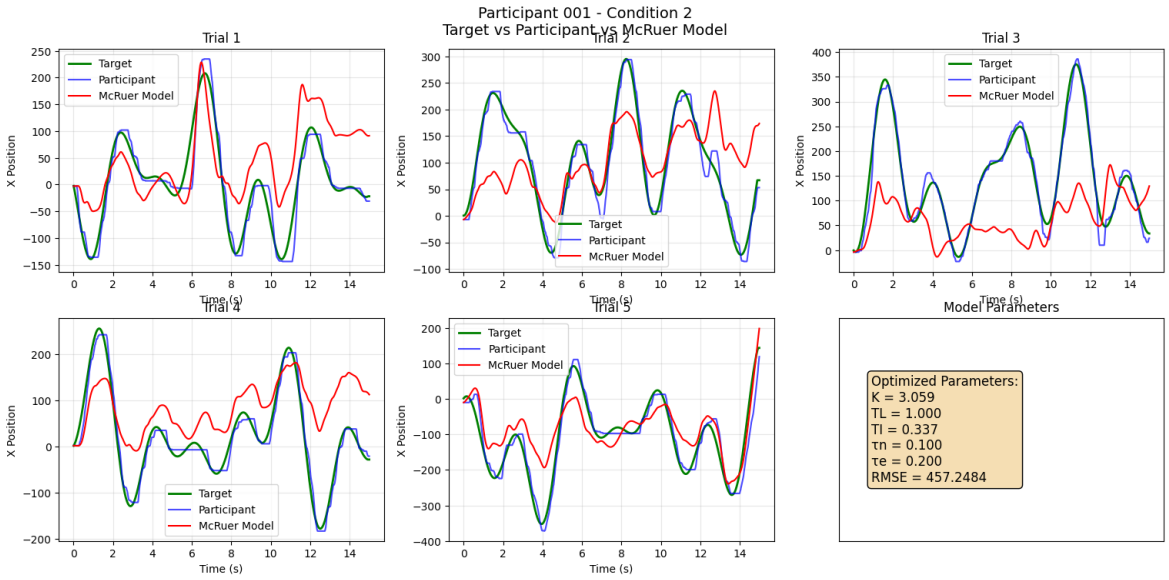

Figure B.2: Experimental results of participant 001, condition 2. Legend bottom-right displaying the optimized McRuer model parameters for generating the model path trying to identify the control behavior for this participant and condition. Green line: Target path. Blue line: Participant path. Red line: Model path.

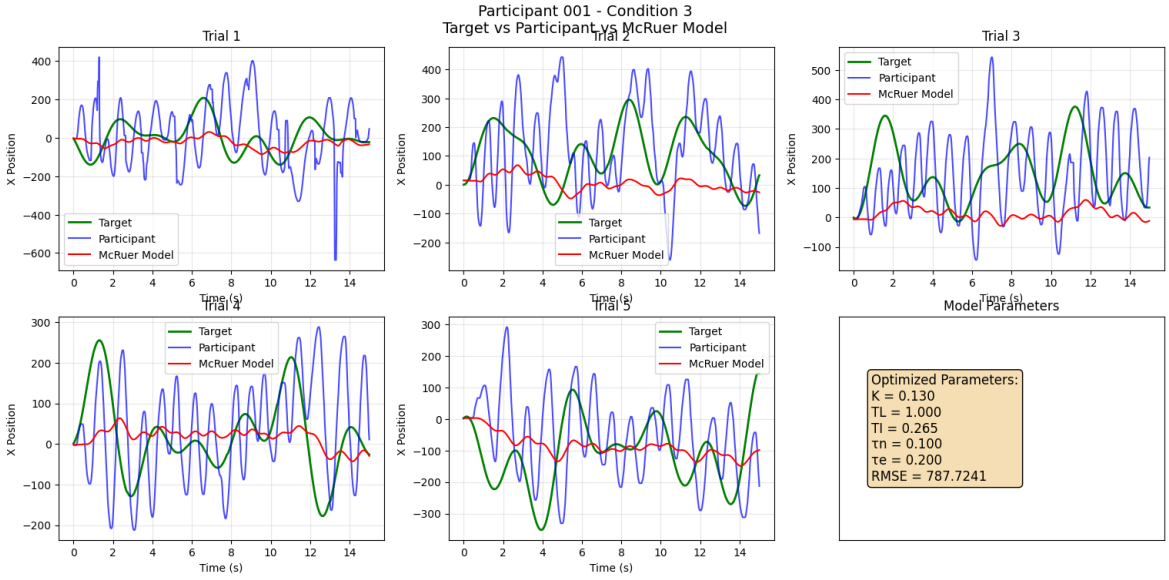

Figure B.3: Experimental results of participant 001, condition 3. Legend bottom-right displaying the optimized McRuer model parameters for generating the model path trying to identify the control behavior for this participant and condition. Green line: Target path. Blue line: Participant path. Red line: Model path.

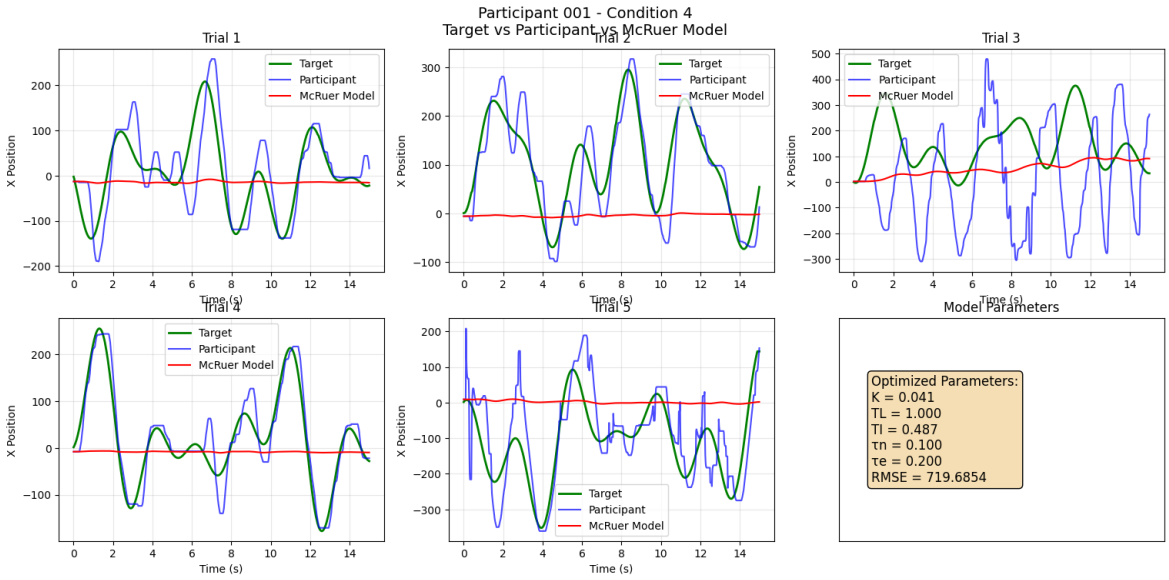

Figure B.4: Experimental results of participant 001, condition 4. Legend bottom-right displaying the optimized McRuer model parameters for generating the model path trying to identify the control behavior for this participant and condition. Green line: Target path. Blue line: Participant path. Red line: Model path.

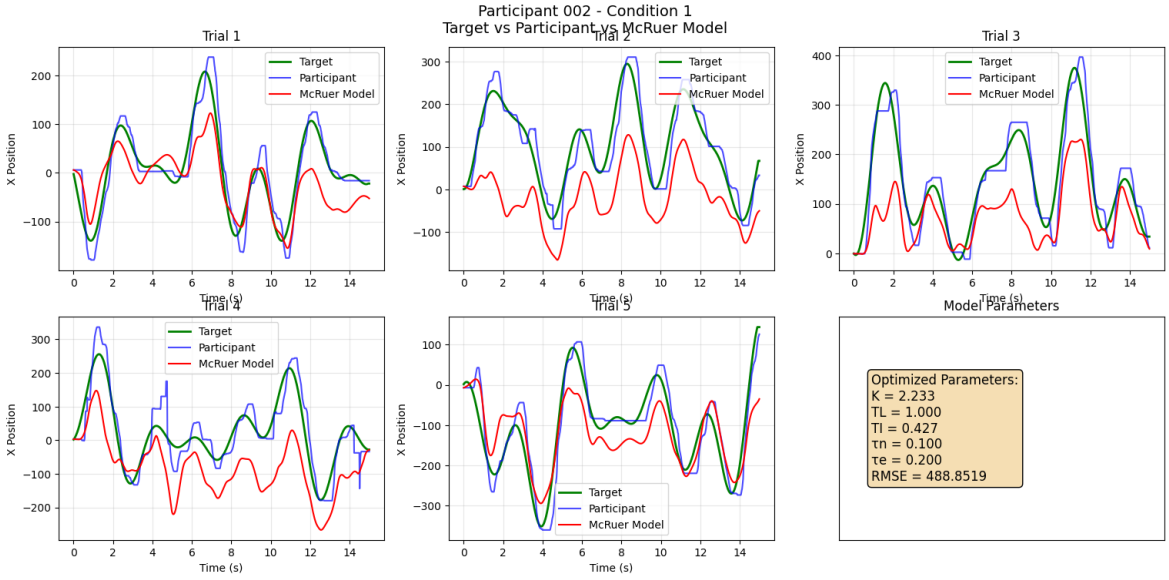

Figure B.5: Experimental results of participant 002, condition 1. Legend bottom-right displaying the optimized McRuer model parameters for generating the model path trying to identify the control behavior for this participant and condition. Green line: Target path. Blue line: Participant path. Red line: Model path.

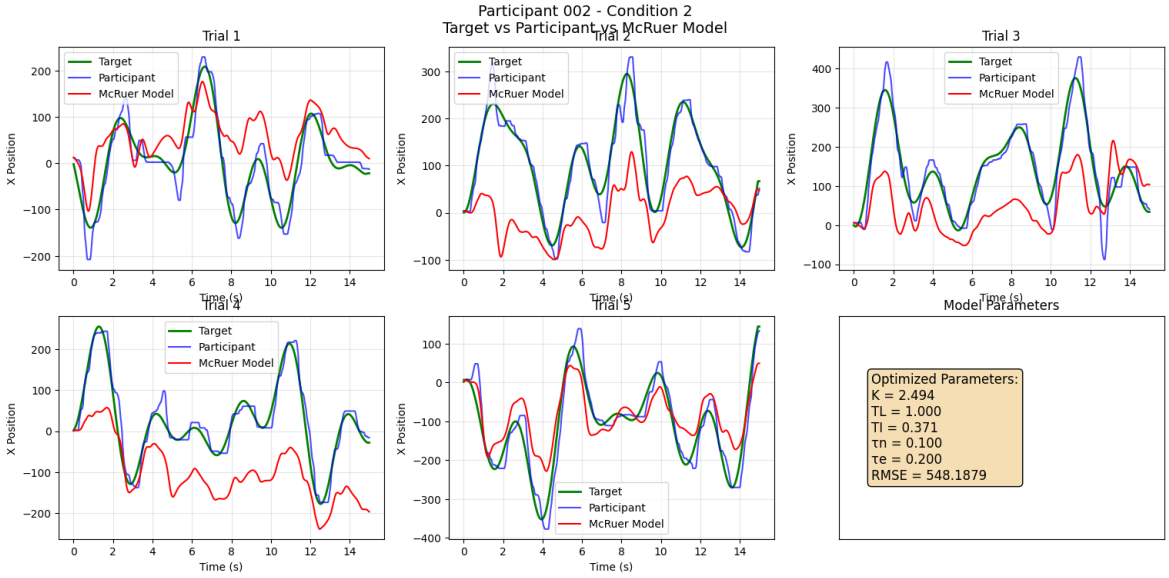

Figure B.6: Experimental results of participant 002, condition 2. Legend bottom-right displaying the optimized McRuer model parameters for generating the model path trying to identify the control behavior for this participant and condition. Green line: Target path. Blue line: Participant path. Red line: Model path.

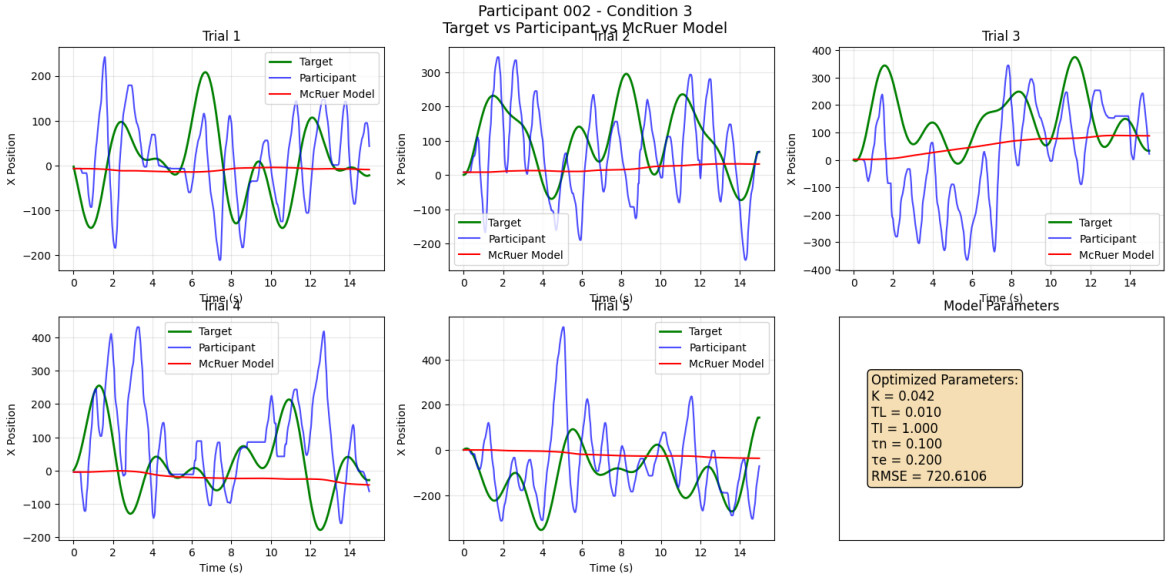

Figure B.7: Experimental results of participant 002, condition 3. Legend bottom-right displaying the optimized McRuer model parameters for generating the model path trying to identify the control behavior for this participant and condition. Green line: Target path. Blue line: Participant path. Red line: Model path.

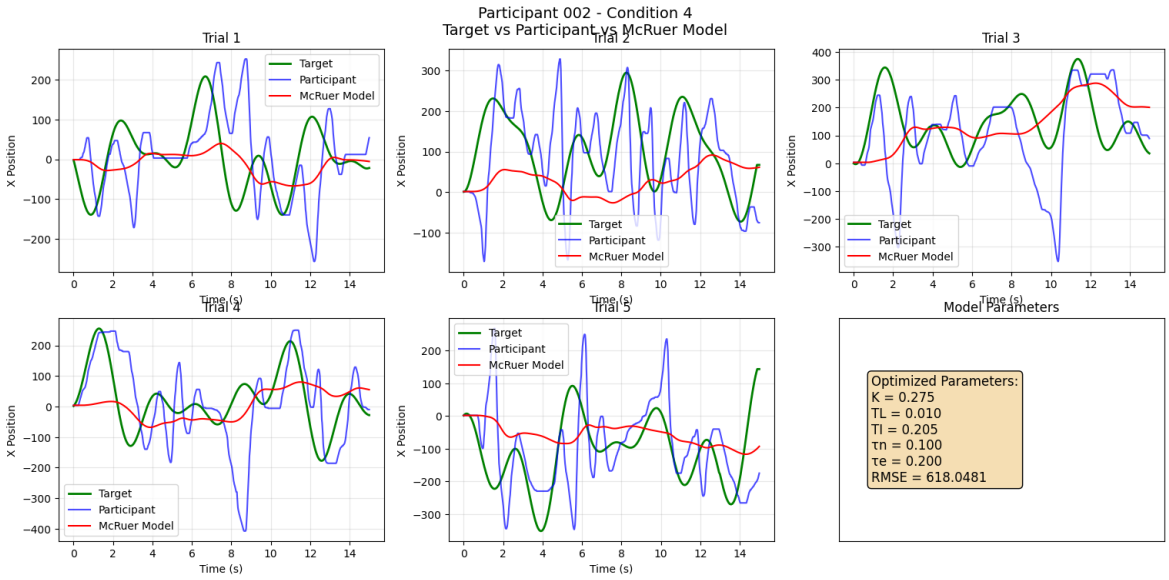

Figure B.8: Experimental results of participant 002, condition 4. Legend bottom-right displaying the optimized McRuer model parameters for generating the model path trying to identify the control behavior for this participant and condition. Green line: Target path. Blue line: Participant path. Red line: Model path.

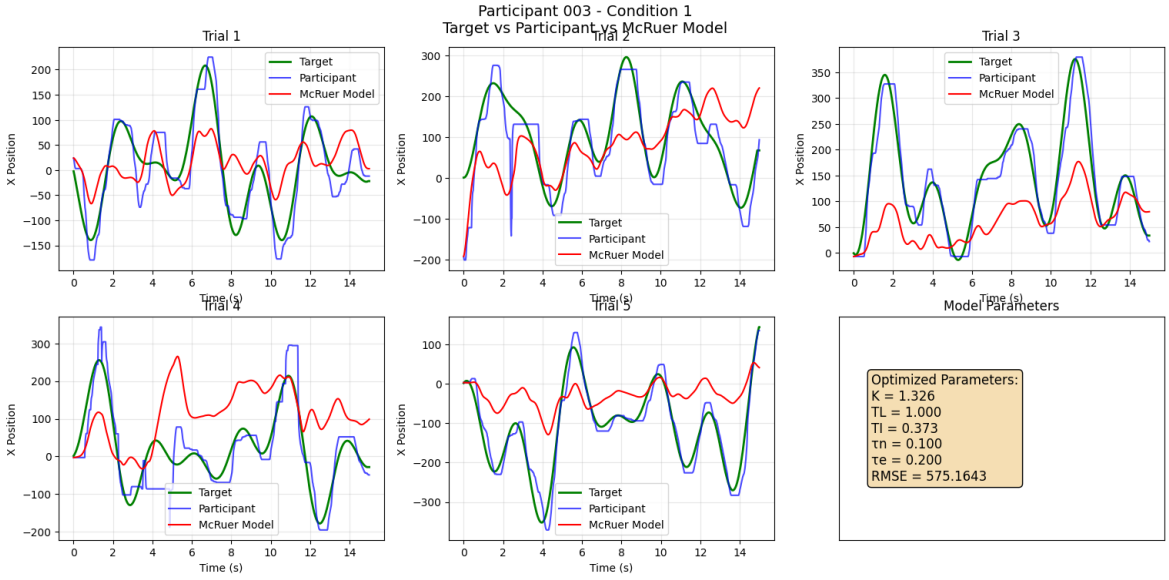

Figure B.9: Experimental results of participant 003, condition 1. Legend bottom-right displaying the optimized McRuer model parameters for generating the model path trying to identify the control behavior for this participant and condition. Green line: Target path. Blue line: Participant path. Red line: Model path.

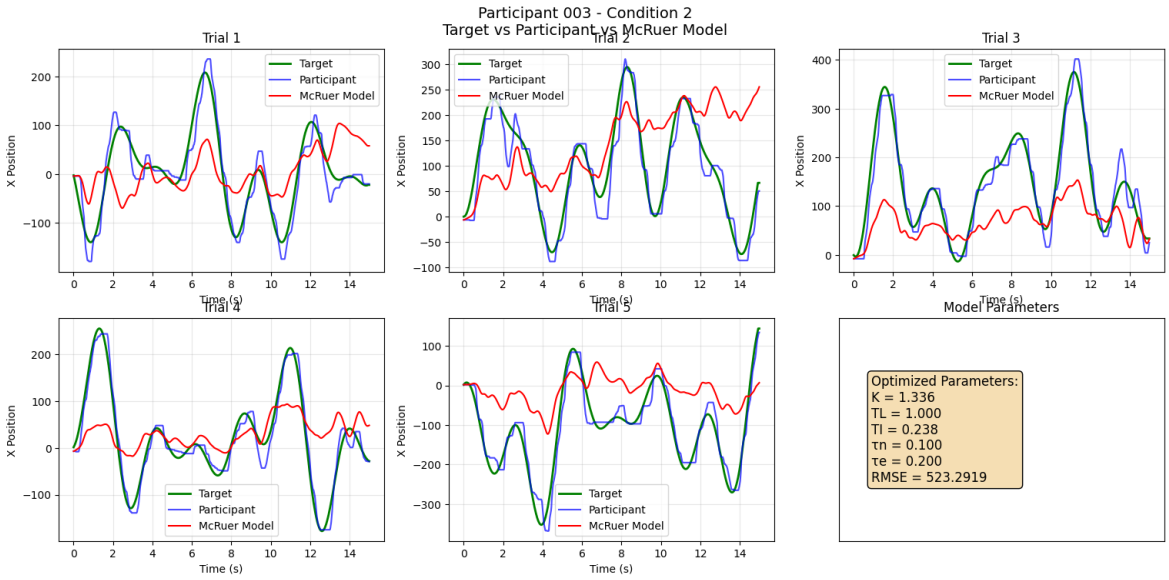

Figure B.10: Experimental results of participant 003, condition 2. Legend bottom-right displaying the optimized McRuer model parameters for generating the model path trying to identify the control behavior for this participant and condition. Green line: Target path. Blue line: Participant path. Red line: Model path.

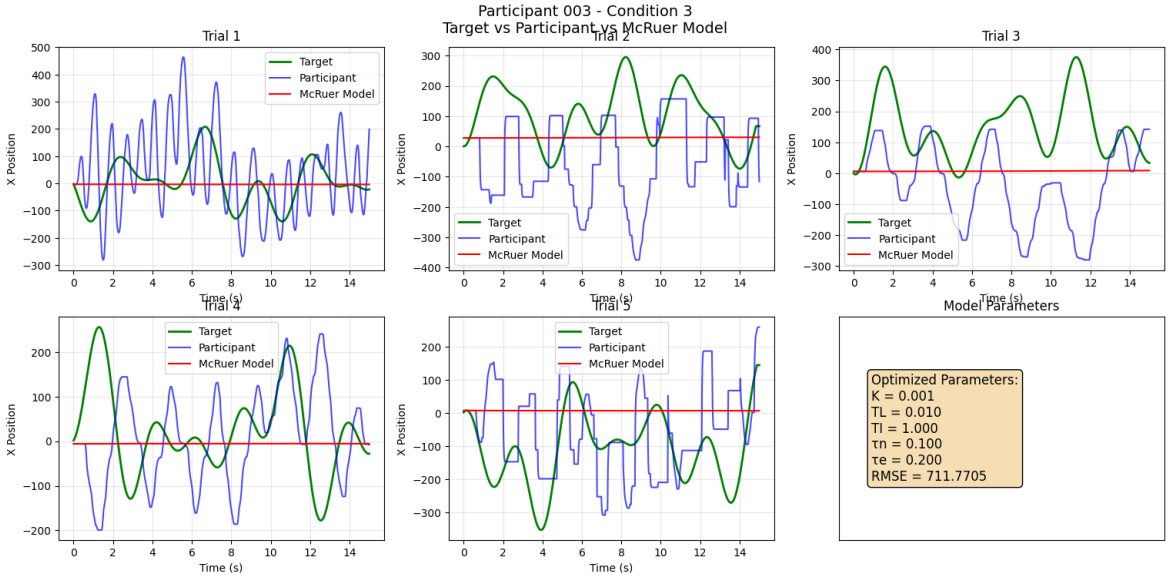

Figure B.11: Experimental results of participant 003, condition 3. Legend bottom-right displaying the optimized McRuer model parameters for generating the model path trying to identify the control behavior for this participant and condition. Green line: Target path. Blue line: Participant path. Red line: Model path.

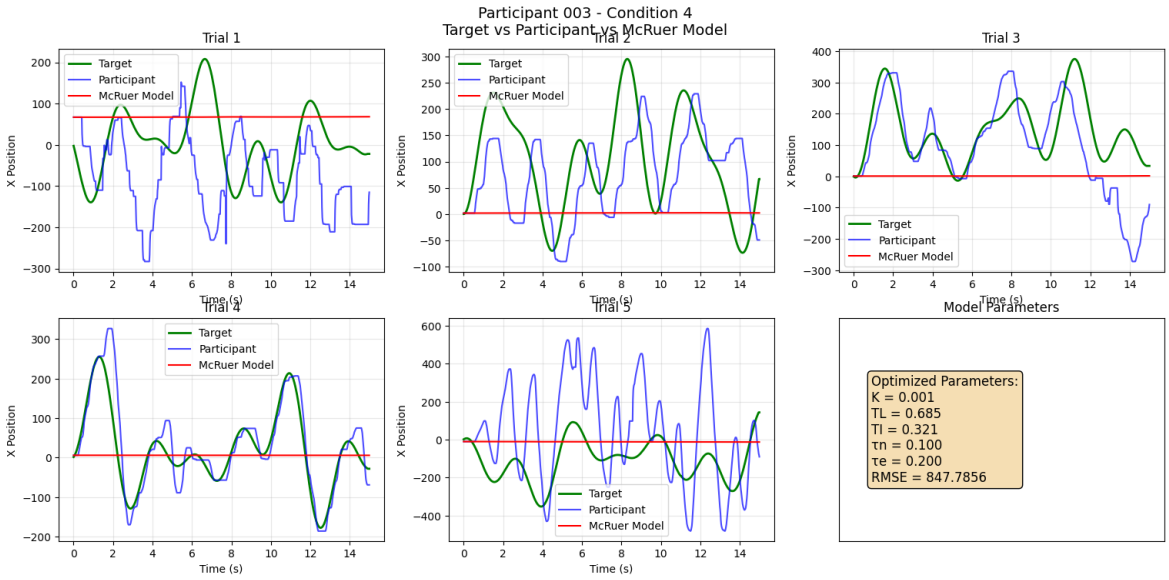

Figure B.12: Experimental results of participant 003, condition 4. Legend bottom-right displaying the optimized McRuer model parameters for generating the model path trying to identify the control behavior for this participant and condition. Green line: Target path. Blue line: Participant path. Red line: Model path.

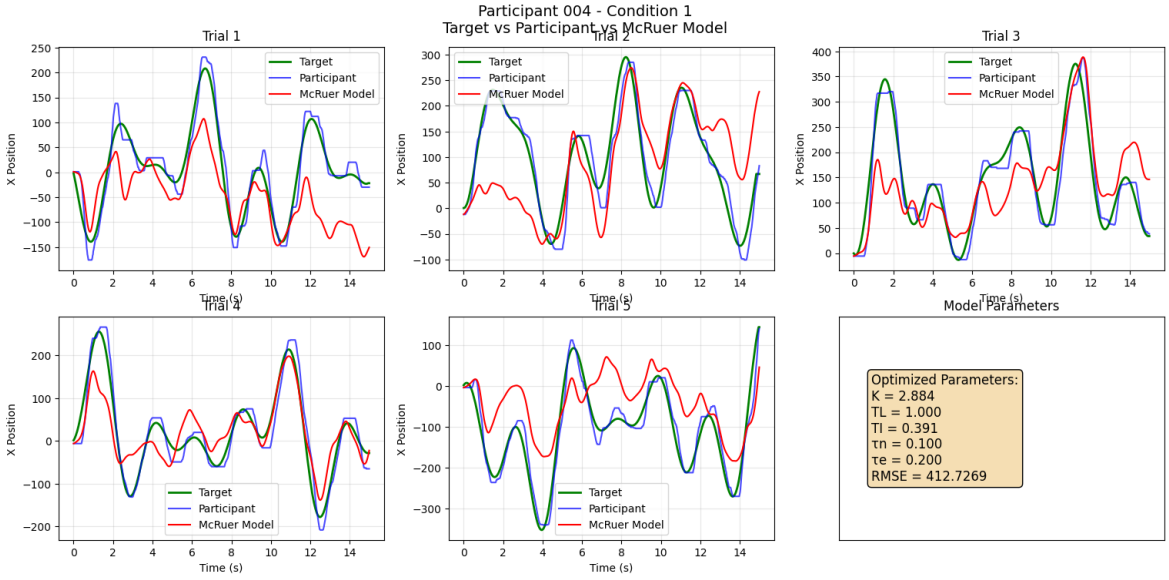

Figure B.13: Experimental results of participant 004, condition 1. Legend bottom-right displaying the optimized McRuer model parameters for generating the model path trying to identify the control behavior for this participant and condition. Green line: Target path. Blue line: Participant path. Red line: Model path.

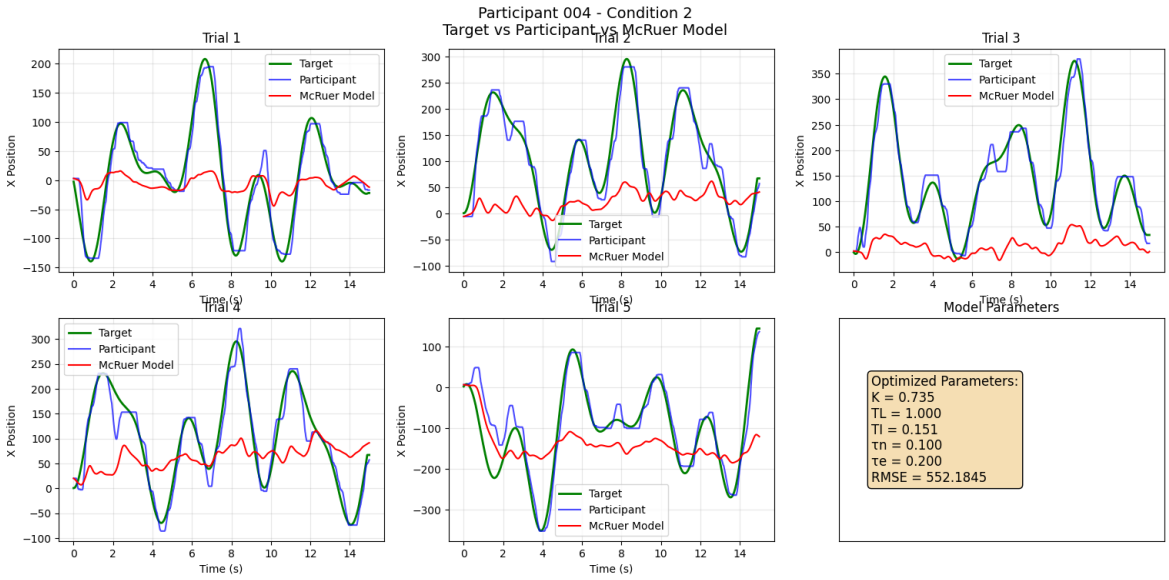

Figure B.14: Experimental results of participant 004, condition 2. Legend bottom-right displaying the optimized McRuer model parameters for generating the model path trying to identify the control behavior for this participant and condition. Green line: Target path. Blue line: Participant path. Red line: Model path.

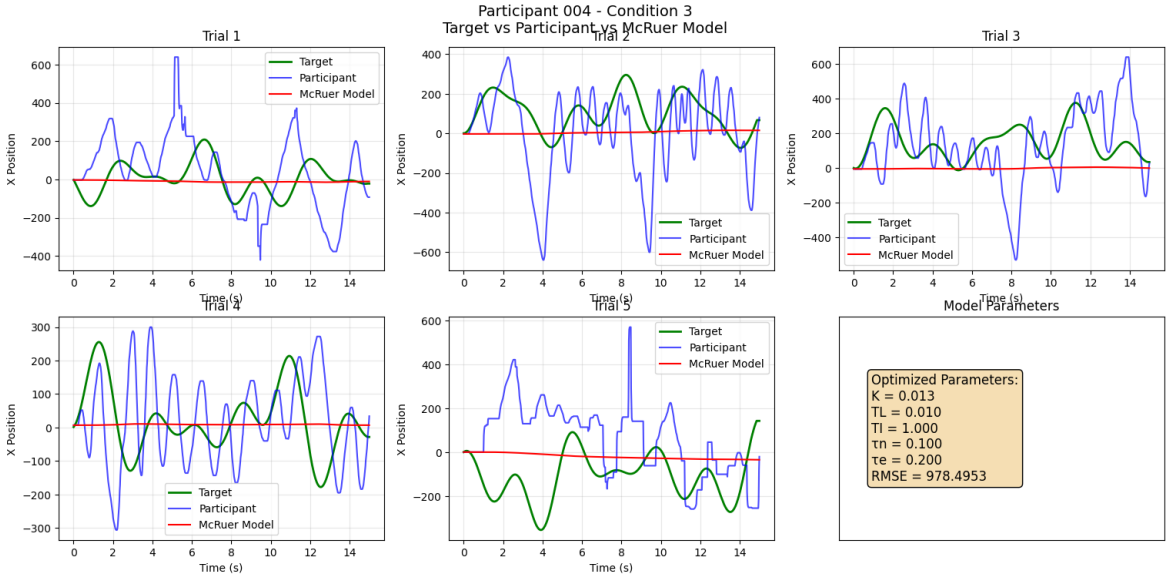

Figure B.15: Experimental results of participant 004, condition 3. Legend bottom-right displaying the optimized McRuer model parameters for generating the model path trying to identify the control behavior for this participant and condition. Green line: Target path. Blue line: Participant path. Red line: Model path.

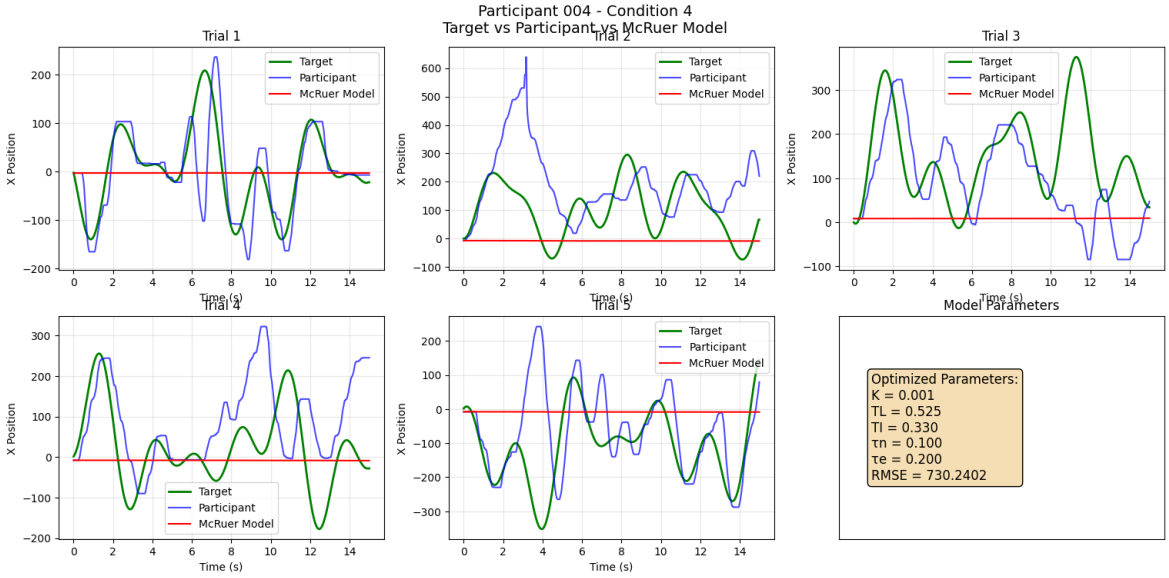

Figure B.16: Experimental results of participant 004, condition 4. Legend bottom-right displaying the optimized McRuer model parameters for generating the model path trying to identify the control behavior for this participant and condition. Green line: Target path. Blue line: Participant path. Red line: Model path.

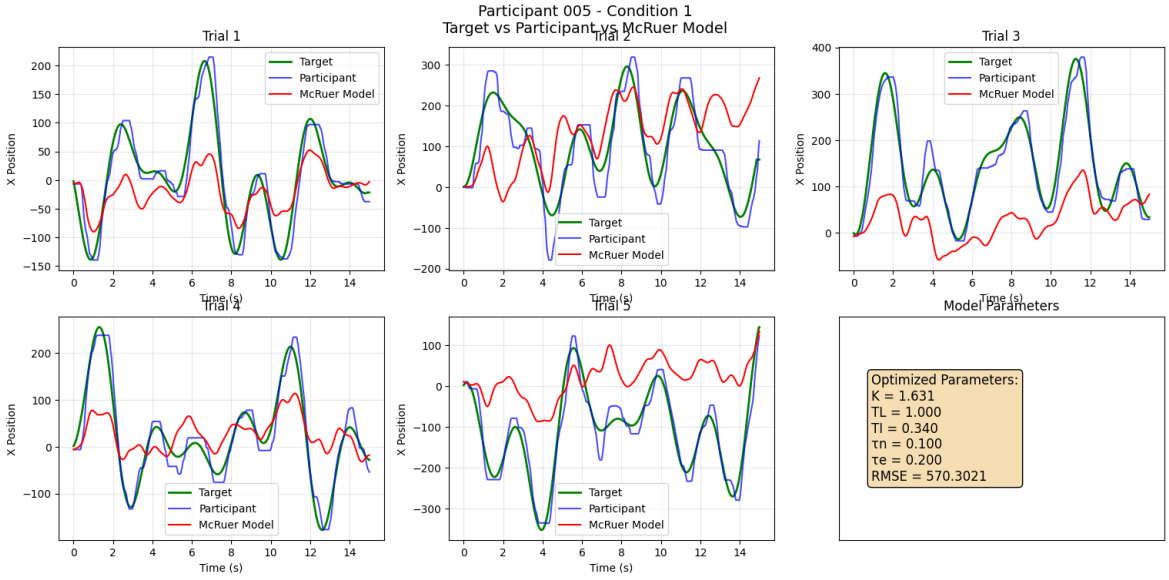

Figure B.17: Experimental results of participant 005, condition 1. Legend bottom-right displaying the optimized McRuer model parameters for generating the model path trying to identify the control behavior for this participant and condition. Green line: Target path. Blue line: Participant path. Red line: Model path.

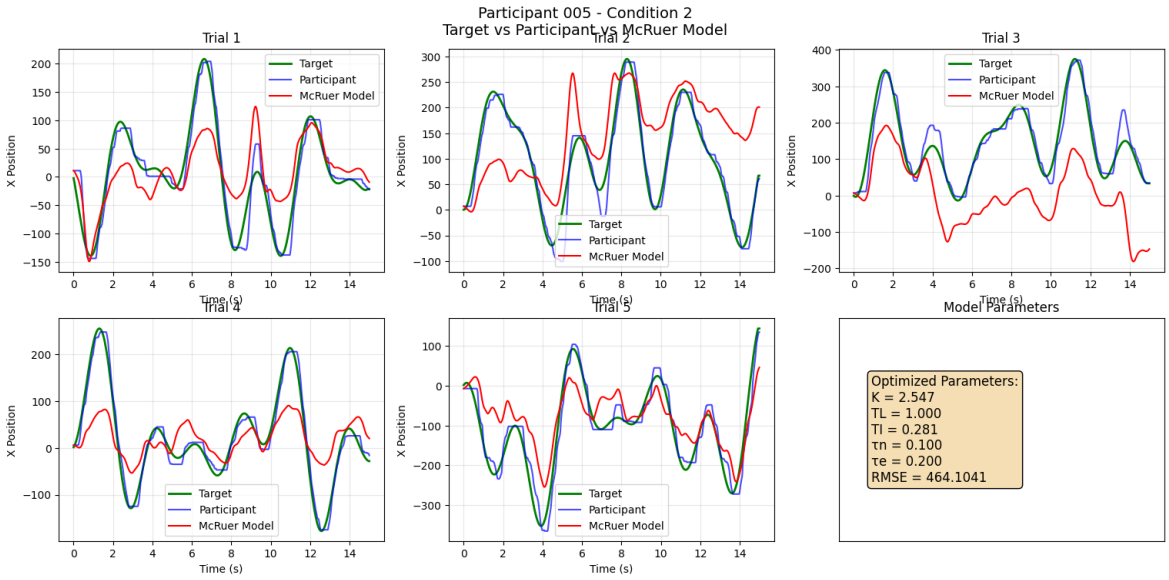

Figure B.18: Experimental results of participant 005, condition 2. Legend bottom-right displaying the optimized McRuer model parameters for generating the model path trying to identify the control behavior for this participant and condition. Green line: Target path. Blue line: Participant path. Red line: Model path.

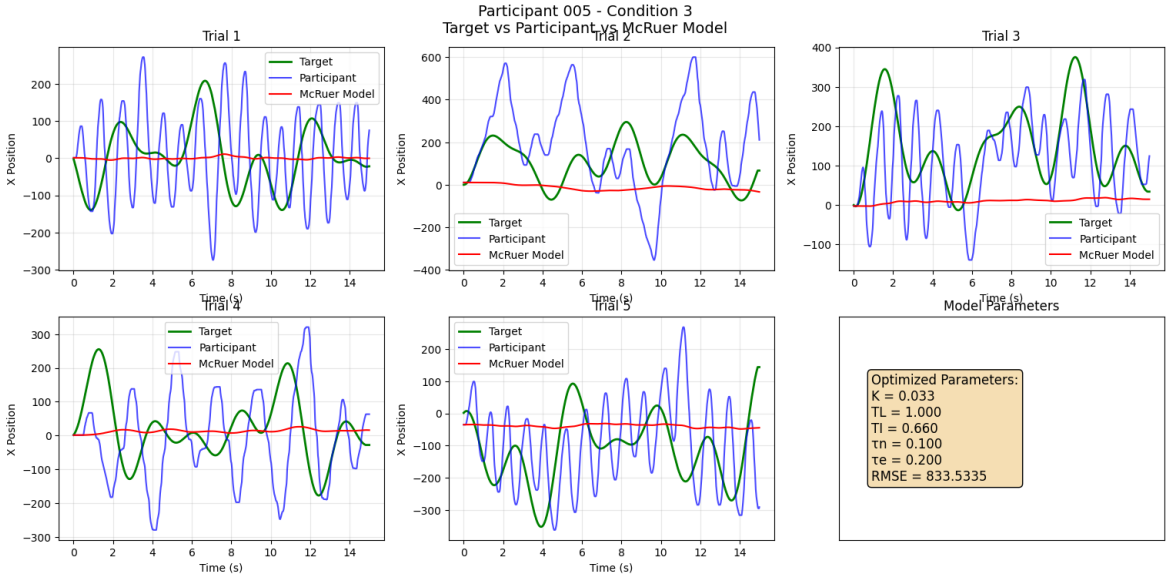

Figure B.19: Experimental results of participant 005, condition 3. Legend bottom-right displaying the optimized McRuer model parameters for generating the model path trying to identify the control behavior for this participant and condition. Green line: Target path. Blue line: Participant path. Red line: Model path.

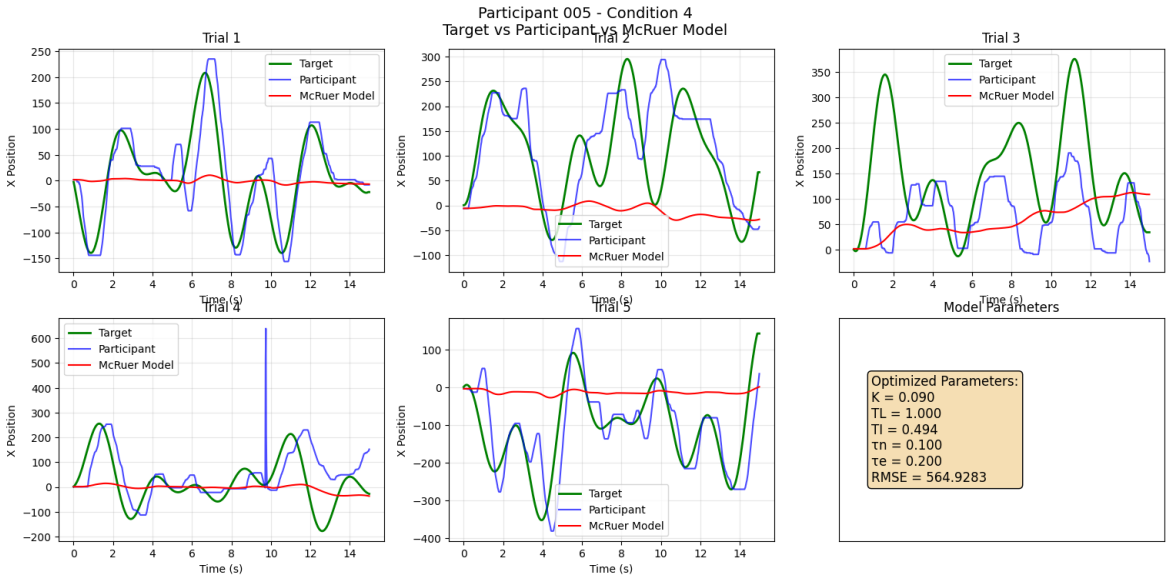

Figure B.20: Experimental results of participant 005, condition 4. Legend bottom-right displaying the optimized McRuer model parameters for generating the model path trying to identify the control behavior for this participant and condition. Green line: Target path. Blue line: Participant path. Red line: Model path.

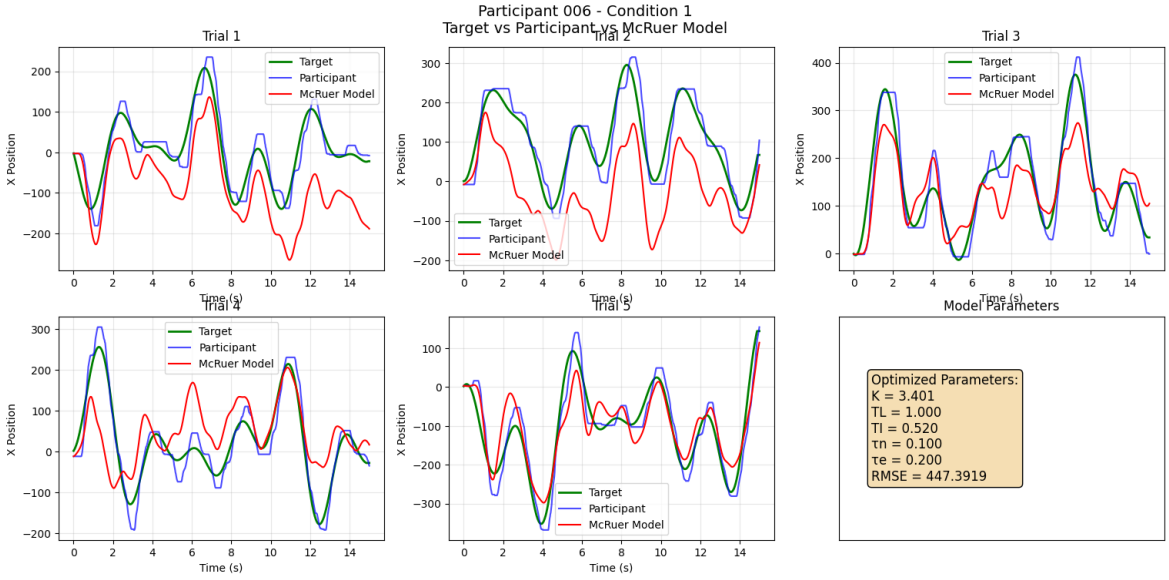

Figure B.21: Experimental results of participant 006, condition 1. Legend bottom-right displaying the optimized McRuer model parameters for generating the model path trying to identify the control behavior for this participant and condition. Green line: Target path. Blue line: Participant path. Red line: Model path.

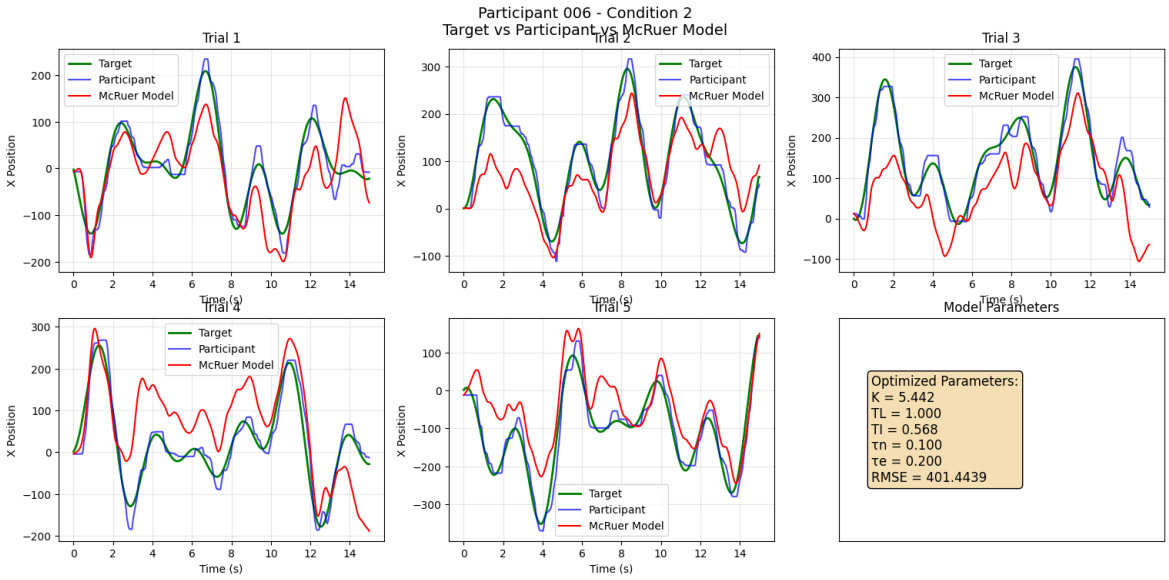

Figure B.22: Experimental results of participant 006, condition 2. Legend bottom-right displaying the optimized McRuer model parameters for generating the model path trying to identify the control behavior for this participant and condition. Green line: Target path. Blue line: Participant path. Red line: Model path.

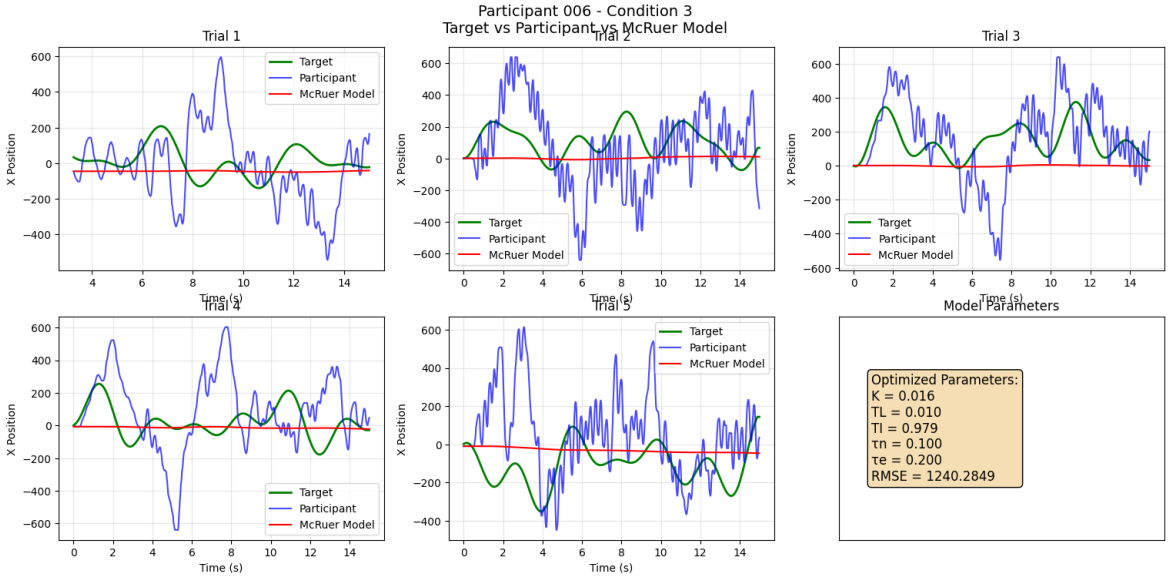

Figure B.23: Experimental results of participant 006, condition 3. Legend bottom-right displaying the optimized McRuer model parameters for generating the model path trying to identify the control behavior for this participant and condition. Green line: Target path. Blue line: Participant path. Red line: Model path.

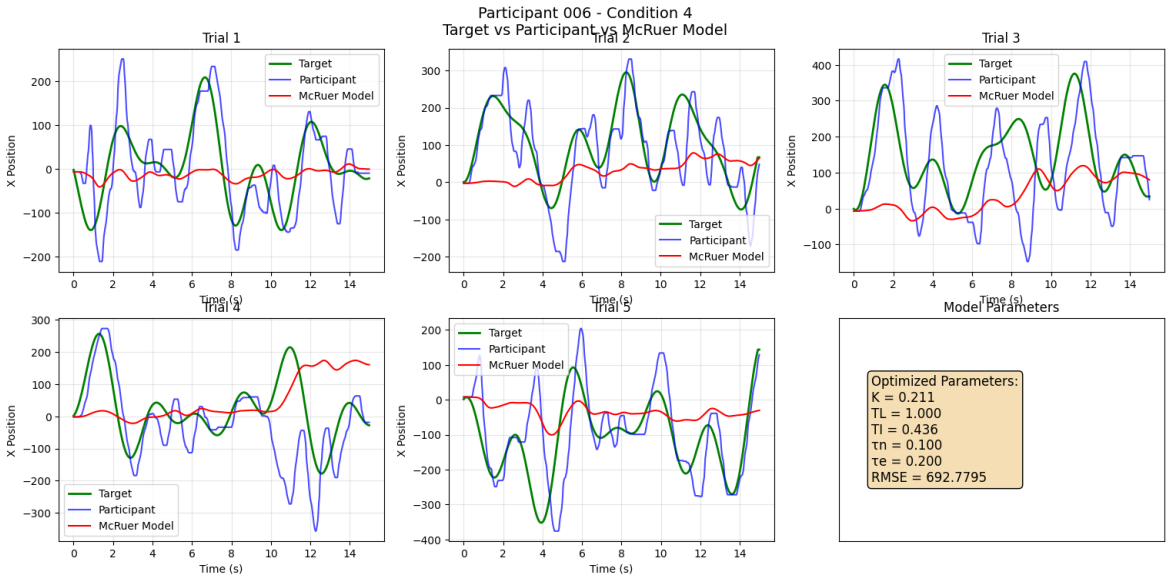

Figure B.24: Experimental results of participant 006, condition 4. Legend bottom-right displaying the optimized McRuer model parameters for generating the model path trying to identify the control behavior for this participant and condition. Green line: Target path. Blue line: Participant path. Red line: Model path.

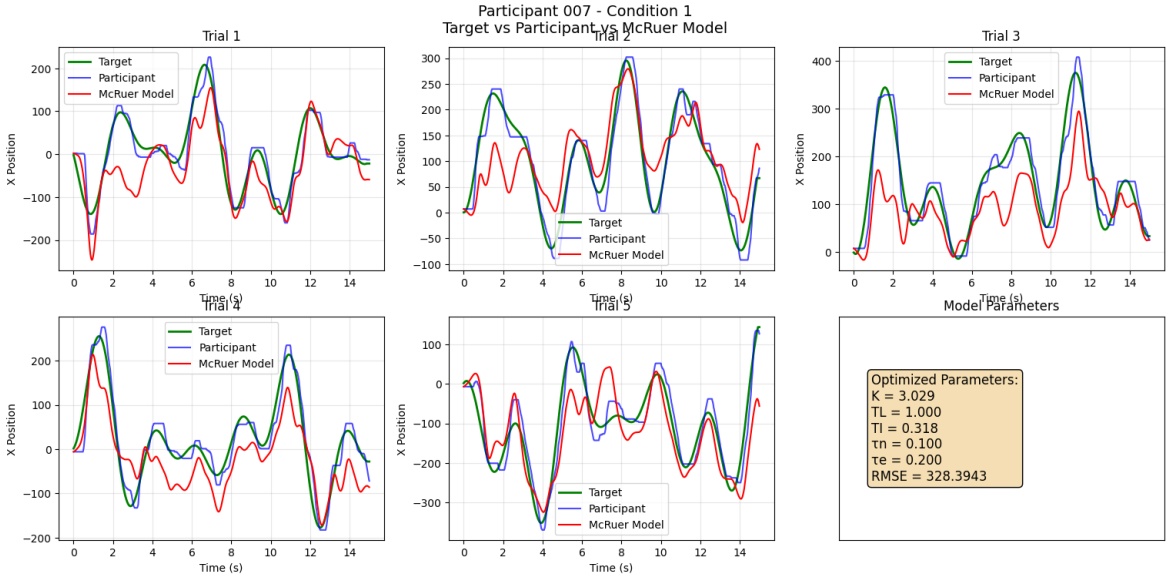

Figure B.25: Experimental results of participant 007, condition 1. Legend bottom-right displaying the optimized McRuer model parameters for generating the model path trying to identify the control behavior for this participant and condition. Green line: Target path. Blue line: Participant path. Red line: Model path.

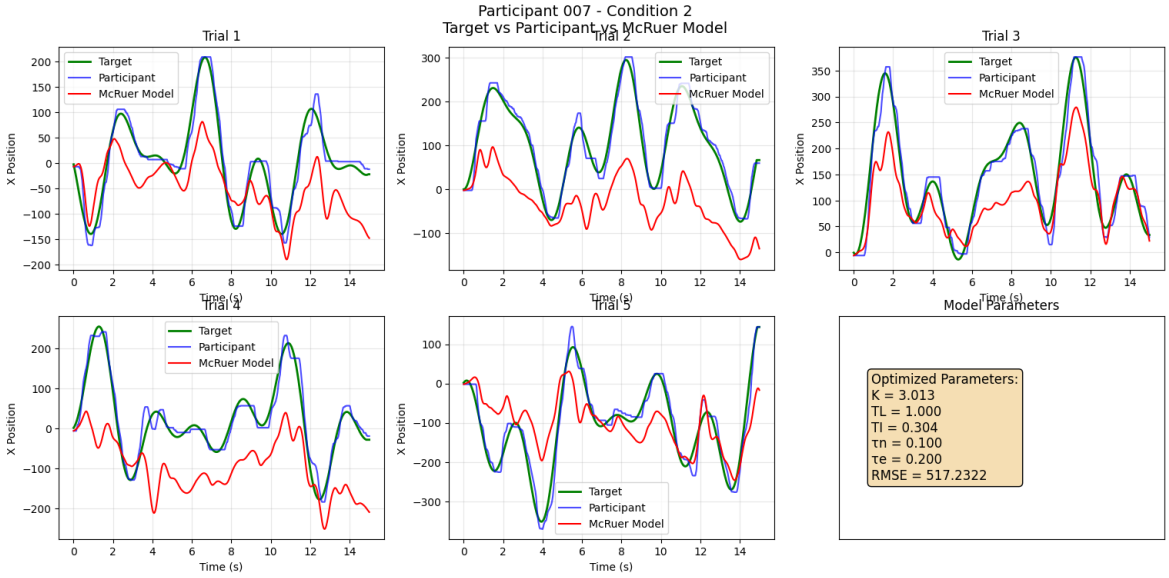

Figure B.26: Experimental results of participant 007, condition 2. Legend bottom-right displaying the optimized McRuer model parameters for generating the model path trying to identify the control behavior for this participant and condition. Green line: Target path. Blue line: Participant path. Red line: Model path.

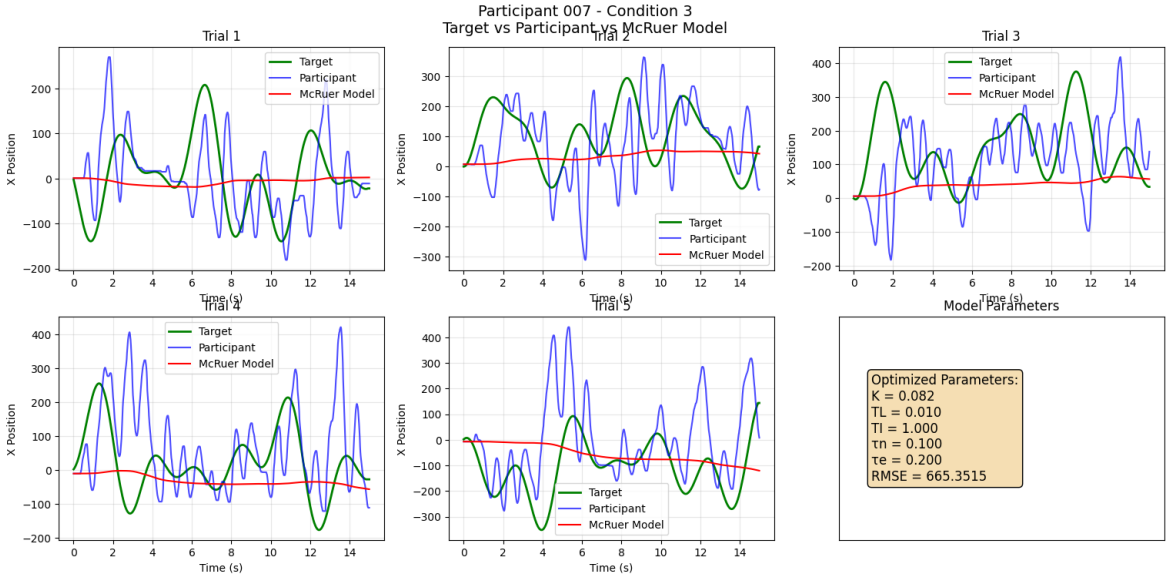

Figure B.27: Experimental results of participant 007, condition 3. Legend bottom-right displaying the optimized McRuer model parameters for generating the model path trying to identify the control behavior for this participant and condition. Green line: Target path. Blue line: Participant path. Red line: Model path.

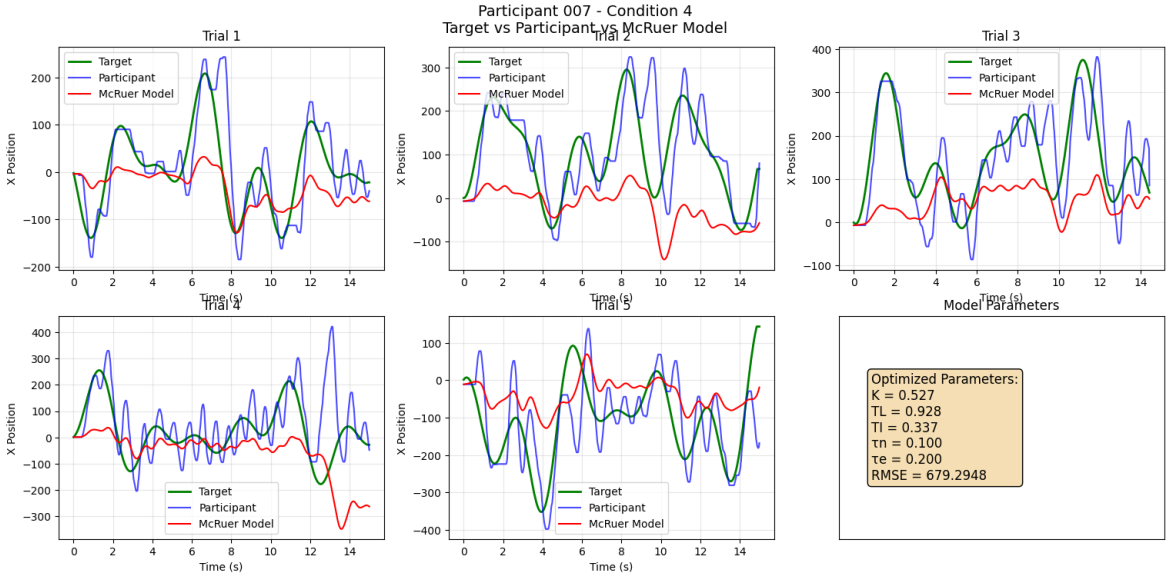

Figure B.28: Experimental results of participant 007, condition 4. Legend bottom-right displaying the optimized McRuer model parameters for generating the model path trying to identify the control behavior for this participant and condition. Green line: Target path. Blue line: Participant path. Red line: Model path.

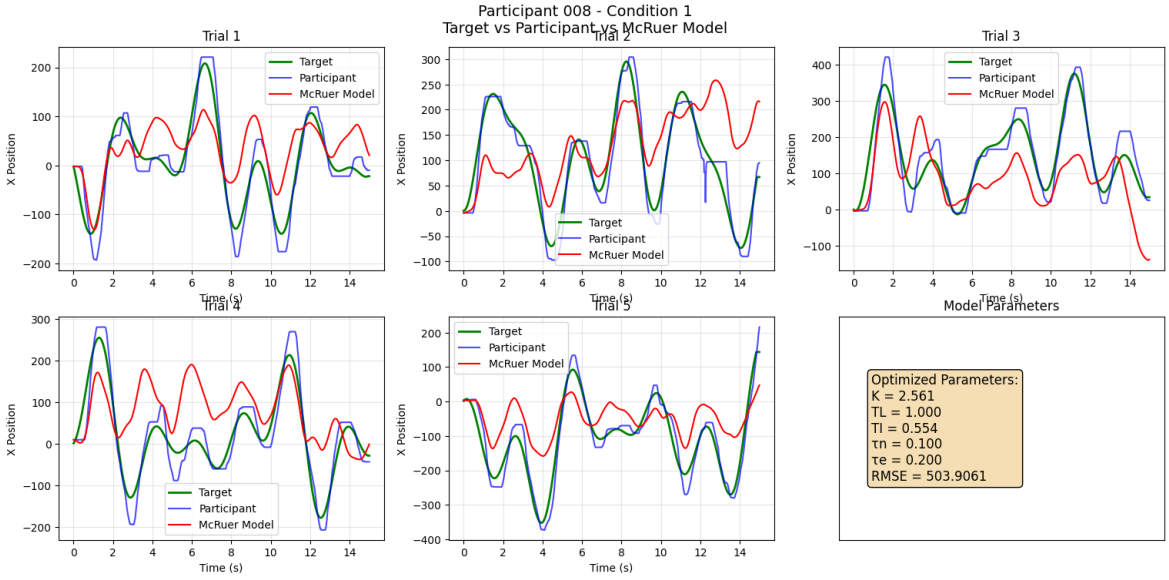

Figure B.29: Experimental results of participant 008, condition 1. Legend bottom-right displaying the optimized McRuer model parameters for generating the model path trying to identify the control behavior for this participant and condition. Green line: Target path. Blue line: Participant path. Red line: Model path.

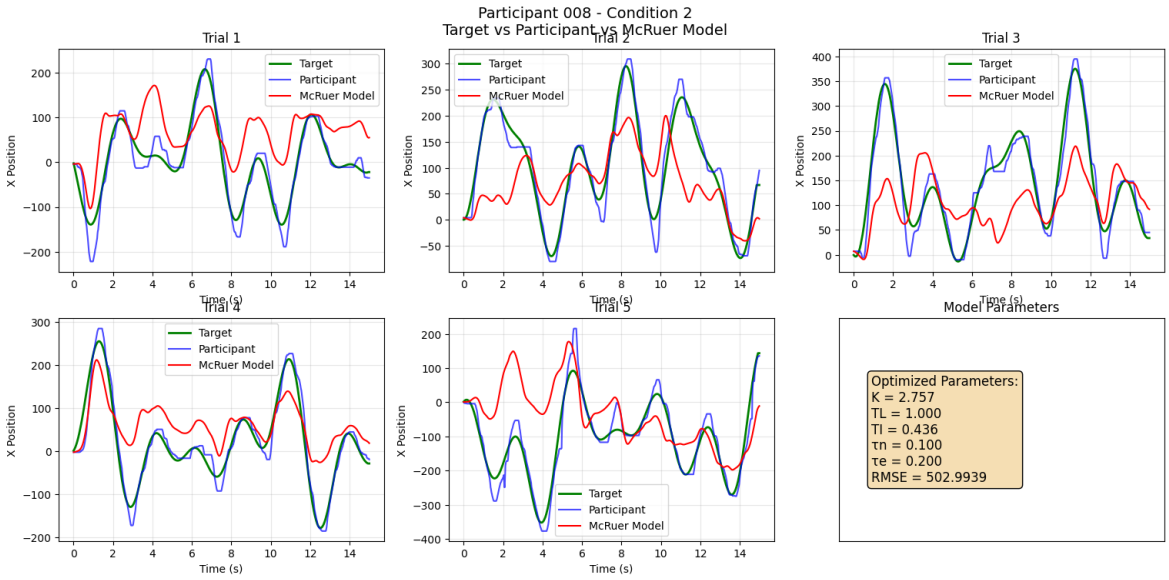

Figure B.30: Experimental results of participant 008, condition 2. Legend bottom-right displaying the optimized McRuer model parameters for generating the model path trying to identify the control behavior for this participant and condition. Green line: Target path. Blue line: Participant path. Red line: Model path.

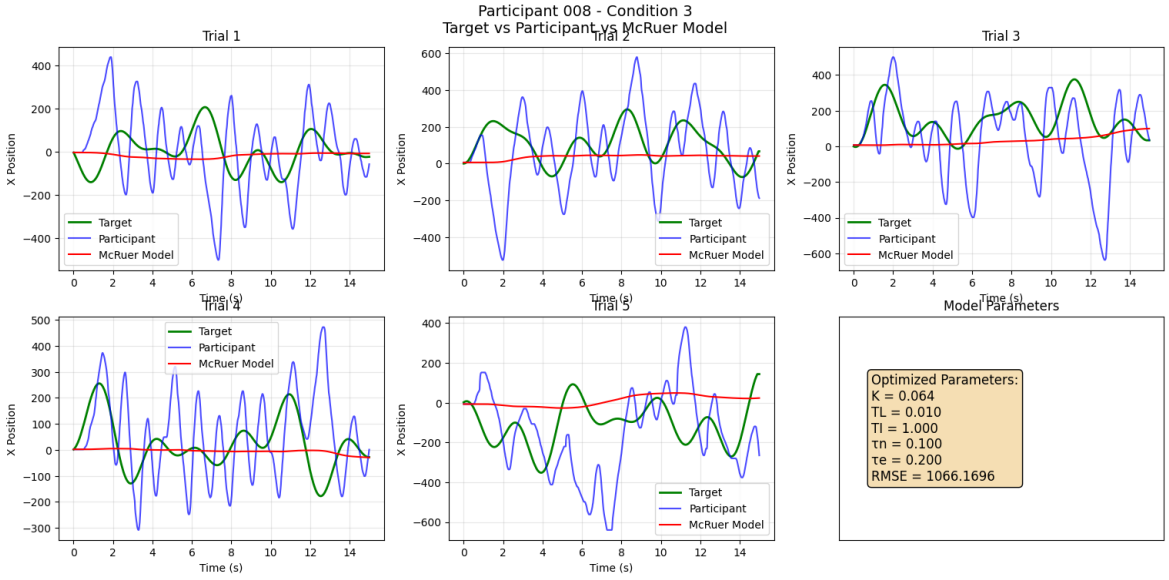

Figure B.31: Experimental results of participant 008, condition 3. Legend bottom-right displaying the optimized McRuer model parameters for generating the model path trying to identify the control behavior for this participant and condition. Green line: Target path. Blue line: Participant path. Red line: Model path.

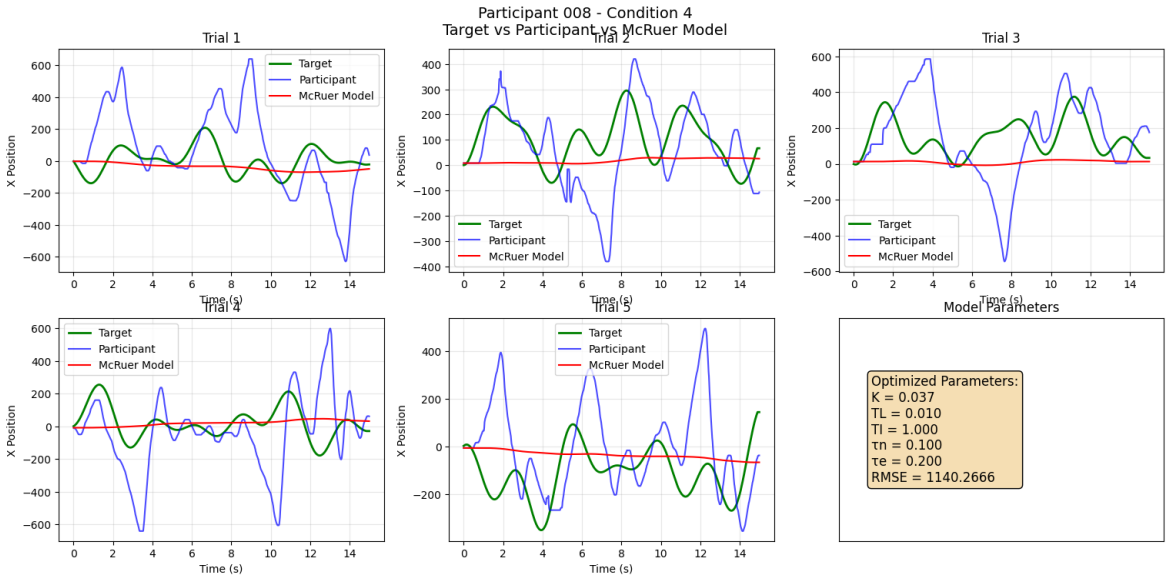

Figure B.32: Experimental results of participant 008, condition 4. Legend bottom-right displaying the optimized McRuer model parameters for generating the model path trying to identify the control behavior for this participant and condition. Green line: Target path. Blue line: Participant path. Red line: Model path.

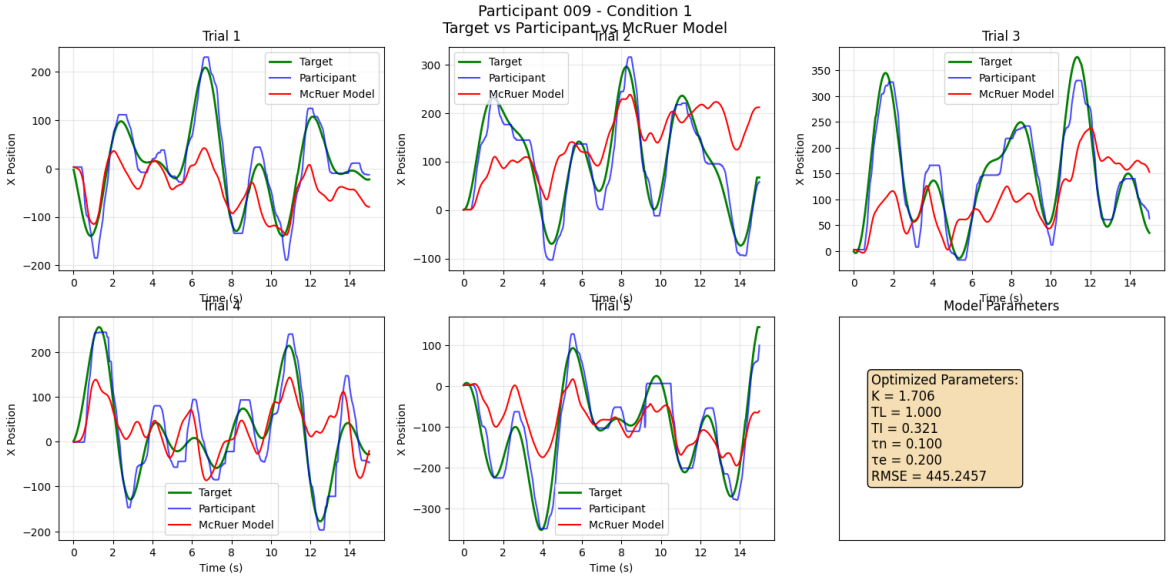

Figure B.33: Experimental results of participant 009, condition 1. Legend bottom-right displaying the optimized McRuer model parameters for generating the model path trying to identify the control behavior for this participant and condition. Green line: Target path. Blue line: Participant path. Red line: Model path.

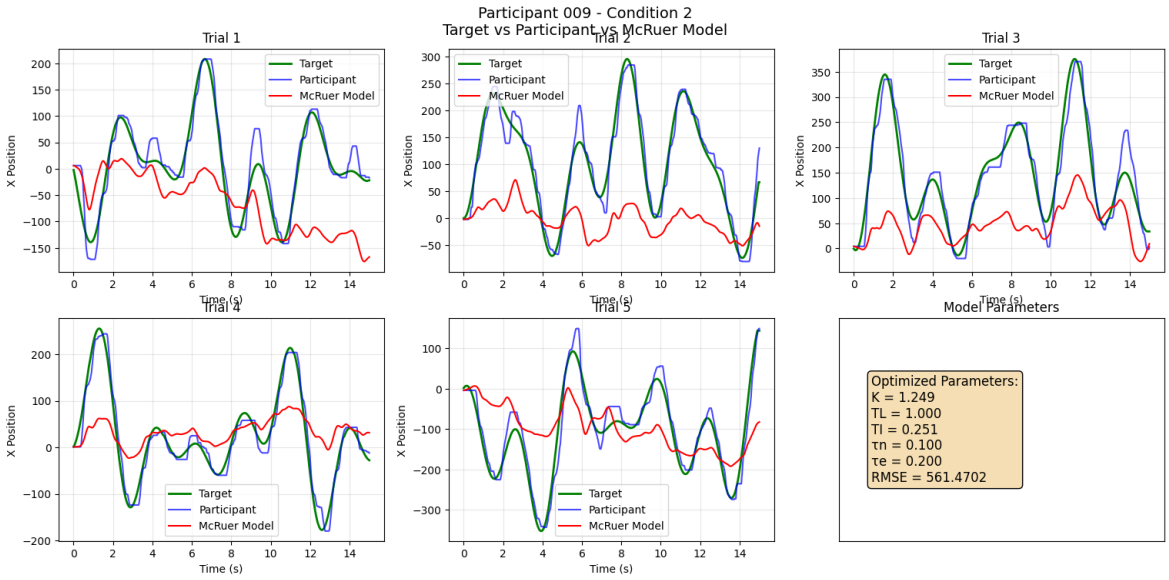

Figure B.34: Experimental results of participant 009, condition 2. Legend bottom-right displaying the optimized McRuer model parameters for generating the model path trying to identify the control behavior for this participant and condition. Green line: Target path. Blue line: Participant path. Red line: Model path.

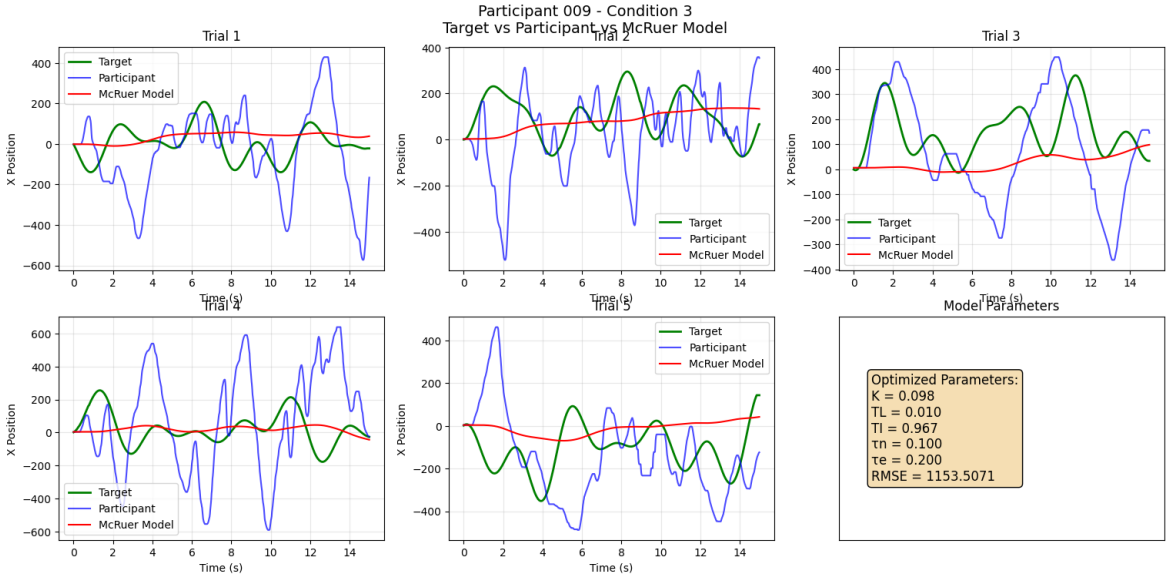

Figure B.35: Experimental results of participant 009, condition 3. Legend bottom-right displaying the optimized McRuer model parameters for generating the model path trying to identify the control behavior for this participant and condition. Green line: Target path. Blue line: Participant path. Red line: Model path.

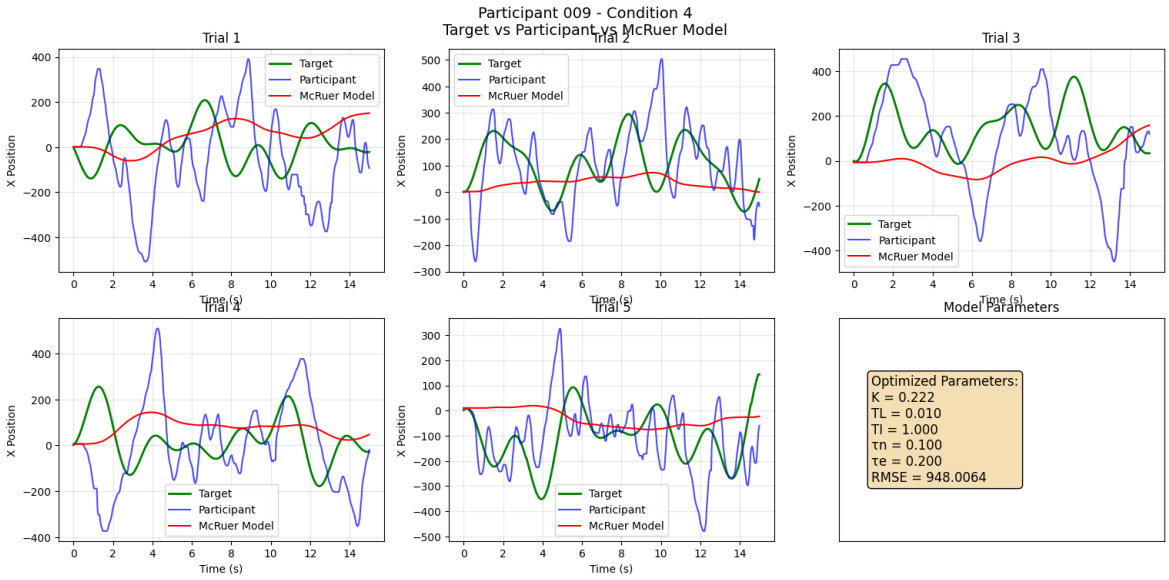

Figure B.36: Experimental results of participant 009, condition 4. Legend bottom-right displaying the optimized McRuer model parameters for generating the model path trying to identify the control behavior for this participant and condition. Green line: Target path. Blue line: Participant path. Red line: Model path.

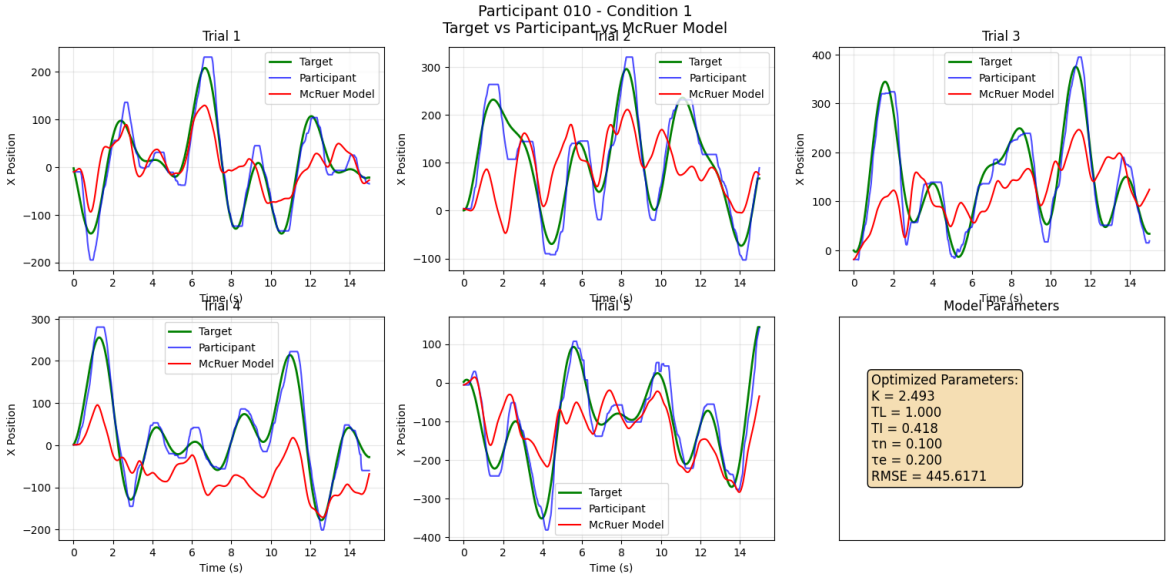

Figure B.37: Experimental results of participant 010, condition 1. Legend bottom-right displaying the optimized McRuer model parameters for generating the model path trying to identify the control behavior for this participant and condition. Green line: Target path. Blue line: Participant path. Red line: Model path.

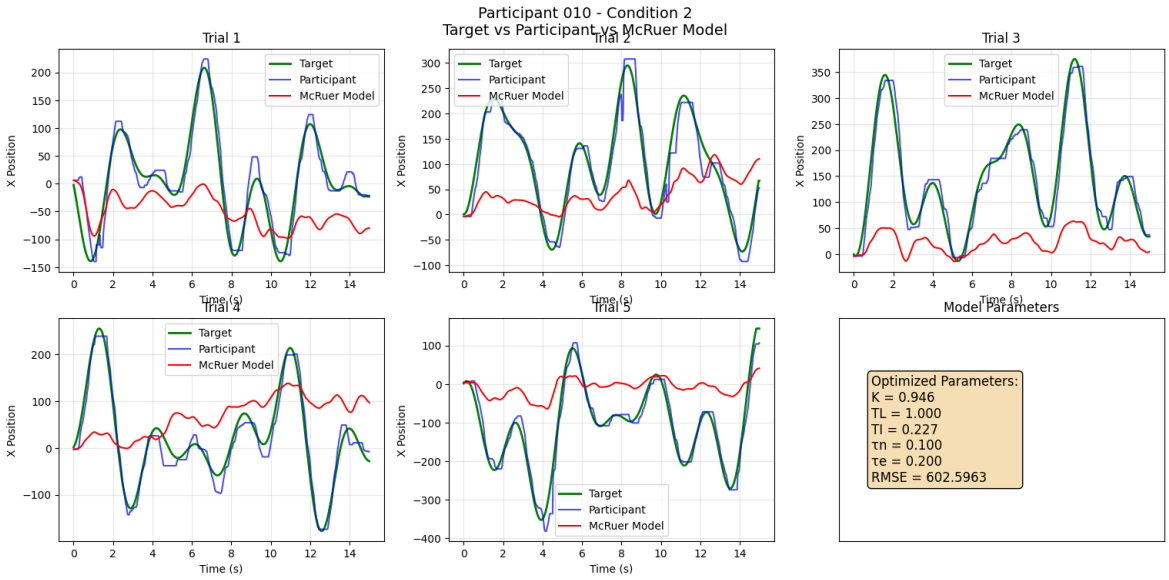

Figure B.38: Experimental results of participant 010, condition 2. Legend bottom-right displaying the optimized McRuer model parameters for generating the model path trying to identify the control behavior for this participant and condition. Green line: Target path. Blue line: Participant path. Red line: Model path.

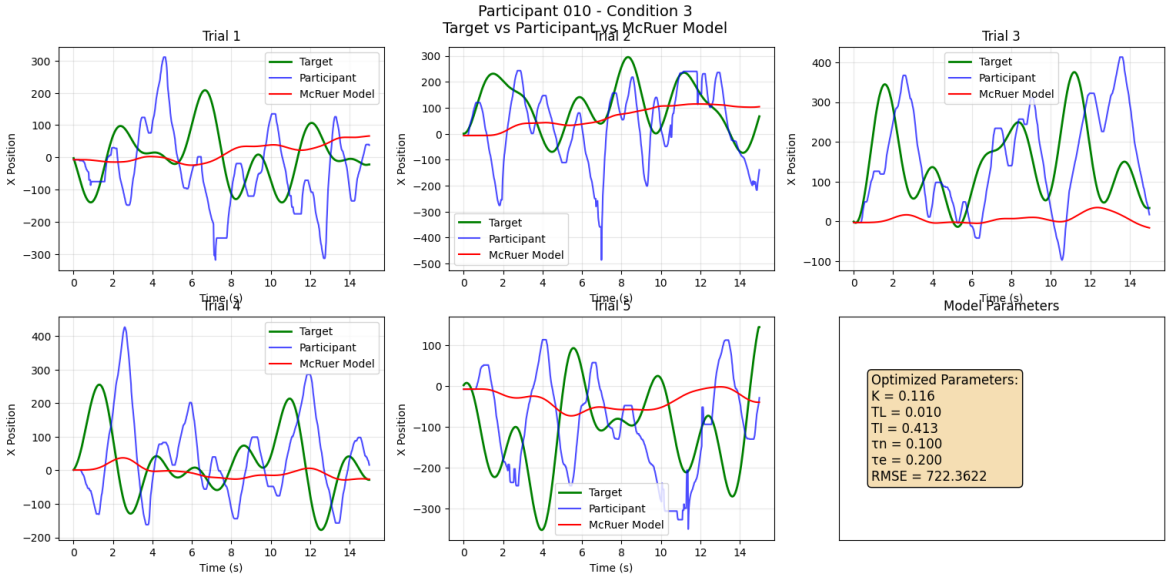

Figure B.39: Experimental results of participant 010, condition 3. Legend bottom-right displaying the optimized McRuer model parameters for generating the model path trying to identify the control behavior for this participant and condition. Green line: Target path. Blue line: Participant path. Red line: Model path.

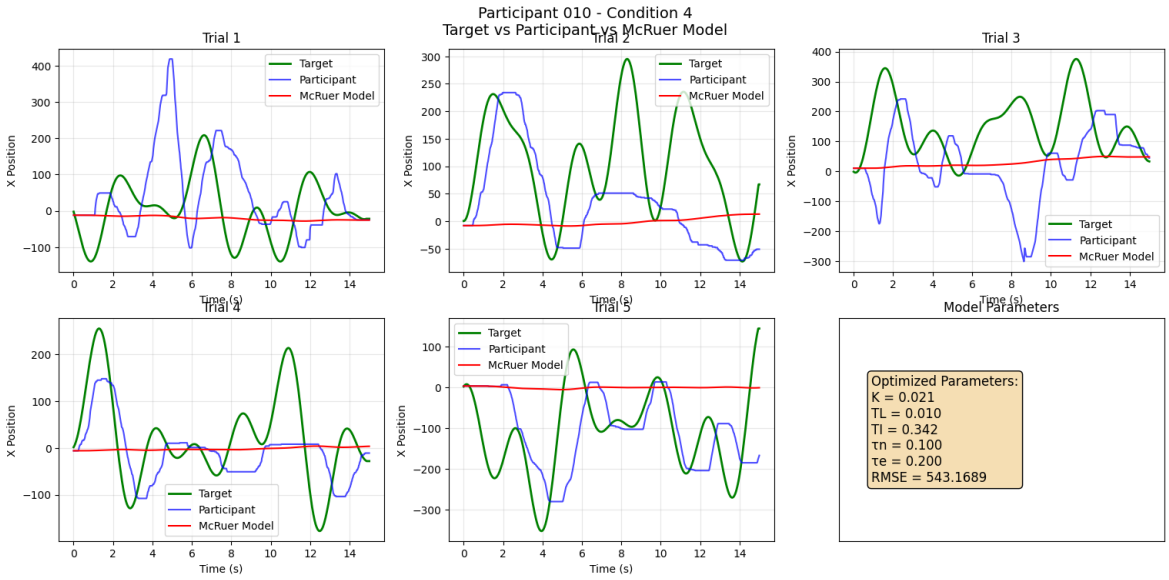

Figure B.40: Experimental results of participant 010, condition 4. Legend bottom-right displaying the optimized McRuer model parameters for generating the model path trying to identify the control behavior for this participant and condition. Green line: Target path. Blue line: Participant path. Red line: Model path.

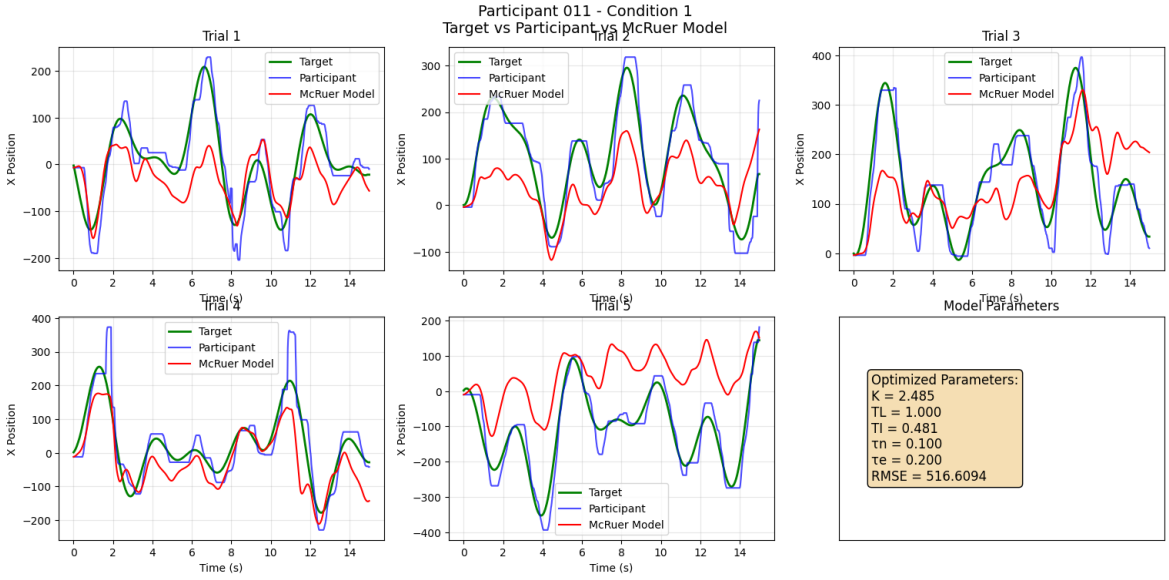

Figure B.41: Experimental results of participant 011, condition 1. Legend bottom-right displaying the optimized McRuer model parameters for generating the model path trying to identify the control behavior for this participant and condition. Green line: Target path. Blue line: Participant path. Red line: Model path.

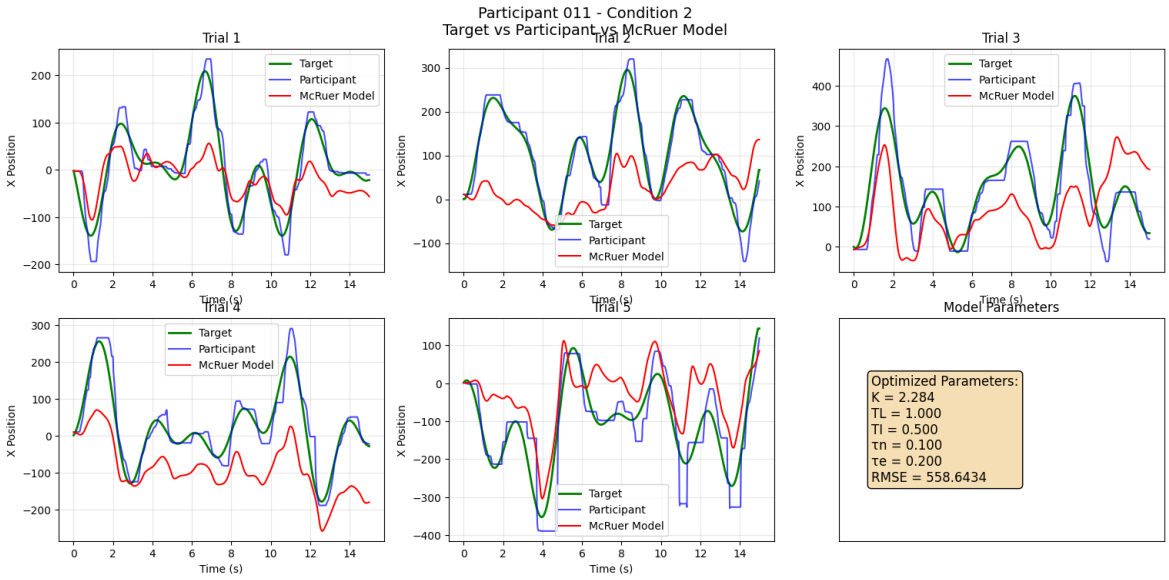

Figure B.42: Experimental results of participant 011, condition 2. Legend bottom-right displaying the optimized McRuer model parameters for generating the model path trying to identify the control behavior for this participant and condition. Green line: Target path. Blue line: Participant path. Red line: Model path.

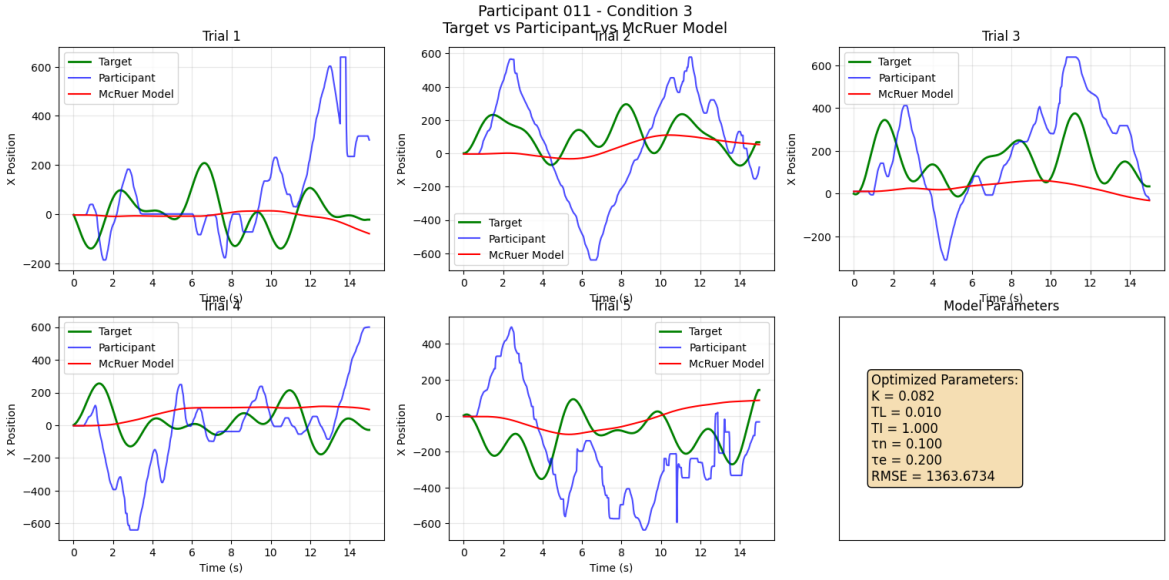

Figure B.43: Experimental results of participant 011, condition 3. Legend bottom-right displaying the optimized McRuer model parameters for generating the model path trying to identify the control behavior for this participant and condition. Green line: Target path. Blue line: Participant path. Red line: Model path.

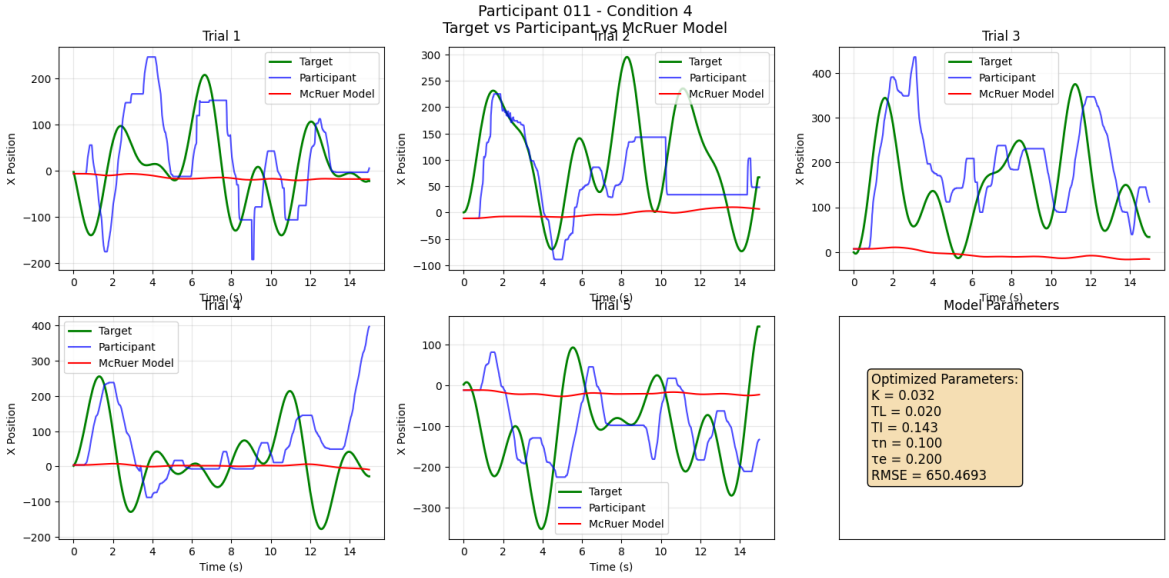

Figure B.44: Experimental results of participant 011, condition 4. Legend bottom-right displaying the optimized McRuer model parameters for generating the model path trying to identify the control behavior for this participant and condition. Green line: Target path. Blue line: Participant path. Red line: Model path.

C

Appendix - Ultraloop Device

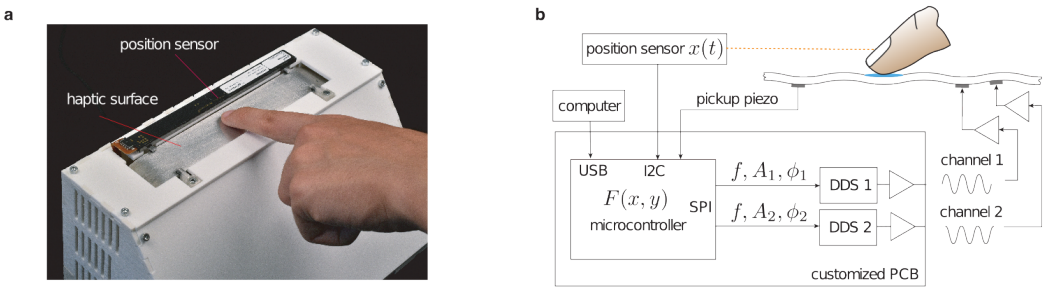

Figure C.1: (a) The study employed an ultrasonic traveling-wave haptic touchpad through which users interacted with the surface to perceive haptic guidance or virtual objects. (b) The system architecture enabled real-time programmable impedance rendering by updating dual output channels to the touchpad according to finger position, which allowed the generation of application-specific features such as bumps, position-dependent friction, and variable impedance profiles. [7]

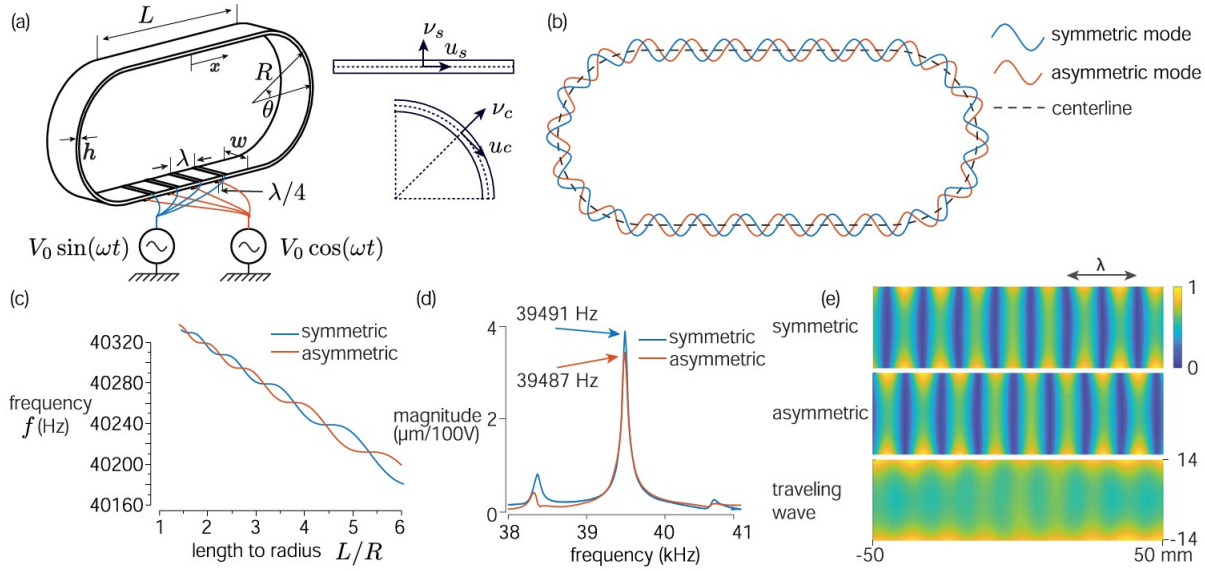

Figure C.2: (a) Schematic view of the Ultraloop. (b) Symmetric and asymmetric mode of the 24th order. (c) Natural frequency of the 24th modes for various length-to-radius ratios. (d) Experimental Bode plot of the two frequency-degenerate modes. (e) Mode shapes of symmetric mode, asymmetric mode and the resulting traveling wave are shown as normalized colormaps. The color at each grid corresponds to the vibration amplitude measured by a laser Doppler vibrometer. Note that the symmetric mode and asymmetric mode are orthogonal to each other.[6]

D

Appendix - Flatloop Device

Figure D.1: The assembly of the complete designed Flatloop device in Onshape.

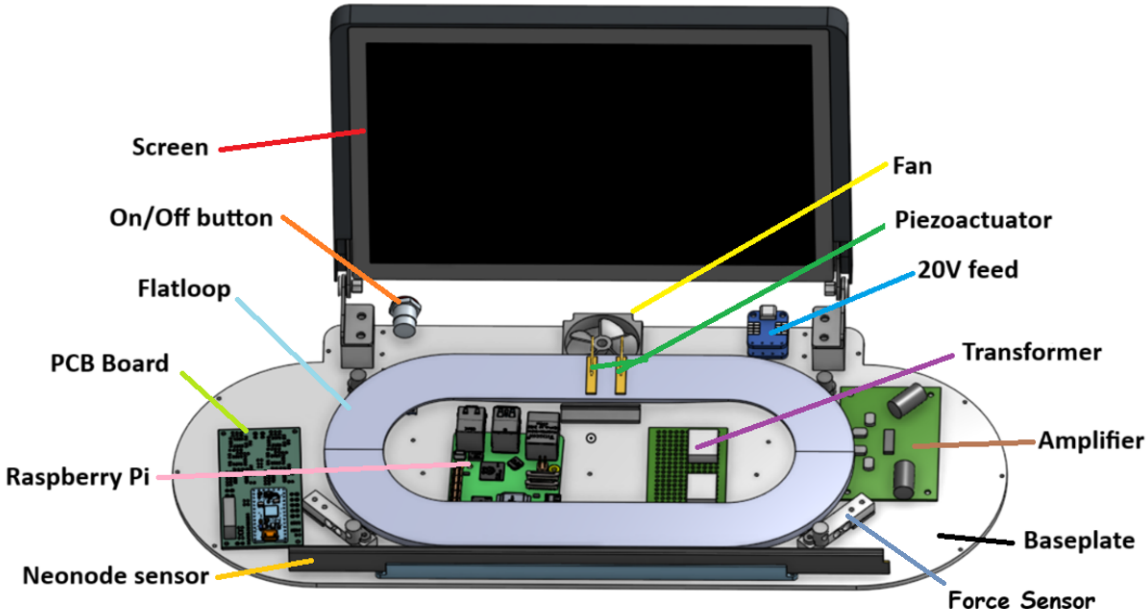

Figure D.2: The components inside the Flatloop device displayed in Onshape.

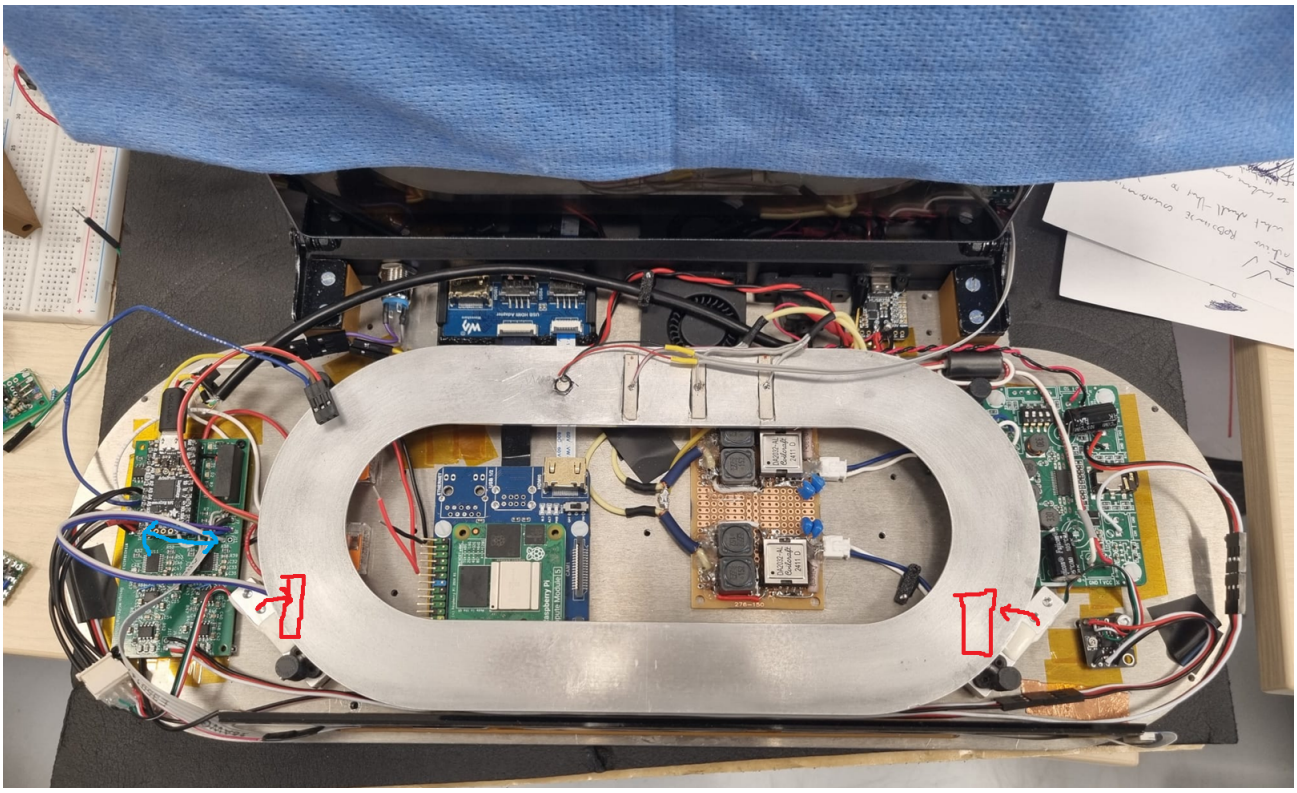

Figure D.3: The components inside the Flatloop device displayed on the real device.

Figure D.4: The complete Flatloop device.